Modeling of the cancer thermal therapies from the perspective of parametric sensitivity and improved treatment planning

Muhammad Jamil

2014

Muhammad Jamil. (2014). Modeling of the cancer thermal therapies from the perspective of parametric sensitivity and improved treatment planning. Doctoral thesis, Nanyang Technological University, Singapore.

https://hdl.handle.net/10356/55390

https://doi.org/10.32657/10356/55390

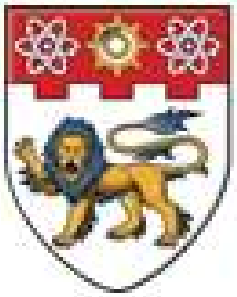

NANYANG TECHNOLOGICAL UNIVERSITY

MODELING OF CANCER THERMAL THERAPIES FROM THE PERSPECTIVE OF PARAMETRIC SENSITIVITY AND IMPROVED TREATMENT PLANNING

MUHAMMAD JAMIL

SCHOOL OF MECHANICAL AND AEROSPACE ENGINEERING

2014

MODELING OF THE CANCER THERMAL THERAPIES FROM THE PERSPECTIVE OF PARAMETRIC SENSITIVITY AND IMPROVED TREATMENT PLANNING

MUHAMMAD JAMIL

School of Mechanical & Aerospace Engineering

A thesis submitted to the Nanyang Technological University
in partial fulfilment of the requirements for the degree of
Doctor of Philosophy

2014

Acknowledgements

This report is completed with the guidance from my supervisor **Associate Professor Eddie Y.K. Ng** from School of Mechanical and Aerospace Engineering, NTU. His incisive comments, erudite knowledge base and the resourceful research methodologies benefited me greatly. Dr. Eddie's continuous help, never ending inspiration, and persistent spirit helped me to overcome the obstacles and achieve my goals in research and life in general. Finally, I would like to express my special thanks to Nanyang Technological University for providing me the opportunity and financial assistance for the postgraduate study.

I would like to express my gratitude to my parents, brothers; Tariq, Asif, Badar and sisters; Asifa and Jamila, who are never short of prayers for me and I'm indebted to them for their unending moral and emotional support. I'm also thankful to my friends Aftab, Fahad, Asif, Shahzada, Zia, Safi, Basit, Nodir, Yousuf, Haseeb, Vinod and Arshad at "Pakistan House" with whom I've shared the ebbs and flows of my postgraduate life. I'm grateful to my lab mates Taureza, Jiao, Liu Dan, Akhil and Chathura for their company. I would also like to extend my gratitude to my nicest Boss Jehanzeb Khan Lodhi for his help and support without whom this endeavour wouldn't have been possible and former colleagues Afzaal sahab, Munawwar and Sheheryar for their support. I would also like to thank my friends and colleagues Shahzad and Adnan Maqsood who supported and helped me during the course of my study.

Table of Contents

List of Figures

List of Tables

Nomenclature

Latin Symbols

A	Frequency factor
$\mathbf{A}$	Global radial basis collocation matrix
A_L	Radial basis collocation matrix for interior domain
A_g	Radial basis collocation matrix for Dirichlet boundary
A_h	Radial basis collocation matrix for Neumann boundary
$\mathbf{a}$	Matrix of unknown coefficients for collocation points
B	Magnetic flux density (Wb/m^2)
B_g	Boundary operator for Dirichlet boundary
B_h	Boundary operator for Neumann boundary
b	Source matrix for collocation points
b_g	Source matrix for collocation points at Dirichlet boundary
b_h	Source matrix for collocation points at Neumann boundary
c	Specific heat [J/(kg.K)]
c_b	Specific heat of blood [J/(kg.K)]
D	Electric displacement (C/ m^2)
E	Electric field intensity (V/m)
F	Fisher statistic
f	Frequency (Hz)
f	Source matrix for open domain
g	Source matrix for Dirichlet boundary
g_I	Radial basis function

$\mathbf{H}$ Magnetic field strength (A/m)

$\mathbf{h}$ Source term for Neumann boundary

$\mathbf{I}$ Identity matrix

$\mathbf{J}$ Current density (A/m^2)

k Thermal conductivity [W/(m.K)]

k_s Protein damage coefficient

k_B Boltzmann constant (J/K)

K_p Proportional gain

K_i Integral gain

K_d Derivative gain

L Characteristic length (m)

$\mathbf{L}$ Differential operator on the inner domain

L Length of the side of numerical domain (m)

n Number of parameters

N Number of runs/experiments

N_s Number of source points

P Probability value

$\mathbf{P}$ Set of collocation points p in interior of domain

p Number of predictors

$\mathbf{Q}$ Set of collocation points q on Dirichlet boundary

Q Volumetric heat generation rate (W/m^3)

Q_p Rate of heat loss per unit volume due to blood flow (W/m^3)

Q_m Metabolic heat generation rate (W/m^3)

Q_r Spatial heat source (W/m^3)

q Heat flux (W/m^2)

q_i	Mean effect of factor i
R	Coefficient of determination
R	Radius of ablation zone (m)
R_u	Universal gas constant [J/(mol.K)]
R	Set of collocation points r on Neumann boundary
S	Set of collocation points s on the interface
sf	Shape factor
SS_i	Sum of squares due to factor i
T	$\mathrm{Temperature\ (K)}$
T_0	Body core temperature (K)
T_a	Arterial blood temperature (K)
T_c	Temperature of the cooling pad (K)
T^h	Temperature in domain h (K)
T_v	Venous blood temperature (K)
$\tilde{T}$	Approximate solution for temperature (K)
t	Time (s)
U	Applied Potential
V_e	Volume of electrode in spherical ablation model (m^3)
V_e'	Volume of electrode in ellipsoidal ablation model (m^3)
V_i	Ablation volume for experiment i
V	Applied voltage
Z	Major axis diameter of ablation zone (m)

Greek Symbols

β	Regression parameter
Γ	Interface boundary
ΔE	Tissue activation energy (J/mol)
ΔG	Gibbs free energy (J)
ε	Error or residual
ε	Permittivity of the material (F/m)
ε'	Ordinary least squares residual
ε_0	Permittivity of the free space (F/m)
ε_r	Relative permittivity or dielectric constant (F/m)
η_i	Effect of parameter at experiment i
Λ	Matrix for interface
λ	Wavelength of the EM wave (m)
μ	Permeability of the material (H/m)
μ_0	Permeability of free space (H/m)
ρ	Density (kg/m^3)
ρ_b	Density of blood (kg/m^3)
ρ_c	Electric charge density (C/ m^3)
σ	Electrical conductivity of the material ($\Omega^{-1}m^{-1}$)
τ	Heterogeneity index
τ_e	Effective relaxation time (s)
Φ	RBF collocation matrix
φ	Electric scalar potential (V)
Ω	Thermal damage coefficient

Ω	Interior domain
Ω_1	Healthy tissue domain
Ω_2	Tumor domain
Ω'	Heating area
ω	Angular frequency of the power source (rad/s)
ω_b	Blood perfusion rate (1/s)
ω_g	Weight for Dirichlet boundary
ω_h	Weight for Neumann boundary
$\partial\Omega_g$	Dirichlet boundary
$\partial\Omega_h$	Neumann boundary

Superscripts

-	Average
^	Predicted value
1	Interior material
2	Exterior material

Subrscripts

1	Tissue domain
2	Tumor domain
a	Artery
b	Blood

c	Body core
e	Domain number
g	Dirichlet boundary
h	Neumann boundary
L	Interior domain
met	Metabolic heat
p	perfusion

Abbreviations

Adj MS	Adjusted Mean Sum of Squares
ANOVA	Analysis of Variance
ARE	Average relative error
DF	Degrees of Freedom
IMQ	Inverse multiquadratic
MNE	Minimum number of experimental combinations
OA	Orthogonal arrays
RBFs	Radial Basis Functions
RBCM	Radial Basis Collocation Method
S/N	Signal to Noise ratio
SS	Sum of Squares
SSE	Sum of squared error
SSR	Sum of squared due to regression
SST	Sum of squared total

Summary

Cancer is the leading cause of death in the world. According to WHO in 2008 cancer was responsible for 13% of the total deaths worldwide. In America 1 out of 4 deaths is caused by cancer which constitutes the second highest mortality rate after heart disease. In Singapore it causes the highest number of deaths that accounts for1 out of 3 deaths. Although the 5 year survival rate has increased gradually over the past decades, there hasn't been a drastic reduction in the cancer related mortality. The gradual improvement in survival rate is attributed to early detection and better treatment modalities. From treatment point of view these factors translate to better diagnostic capabilities and enhanced therapeutic output. The scope of this thesis covers the latter which relates to better prognosis owing to improved efficacy of the treatment. There are many treatment modalities that have been used to treat cancer but none of them can be qualified as sole treatment modality for all types and tumour sites. So the researchers resort to different treatments by harnessing its congruent attributes for best results against a particular cancer.

Thermal therapies are the genre of therapies which use the lethal effect of heat for treatment purpose. The scope of this thesis covers the improved efficacy of the thermal therapies of capacitive hyperthermia and radiofrequency ablation (RFA). Additionally, it deals with the simulation of bioheat transfer with a novel numerical method that makes use of its meshless characteristic to provide the optimum simulation results.

For a particular therapy to be applied, it is imperative that the effect of all the parameters be known perceptively. Firstly, the factors involved in the capacitive

hyperthermia were ranked which provided a broader guideline for the emphasis that needs to be cast upon each factor during the therapy.

Moreover, capacitive hyperthermia was analyzed from a physical perspective. Physical parameters like depth of tumour, size of tumour, size of electrodes and position of electrodes were considered. Their effect on the maximum achievable temperature inside the biological domain was considered and a multiple regression based prediction model was formulated based on the physical parameters. Two indices namely treatment index and damage index, were defined which correspond to achievement of treatment objective and efficiency of tumour killing respectively.

A novel meshless method known as Radial Basis Collocation Method (RBCM) has been applied to simulate the heterogeneous conduction and bioheat transfer problem. RBCM is a meshless method that uses radial basis function (RBF) interpolation to obtain the solution. RBFs hold many advantages like exponential convergence, less dependence on the dimensionality of the problem, ability to deal with complex geometries and ease of implementation, which can be harnessed to one's benefit. RBCM was successfully applied to simulate the heterogeneous heat conduction and remained consistent even for extreme heterogeneities. RBCM was successfully applied to solve the bioheat transfer problem. Firstly, a homogeneous bioheat problem was simulated and comparison with the analytical solution showed that RBCM provided accurate solution. Furthermore, RBCM was extended to the simulation of heterogeneous bioheat transfer problem. It was concluded that features of RBCM such as accuracy, point based data dependency, ease of

implementation along with its meshless property make it an attractive alternative to the other numerical methods available.

Under the scope of the thesis, research was carried out to analyze the efficacy of radiofrequency ablation (RFA) for varying electrothermal parameters under the framework of fixed temperature control. An attempt has been made to study the RFA for the effect of thermal conductivity, electrical conductivity and blood perfusion rate with Taguchi's design of experiments methodology. Their combined effect was analyzed quantitatively in different tissues. It was found that ablation volume for temperature control algorithm is mostly affected by blood perfusion followed by electrical conductivity and thermal conductivity. Smallest ablation volume was observed in kidney tissue while largest lesion volume was obtained in muscle tissue. Based on the results some insightful corollaries were drawn which may be translated as qualification of RFA for the respective tissue treatment protocol. Moreover, quantification of parameter sensitivity translates to efficient design of control algorithm for power delivery. It is intended that these conclusions will help the radiologist in the treatment planning stage and would serve as broad guidelines for the application of RFA in varying biological environment.

Radiofrequency ablation (RFA) has been increasingly used in treating cancer for multitude of situations to various tissue types. In order to perform the therapy safely and obtain reliable results, the effect of the critical parameters needs to be known beforehand. In this study we have analyzed the effect of electrical conductivity, thermal conductivity and blood perfusion rate of the tumour and surrounding normal tissue on the RFA under the framework of automatic temperature control.

Temperature dependent variations in the parameters were incorporated for better clinical relevance. Ablation volume was chosen as the characteristic to be optimized and temperature control was achieved via PID controller. The effect of all 6 parameters each having 3 levels was quantified with minimum number of experiments harnessing the Taguchi orthogonal arrays' fractional factorial characteristic. It was observed that as the blood perfusion increases, the ablation volume decreases. Electrical conductivity of the tumour and the surrounding normal tissue has an opposite effect on the ablation volume. Increasing electrical conductivity of the tumour results in increase of ablation volume whereas increase in normal tissue conductivity tends to decrease the ablation volume and vice versa. Similarly, increasing thermal conductivity of the tumour results in enhanced ablation volume whereas an increase in thermal conductivity of the surrounding normal tissue has a debilitating effect on the ablation volume and vice versa. With increase in the size of the tumour (i.e., 2cm to 3cm) the effect of each parameter is not harmonious. Their effect varies with change in size of the tumour that is shown by the different gradient observed in ablation volume. Most important is the relative insensitivity of ablation volume to blood perfusion rate for smaller tumour size (2 cm) which is also in accordance with the previous results presented in literature.

Finally research was carried out for accurate prediction of the outcome of the therapy based on the simplified models which are fast and require only few parameters. These include spherical and ellipsoidal models. FEM simulation showed that the gradient of ablation volume for different tissue types is also different owing to varied electrical and thermal properties. The effect of maximum allowable

temperature also affects the shape as well as the evolution of ablation volume. Comparison of simplified models with FEM results was carried out and it was concluded that for various tissues simplified models provide good results with an accuracy of more than 90 percent in some cases. Generally, the prediction is poor at shorter times however it becomes gradually more accurate as the treatment time progresses. Additionally the predictions become more accurate as the set point temperature increases.

Chapter 1: Introduction

1.1 Background

For the past 50 years, although there have been leaps and bounds in our understanding of genetics, molecular and cellular underpinnings of cancer, yet there are no significant changes in the age adjusted mortality from cancer as it remains one of the leading causes of death in the world. According to World Health Organization (WHO) cancer is the leading cause of death which accounted for 13% of the total deaths in the world [1]. In United States, 1 out of 4 deaths is caused by cancer which is the second highest mortality rate after heart disease [2]. Likewise, in Singapore cancer causes the most deaths and is responsible for one third of the total deaths [3].

Cancer is characterised by uncontrolled growth of abnormal cells owing to internal or external factors. The internal stimuli can be inherited mutations, immune system, lifestyle or genetics. The external stimuli can be radiations, chemicals known as carcinogens, tobacco or certain viral infections. Excessive cell division results in a lump of mass known as tumour which in later stages of cancer can cause the abnormal cells to invade other organs of the body. This process is known as metastasis and is responsible for most of the death caused by cancer.

Cancer can be controlled by adopting multiple strategies that deal with prevention, detection and treatment regimes. Prevention regime includes keeping a healthy lifestyle, minimizing exposure to external factors, using UV and radiation protection, controlling the diseases which can deteriorate to cause cancer like Hepatitis B, C and HIV.

Detection caters to imaging modalities like improved resolution of CT scan and MRI which favour early detection of the disease. It also deals with the post treatment (imaging, monitoring) patient care. Treatment regime is concerned with the treatment modalities used for the cancer treatment. It includes better treatment planning and simulation tools, enhanced therapeutic output and palliative care. There are a number of treatment modalities available such as radiation therapy, chemotherapy, thermal therapies etc. An overlap exists between the detection and treatment regimes as repetitive imaging modalities are also an essential part of gauging the therapeutic output.

Therapeutic outcome is dependent on many factors. In order to carry out a successful medical procedure the effect of each parameter on the outcome must be known. The improvement in treatment modalities can be achieved in terms of better treatment planning and enhanced treatment efficacy. Biological tissues are complex structures and their physical, electrical and thermal properties vary greatly. One variation can be the intra-patient variation caused by the location, size and the type of the tissue. Other variation can be the inter-patient variation encountered which can be attributed to physical and biological variations. Physicians come across multitude of situations where it becomes practically impossible to predict the outcome. Physician's judgement needs to take into consideration all the factors like the risk involved, ethical guidelines and potential side effects. Therapeutic advantage in terms of enhanced efficacy needs to be weighed against the risks involved in the therapy. In such situations, simulation tools present themselves as the prime choice; offsetting the general in vivo limitations and enhancing the physician's foresight by

parameter optimization to avoid undesirable results pre-emptively. Utilizing the rigorous simulation tools combined with more efficient and robust numerical techniques can go a long way to improve the patient care and mitigation of inadequacies.

1.2 Scope of the Thesis

Scope of this research relates to cancer prognosis that deals with treatment protocols for enhanced therapeutic outcome via efficacy, treatment planning and simulation improvement. Specifically, it deals with improving the capacitive hyperthermia and RFA within the framework of thermal therapies. Concurrently, it also includes the simulation part of the cancer treatment that deals with the numerical algorithms adopted in the therapy. Thermal medicine is the genre of therapies that apply the curative effect of heat to treat cancer. Heat can either flow into the body as in the case of hyperthermia and ablation or it can flow out of the body as in the case of cryoablation.

Within the framework of treatment simulation, numerical methods possessing the favourable properties that are congruent with the simulation requirements can be advantageous to further the treatment efficacy. Furthermore, it is also the intention to stipulate the mathematical framework by harnessing the statistical and numerical techniques that are efficient and accurate to predict and pre-empt the treatment outcome.

1.3 Research Objectives and Specific Aims

This research deals with the capacitive hyperthermia, RFA and implementation of a novel numerical technique within the framework of bioheat transfer.

In capacitive hyperthermia, the electrodes are capacitively coupled and the heating effect is caused by the current flowing from one electrode to another. In RFA, conductive electrodes are positioned inside the tumour under image guidance, and a dispersive pad is placed elsewhere on the body which acts as ground (sink) to complete the circuit.

1.3.1 Aims Related to Parametric Sensitivity

1. This research aims to study the effect of each of electrothermal parameter involved in capacitive hyperthermia. This can be extended further and manifested as to *rank the parameters* that affect the bioheat transfer.

2. To evaluate the effect of tumour and equipment morphology along with tunable parameters involved in the capacitive hyperthermia. The morphology involves size of the tumour, depth of tumour, size of electrodes and position of electrode. Tunable parameters include the voltage and frequency of the applied field.

3. To obtain the *parametric sensitivity of RFA* without violating the entailing limitations. The limitations here refer to the maximum or threshold temperature value that cannot be exceeded during the course of the therapy in order to avoid the boiling. It also aims to stipulate the therapeutic output under combined effect of parameters.

4. To quantify the *parameter sensitivity of RFA* for the case of concentric tumour model under fixed temperature control. It can be extended to the response of parameter sensitivity in the wake of varying tumour morphology.

1.3.2 Aims Related to Predictive Models

1. To lay a mathematical framework utilizing the statistical techniques to predict the outcome in capacitive hyperthermia. Statistical techniques refer to multiple regression and experimental design. The physical as well as tunable parameters are fed into the model for prediction.

2. To put forth simplified prediction models for implementation in RFA for various tissue types under the framework of fixed temperature control. Tissue types include fat, bone, liver, lung and kidney etc. and simplified models here refer to ellipsoidal and spherical approximations for calculation of ablation volume.

1.3.3 Aims Related to Simulation Tools

To implement a novel numerical method that is easy to implement and at the same time robust enough to capture the correct physics of the heat transfer phenomenon in biological tissues. Meshless methods possess the congruent features to those stipulated above and this research predominantly aims to harness their aforementioned pros for simulation of bioheat transfer.

1.4 Methodology

In this work, experimental design methodology has been used for the parametric sensitivity analysis. In the context of large parameters involved, Taguchi's orthogonal arrays have been used which rely on their fractional factorial characteristic to give the optimum results with minimum number of experimental runs [4-6]. Multiple linear regression analysis was utilized to chalk out a predictive model based on the physical and tunable parameters involved. Analysis of variance (ANOVA) was coupled with Taguchi experimental design in carrying out the ranking of parameters.

For the implementation of meshfree numerical method, a novel Radial Basis Collocation Method (RBCM) was implemented in Matlab. The RBCM was first used for the simulation of heat transfer in heterogeneous conduction and it was implemented in the simulation of cases with extreme heterogeneities. It was extended further for simulation of Pennes bioheat transfer equation. Initially, the RBCM was applied to homogeneous bioheat problem and results were benchmarked against the analytical solution. Later it was used in the simulation of heterogeneous bioheat transfer problem with promising results.

1.5 Organization of the Thesis

Chapter 1

In this chapter, a concise background of the research area is given. The intention is to start with a broader perspective about the field and build an argument for motivation about the study and then narrow it down to proposed research objectives and the methodology to achieve those objectives. At the end of the chapter, a concise and systematic outline of the report is presented.

Chapter 2

Literature review is an important aspect of carrying out research and to find out the knowledge gaps. Learning from literature survey helps to understand and solve the problems. It also helps to analyze the problem and make useful conclusions out of the results or findings. Chapter 2 describes the relevant literature about the thermal therapy within the scope of this thesis. The chapter has three main streams namely heat transfer, electromagnetics and meshless methods. These streams correspond to

the objectives outlined in Chapter 1. Heat transfer stream deals with the various heat transfer models presented in literature which differ in terms of complexity, implementation and underlying methodology. It also includes the quantification of the lethal effect of temperature via different indices presented in the literature. Electromagnetics stream deals with the basic theory related to electromagnetics which is based on the Maxwell's equations. It further deals with the concomitant tuning and simplifications when these equations are applied under the framework of thermal therapies. Meshless methods stream caters to the literature related to meshless approaches. It falls under the broader scope of this research which is to implement a novel meshless method that is simple to implement and yet comprehensive enough to provide reliable results by capturing the true physics.

Chapter 3

Chapter 3 presents the results of ranking of parameters in bioheat transfer for hyperthermia therapy. It deals with the capacitive hyperthermia and intricate details regarding different parameters involved are quantitatively analyzed. Systematic variation of parameters is done to obtain concrete results regarding the parameters affecting the bioheat transfer.

Chapter 4

In chapter 4, the hyperthermia therapy has been analyzed from a physical perspective. The influence of physical parameters like size of tumour, depth of tumour, electrode size etc. on the outcome of the therapy is presented. Moreover, a prediction model based on multiple linear regression is also formulated which

presents itself as a quick alternative to rigorous and time consuming simulation methodologies.

Chapter 5

Chapter 5 deals with the application of novel radial basis collocation method. Firstly the method is benchmarked against a particular heterogeneous conduction problem presented in literature and then its application is extended for extreme heterogeneous problems. Similarly, the RBCM is applied to 2D homogeneous bioheat problem with various perfusion rates and results are compared with the analytical solution. Furthermore, it is extended to 2D heterogeneous bioheat problem and its merits and demerits compared to other methods are presented.

Chapter 6

Chapter 6 covers the application of RFA for different tissue types. Firstly, the effect of various parameters on different tissue types is evaluated with the restriction that the maximum steady state temperature doesn't increase above the threshold temperature. Additionally a concentric tumour model is analyzed under fixed temperature control framework and the effect of various parameters is quantified for tumour and surrounding normal tissue properties. Furthermore, it also includes the prediction of ablation volume by utilizing simplified models i.e. spherical and ellipsoidal approximations.

Chapter 7

Chapter 7 of the thesis summarizes the conclusions of the research regarding control and heat transfer. Additionally it outlines the contributions, limitations and future directions for the current research.

Chapter 2: Literature Review

2.1 Bioelectromagnetics

Bioelectromagnetics is the study of how electric and magnetic fields interact with the body. The importance of this field has become critical as we are increasingly exposed to lot of electromagnetic field sources. These include radio waves, radar, television signal, mobile phones etc. For accurate exposure calculations, Maxwell's equations are a set of equations that form the framework of all the classical electromagnetic (EM) field theory. There are two distinct levels of interaction between EM and biological material to be studied [7].

1. Macroscopic

2. Microscopic

The effect at both levels cannot be considered independently. At the macroscopic level, energy penetration and dissipation phenomena are taken into consideration while at the microscopic level, interaction mechanisms should also be considered at smaller extents. The effect of interaction of EM waves with biological tissues can be classified as the result of three phenomena [7],

1. The penetration of EM waves into the living system and their propagation in it
2. The primary interaction of the waves with biological tissues
3. The possible secondary effects induced by the primary interaction.

It is therefore difficult to fully characterize the propagation of EM field in the human body as biological tissues are complex in structure and non homogenous in nature. This is because the human body is made up of a large number of different tissue

materials, each of them having specific properties. So the properties of the body vary depending on the organ or area under consideration. These properties have been studied at length in the last few decades from 10 Hz to 10 GHz [8]. Since biological tissues are mainly made up of water, they act neither as a conductor nor a dielectric, rather as a dielectric with losses. The wetter the tissue is, the more loss the tissue will experience.

However, computers allow highly accurate evaluations of dosimetry for biological tissues. An EM wave consists of a varying electric field and a varying magnetic field. Propagation of electric and magnetic field is described by the differential form of the Maxwell's equations:

$$\nabla \times \mathbf{H} = \mathbf{J} + \frac{\partial \mathbf{D}}{\partial \mathrm{t}} \tag{2.1}$$

$$\nabla \times \mathbf{E} = -\frac{\partial \mathbf{B}}{\partial \mathrm{t}} \tag{2.2}$$

$$\nabla . \mathbf{B} = 0 \tag{2.3}$$

$$\nabla . \mathbf{D} = \rho_c \tag{2.4}$$

with the constitutive relationships as below:

$$\mathbf{B} = \mu \mathbf{H} \tag{2.5}$$

$$\mathbf{D} = \varepsilon \mathbf{E} \tag{2.6}$$

$$\mathbf{J} = \sigma \mathbf{E} \tag{2.7}$$

where $\mathbf{E}$ is the electric field in Volts per meter (V/m), $\mathbf{H}$ is the magnetic field in Amperes per meter (A/m), $\mathbf{J}$ is the current density in Amperes per square meter (A/m^2), $\mathbf{B}$ is the magnetic flux density in Weber per square meter (Wb/m^2), $\mathbf{D}$ is the electric displacement in Coulombs per square meter (C/m^2), μ is the permeability in Henries per meter (H/m), ε is the permittivity in Farads per meter (F/m), and σ is the conductivity in $\Omega^{-1}m^{-1}$, ρ_c is electric charge density in Coulombs per cubic meter (C/m^3) and time is represented by t.

In general, three different quantities explain the permittivity of a medium: ε, ε_0, and a dimensionless quantity known as the relative permittivity ε_r or the dielectric constant, which is defined as the permittivity relative to that of free space ($\varepsilon_0 = 8.854 \times 10^{-12}$ F/m)[9].

For special case of thermal therapy problems, μ is constant, ∂/∂t is the equivalent of jω where ω is the angular frequency (rad/s) at which the power is excited, ρ_c is zero as there is no residual charge, and j is $\sqrt{-1}$.

For isotropic, linear, and nonmagnetic media, Maxwell's equations in the steady-state form can be written in terms of Faraday's law:

$$\nabla \times \mathbf{E} = -j\omega\mathbf{B} \quad \text{(Faraday's Law)} \tag{2.8}$$

$$\nabla \times \mathbf{B} = \mathbf{J} + j\omega\varepsilon\mathbf{E} \quad \text{(Ampere's law)} \tag{2.9}$$

2.1.1 Nature of Electromagnetic Interaction

Maxwell's equations are applicable over a large frequency range as can be seen from the Figure 2.1 but the behaviour of EM waves is not the same over the whole frequency range.

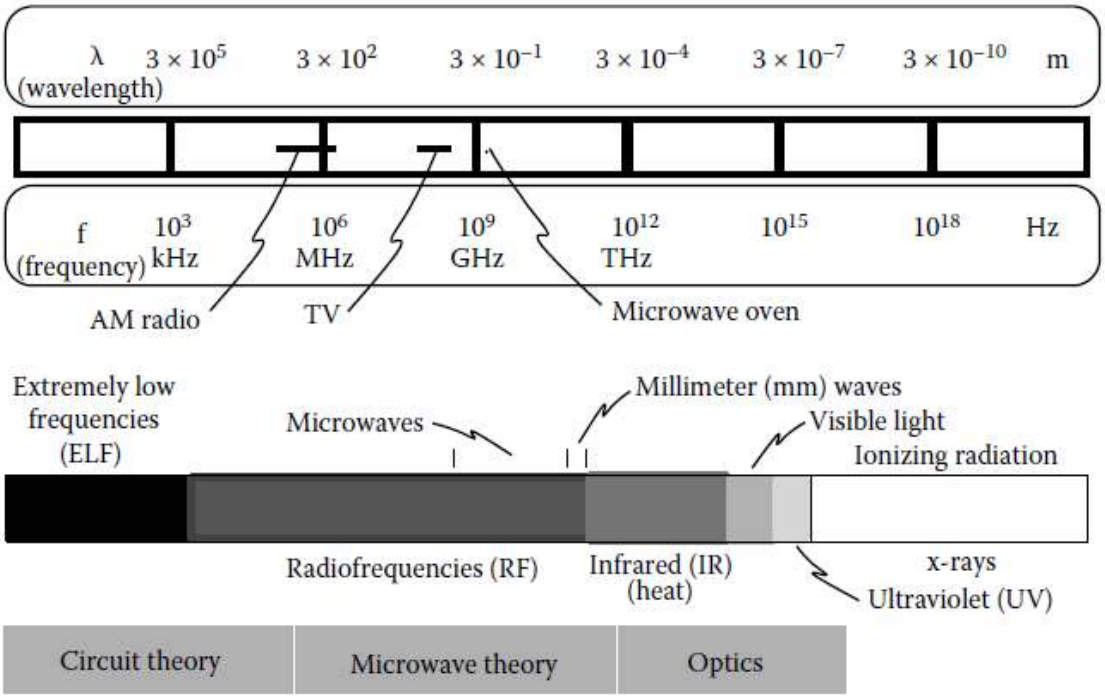

Figure 2.1: Electromagnetic frequency spectrum [10]

The interaction of EM waves and corresponding effects depend on two factors [10]:

1. Size of the Object
2. Frequency of EM wave used

The electromagnetic depends rather on the size of the object as compared to the wavelength of the wave. Suppose λ is the wavelength and L is the characteristic length of the object, then EM behaviour is dependent on the relative size between λ and L. This interdependence of size and wavelength is summarized in Table 2.1.

Table 2.1: Summary of EM behavior for size-wavelength regimes [10]

When $\lambda >> L$ (low frequency for most typical devices)	Electric circuit theory and quasi-static EM field theory are used. Propagation effects are negligible. E and B are uncoupled. Energy is transmitted by wires and cables, but not in beams through the air.
When $\lambda \approx L$ (medium frequency for most typical devices)	Microwave theory is used. Propagation effects dominate. E and H are strongly coupled. Energy is transmitted through cables, hollow waveguides, and beamed through the air.
When $\lambda << L$ (high frequency for most typical devices)	Optics and ray theory are used. Propagation effects dominate. Energy is beamed through the air and is not transmitted through metallic cables or along metallic wires, but can be transmitted through optical fibers.

2.1.2 Quasi Static Approximation

Typical cell diameter is about 100 microns which is, for most used frequencies, much smaller than the wavelength of the EM waves. So the interaction of EM waves with cell will be governed by $\lambda >> L$ category. This situation is shown in Figure 2.2.

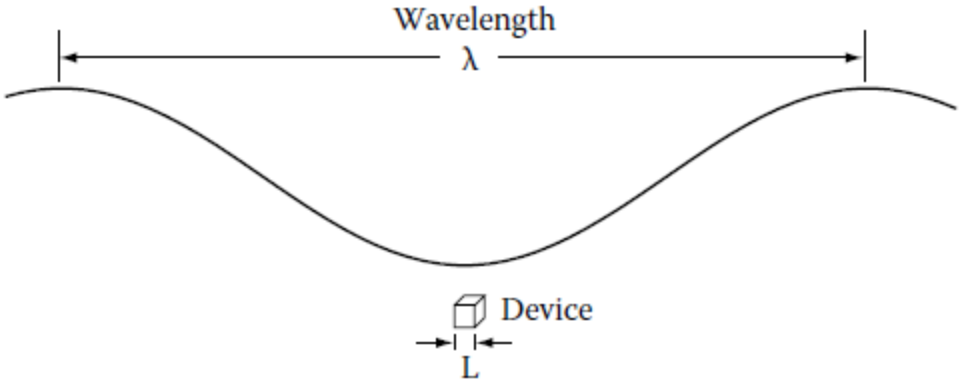

Figure 2.2: EM regime when wavelength is much larger compared to device length [10]

As the size of the object under consideration is very small as compared to wavelength of the applied field, electric field $\mathbf{E}$ and magnetic flux density $\mathbf{B}$ are uncoupled. The fields $\mathbf{E}$ and $\mathbf{B}$ can be assumed to be Quasi Static. Quasi static means, that the extent of variation of $\mathbf{E}$ and $\mathbf{B}$ fields is not that much and is very similar in characteristic to static fields.

In most cancer therapies, frequencies less than 10 GHz are used. Still at this relatively high frequency, wavelength is about 30mm. If the effect of dielectric properties of cell is considered, wavelength is larger than 3.75mm. As the cell size can be up to 100 microns, which suggests that wavelength (3.75mm) is large compared to the size of the object under consideration.

The quasi static approximation simplifies the Maxwell's equations because the field variant terms can be neglected.

Maxwell's equations (2.1) & (2.2) can be written in a simplified form as:

$$\nabla \times \mathbf{E} = 0 \tag{2.10}$$

$$\nabla \times \mathbf{H} = 0 \tag{2.11}$$

Using equations (2.4) and (2.10), electric field calculations can be made.

Considering the somewhat static nature of $\mathbf{E}$, the scalar potential Φ can be defined as:

$$\mathbf{E} = -\nabla\Phi \tag{2.12}$$

Substituting (2.4) into (2.6) and using (2.12), we get the Poisson's equation:

$$\nabla^2\Phi = -\frac{\rho_c}{\varepsilon} \tag{2.13}$$

In a source free medium (i.e. ρ_c =0), **Poisson's equation** becomes:

$$\nabla^2\Phi = 0 \tag{2.14}$$

Equation (2.14) is known as **Laplace's equation** which can be easily solved to obtain the electric potential inside the object of interest.

2.2 Bioheat Transfer in Blood Perfused Tissues

Bioheat transfer is a complicated phenomenon because of the variation in tissue characteristics and complexity of the vasculature responsible for supplying and retrieving blood from every part of the body. There is an ever increasing need of development for accurate bioheat models because of the advancement in medical technology. Now surgeons and physicians resort to numerical simulations for safety and risk assessment involved in treatment of diseases like cancer, eye surgery etc. Accurate prediction of the desired therapeutic outcome is essential for success of these therapies. Additionally, availability of computational resources at physician's disposal make the task easy.

Over the period of time researchers have presented many bioheat transfer models which differ in complexity, underlying theory and implementation.

Heat transport in blood perfused tissues can be modelled using two approaches [11].

1. Bioheat transfer modelling using simplified approach
2. Bioheat transfer modelling using porous media theory

Porous media theory is more detailed and takes into consideration the porosity, effective tissue conductivity and models the exchange process between tissues, arteries and veins more accurately. The main characteristics of porous media based bioheat modelling are shown in Table 2.2.

In simplified approach the heat transfer is modelled using simplified assumptions about vasculature, thermal interaction between vasculature and tissues, and blood perfusion etc. Although many models have been developed to model bioheat transfer, Pennes bioheat equation [12] has received the most attention. It has been successfully applied to many problems [13-15] and will be discussed here further.

Table 2.2: Main characteristics of porous media approach bioheat models [11]

Bioheat Model	Main Characteristics
Porous media model (local thermal equilibrium principle)	This model modifies the Pennes equation by accounting for the following effects: Variable tissue porosity Effective tissue conductivity Effective tissue capacitance Blood dispersion
Porous media model (local thermal nonequilibrium principle)	This model requires more knowledge about the thermal and anatomic properties of the tissue, the velocity field of the blood, and interstitial convective heat transfer coefficients. This model considers the following effects: Variable tissue porosity Blood dispersion Effective tissue conductivity Effective tissue capacitance

2.2.1 Pennes Bioheat Equation

The first bioheat model was developed by Pennes to model the bioheat transfer in the human forearm. The equation developed by Pennes is given by [12]:

$$\rho c \frac{\partial T}{\partial t} = \nabla . k \nabla T + Q_p + Q_m \qquad (2.15)$$

where ρ, c, k, and Q_m are density, specific heat, thermal conductivity and metabolic heat generation in the tissue respectively. Q_p represents the heat loss due to the blood perfusion.

Heat transfer from blood to tissue is assumed to be function of difference between arterial blood entering the tissue and venous blood leaving the tissue i.e.,

$$Q_p = \rho_b c_b \omega_b (T_a - T_v) \tag{2.16}$$

where T_a and T_v represent the arterial and venous blood temperature. ρ_b, c_b are density and specific heat of blood respectively and ω_b is volumetric rate of blood perfusion in tissue per unit volume.

In modelling the perfusion term, Pennes assumed thermal equilibrium between venous and tissue temperature i.e., $T_v = T$ to give the final bioheat equation as:

$$Q_p = \rho_b c_b \omega_b (T_a - T) \tag{2.17}$$

2.2.2 Other Bioheat Transfer Models

After the pioneering work on bioheat transfer by Pennes, many other bioheat transfer models were presented. The initial Pennes bioheat model was critically analyzed and the assumptions made by Pennes were questioned.

Wulff presented his bioheat model known as Wulff continuum model [16]. He modelled the perfusion term on the temperature difference between the blood and tissue. His final equation includes term containing the local mean blood velocity. The main problem with his model was how to measure the local blood velocity.

Klinger improved the Wulff model and modelled the perfusion term by considering the spatial and temporal variations in blood [17]. In effect it added more details of the physical phenomenon but in hind sight added more complexity and required more variables.

Chen and Holmes considered the tissue as a matrix consisting of solid phase and vasculature and using energy balance applied the volume averaging over the solid and fluid phase to obtain the final equation [18]. They put forth the concept of effective conductivity of the tissue and vascular space as a result of thermal dispersion effect. Unlike Wulff's continuum model, their model catered for the blood to be at different temperature than the tissue and hence considered the effect of convection heat transfer caused by blood flow.

Weinbaum, Jiji and Lemons further modified the effective thermal conductivity concept which included the geometrical and local blood flow features [19]. They based their model on the assumption that arteries and veins have counter current arrangement and the associated blood flow causes simultaneous heating and cooling effects.

The details of these models are given in Table 2.3. It is evident that these models are based on the basic work of Pennes and can be regarded as either modification or extension of original Pennes model.

Lastly, Pennes model is based on the classical Fourier law which assumes that thermal disturbance travels at an infinite speed and small disturbance is felt instantaneously in the body. To incorporate this, non-Fourier models which assume finite propagation speed of thermal disturbance were also presented [20, 21]. Non-Fourier phenomenon has been observed in processes involving very low temperatures, or processes where large amount of energy is deposited in short time scales like laser heating and materials with large heterogeneities. Neither of these is

relevant for the current research, so Pennes bioheat model based on the classical Fourier law is sufficient for this research.

Table 2.3: Main characteristics of bioheat models using simplified approach [11]

Bioheat Model	Assumptions	Main Characteristics
Pennes	Uniform physical properties and metabolic heating Heat transfer from the blood to the tissue is proportional to the temperature difference between the arterial blood entering the tissue and the venous blood leaving the tissue	Simple model Not valid for all tissues
Wulff	Thermal equilibrium between flowing blood and the surrounding tissue Uniform mean blood velocity inside the tissue	Modified version of the Pennes model
Klinger	Constant physical properties	Considers the convective heat transfer caused by the blood flow inside the tissue Considers the spatial and temporal variations of the velocity field and heat source
Chen and Holmes	Utilized two separate volumes: one for solid tissue and one for blood in the vascular space	The total heat transfer by conduction relates to heat transfer by conduction in the solid tissue and in the vascular space The total perfusion term corresponds to the effect of blood flow on tissue temperature around large vessels, heat transfer that takes place as a result of the blood flow, and heat transfer due to the small temperature changes (microvessels) Introduce perfusion conductivity tensor in the bioheat equation. Allows for the blood within the tissue matrix to flow at a temperature different than that of the tissue temperature

(Continued)

Bioheat Model	Assumptions	Main Characteristics
Weinbaum, Jiji, and Lemons	Based on a hypothesis that small arteries and veins are parallel and the flow direction is countercurrent, resulting in counterbalanced heating and cooling effects	Coupled energy equations for artery–vein pair and tissue
	Isotropic blood perfusion between the countercurrent vessels	Utilizes the effective conductivity
Weinbaum and Jiji	The mean tissue temperature is approximated by an average temperature of the bulk mean temperatures inside the blood vessel	Valid when arteries and veins are close, leading to negligible blood perfusion effects
	Assumes that the tissue around the vessel pair is a pure conduction region	Utilizes the effective conductivity

2.2.3 Thermal Therapies

Thermal medicine is the field of medicine in which the curative effect of heat is used for treatment. Depending on the treatment type heat can flow in and out of the body. In treatments like cryoablation the temperature is decreased to -50 ^{o}C and heat flows out of the system [22]. In treatments like hyperthermia or radiofrequency ablation (RFA) heat is supplied to the body to raise the temperature of the body to achieve hyperthermic and ablative conditions. A detailed review of these therapies is shown in Figure 2.3. In Figure 2.3 Investigational Device Exemption (IDE) trials, Premarket Approval (PMA), Ultrasound (US) and Microwave (MW) are also mentioned.

In moderate temperature hyperthermia the temperature of the body is raised to 4-8 ^{o}C above the normal body temperature. Prolonged exposure at these temperatures leads to cell death. In capacitive hyperthermia, two electrodes are capacitively coupled to each other and current flows through the tissue placed between the electrodes.

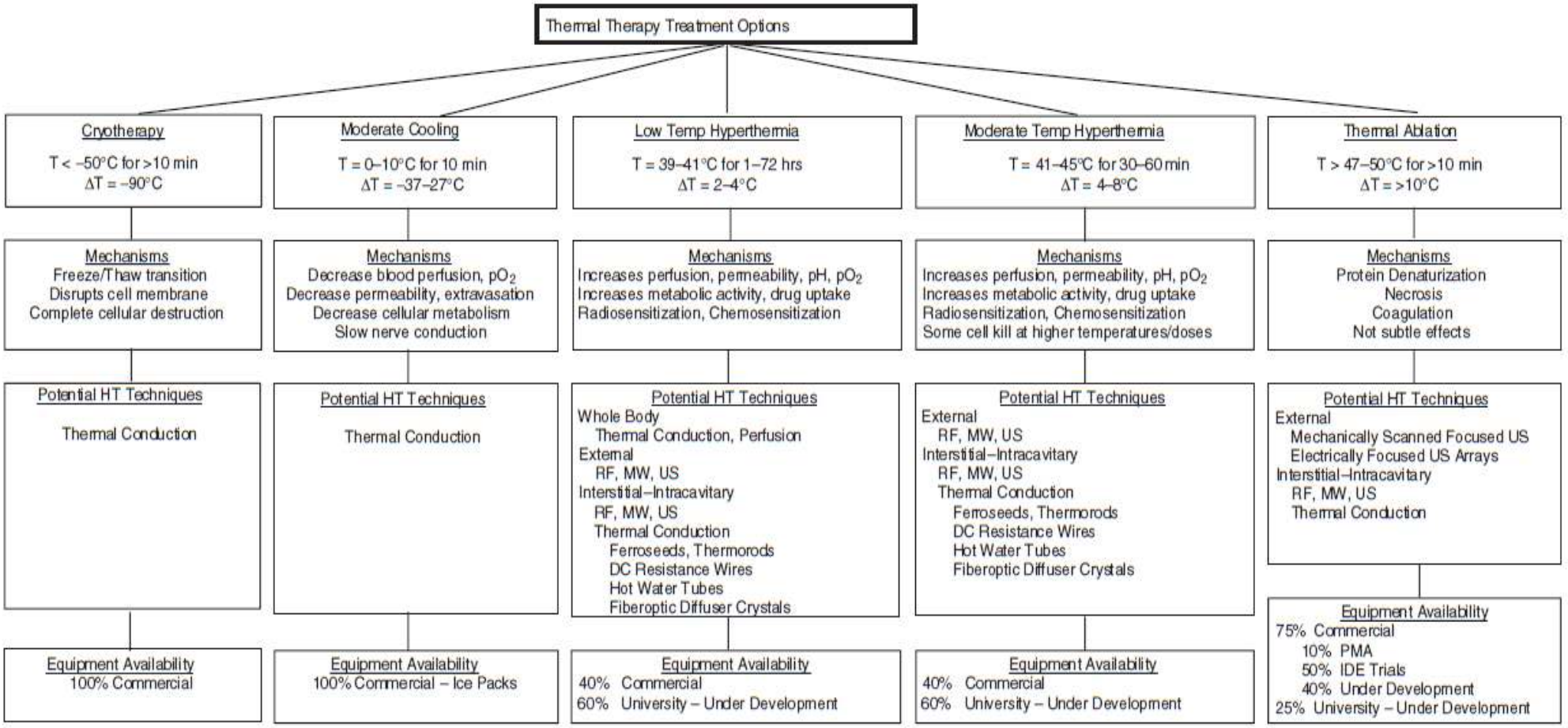

Figure 2.3: Treatment options for therapeutic use of thermal medicine [22]

Typical arrangement for capacitive hyperthermia is shown in Figure 2.4. Potential difference is applied between the electrodes which makes the current flow from one electrode to another.

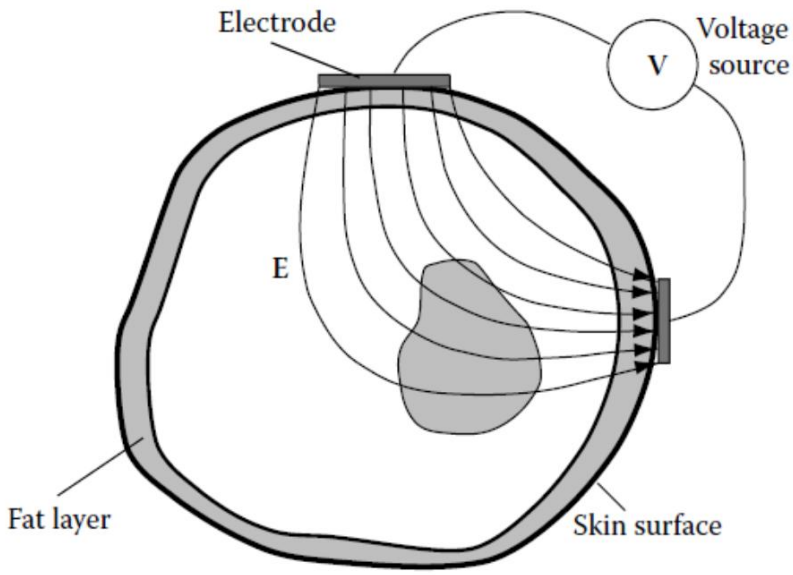

Figure 2.4: Typical setup for capacitive hyperthermia [23]

In RFA the temperature of the biological tissues is raised above the hyperthermic temperatures (i.e. 10 ^{o}C more than the body temperature).

The setup shown for RFA is shown in Figure 2.5. In RFA, an RF electrode is percutaneously inserted to the diseased area under the image guidance. Voltage is applied on the active part of the RF electrode and grounding pads are place elsewhere on the body. Application of voltage on the active RF electrode causes the current to flow through the body which raises the temperature of the body.

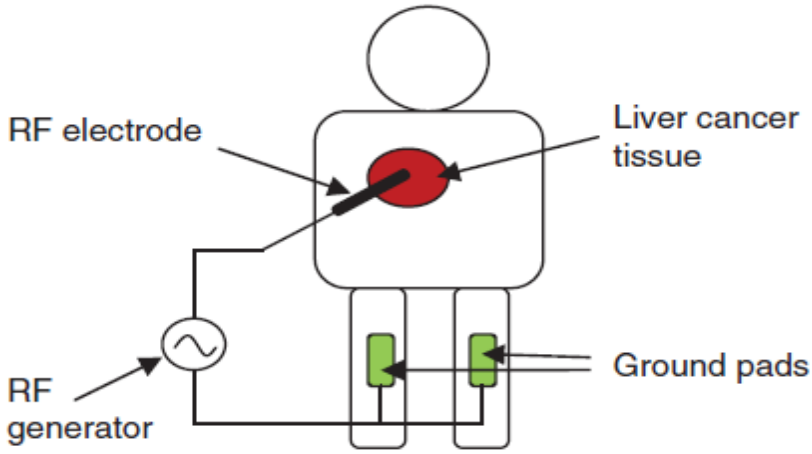

Figure 2.5: Overview of RF ablation procedure [24]

2.2.3.1 Thermal Effects of Electromagnetic Fields

During the RF and capacitive ablation procedures the electrical circuit is complete and current flows inside the body. For capacitively coupled electrodes current flows from one electrode to another. For RF ablation the current flows from the electrode to grounding pad. As the current flows through the body, the free ions (Na, Cl, K etc.) present in the body are agitated and follow the polarity of the RF current (Figure 2.6). Frictional losses due to movement of ions results in generation of heat. This resistive heating is dependent on the properties of the tissue under consideration. Prolonged heating results in temperature increase inside the tissue and subsequently reaches hyperthermic or ablative temperatures.

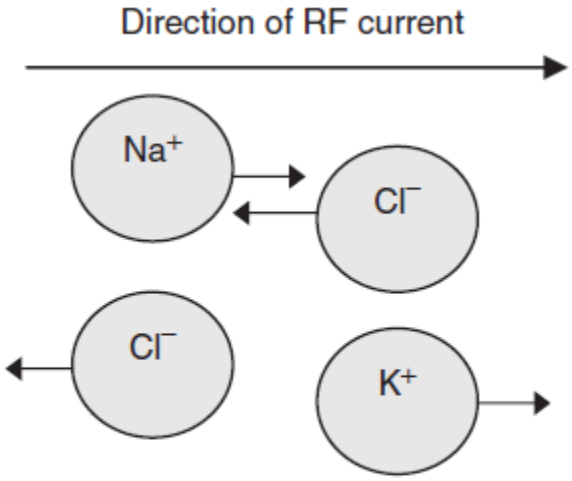

Figure 2.6: Motion of ions inside the tissue driven by RF current [24]

The quantification of the effects of hyperthermia on the cells is a complex problem. This is because hyperthermia therapy activates many mechanisms simultaneously. There are two primary hyperthermia induced effects. One is hyperthermia induced cell death and other is the radiosensitization and chemosensitization caused by hyperthermia.

Hyperthermia induced cell death can be via apoptosis, mitotic catastrophe or heat shock proteins (HSPs). Hyperthermic temperatures cause induction of HSPs which subsequently results in unfolding of hydrophobic groups in cells and causes aggregation of proteins as shown in Figure 2.7. The effect of aggregation is mostly in nucleus as most of the DNA and proteins are concentrated in nucleus. Secondly, nucleus is responsible for critical cell functions like transcription, replication and repair of DNA. This aggregation results in disruption of these cellular functions leads to genome instability and cell death. Although hyperthermia results in protein

aggregation but it doesn't cause any DNA damage via breaking of double strands as is the case of ablation where higher temperatures are achieved.

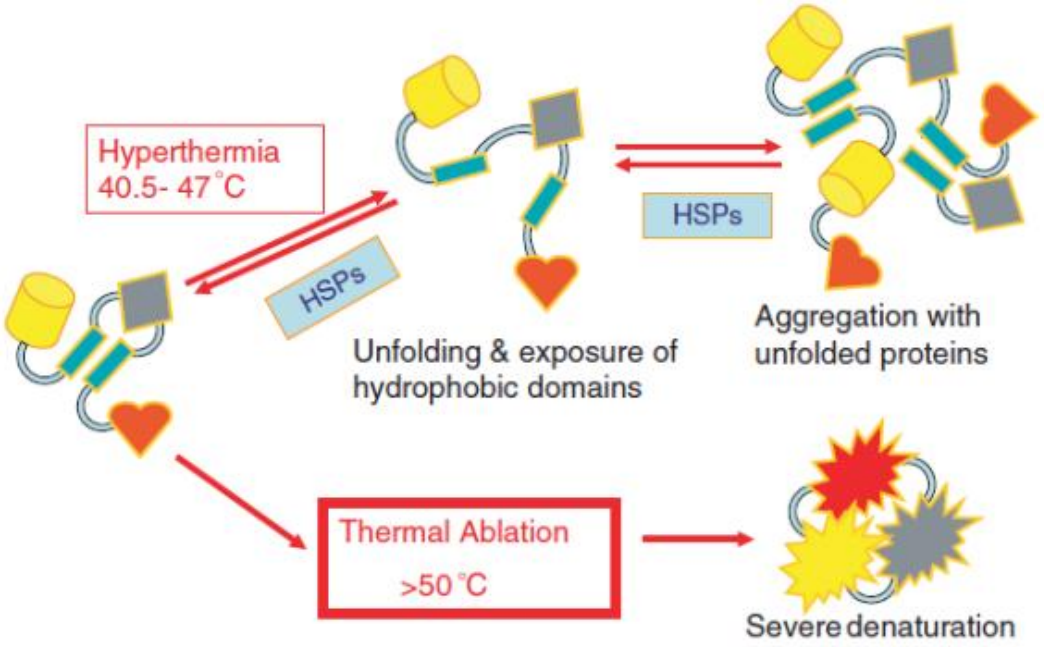

Figure 2.7: Thermal effects of hyperthermia and thermal ablation [25]

Moreover, exposure of cells to hyperthermic temperatures causes the depolarization of the mitochondria and increases the oxygenation and permeability of the plasma membrane which contribute towards sensitization of the cells to hyperthermia and other therapies like chemotherapy and radiation therapy.

Raising the temperature of the body to ablative temperatures results in severe protein denaturation (Figure 2.7). It has also been known that raising the temperature above 50 ^{o}C results in DNA damage [25]. When the temperature is raised above 70 ^{o}C it results in coagulation. Raising the temperature above 100 ^{o}C can cause boiling and charring of tissue [24].

2.2.3.2 Non Thermal Effects of Electromagnetic Fields

Electromagnetic fields also affect the other functions of the body and can cause various non thermal effects.

2.2.3.2.1 Visual Phosphenes

Electromagnetic fields can cause flashing of lights in the eye which is known as visual phosphenes. The electromagnetic field stimulates the retinal cell potentials and results in visual phosphenes.

2.2.3.2.2 Peripheral Nerve Stimulation

Electromagnetic fields depolarize the neural membranes and stimulate the ion channels in the neurons which result in sensation.

2.2.3.2.3 Direct Muscle Cell Excitation

Motor neurons in the muscle can also be activated by exposure to electromagnetic fields and result in direct muscle excitation.

2.2.3.2.4 Electroporation

Exposure of biological cells to high magnitude pulsed fields can produce pores in the cellular membrane of the cell. The electroporation can be permanent or temporary depending on the field magnitude.

2.2.3.2.5 Audio Effects

Very high electromagnetic fields can produce a thermoelastic wave in the head which can be detected by the auditory mechanism of the ear.

2.2.3.2.6 Magnetohydrodynamic Effects

Very strong magnetic fields can exert forces on the ions present in the blood. The forces are applied on the ions which are perpendicular to the applied magnetic field and can result in vertigo and taste sensations.

2.2.4 Evaluation of Thermal Damage

Critical temperature can be used as the easiest way to quantify the thermal damage. But thermal injury also depends on the thermal history such as heating rate, hold time and final temperature. There have been models developed to quantify damage of tissue, cell or vasculature.

Following approaches have been used for quantification of thermal damage [20].

1. Critical thermal load approach
2. Arrhenius burn integration approach
3. Approach based on enzyme-catalyzed reactions
4. Simplified approach based on the isotherm contour

2.2.4.1 Critical Thermal Load Approach

Critical thermal load approach assumes that equal thermal damage induced is a function of cumulative dose.

Using this approach thermal damage Ω can be quantified by the following equation:

$$\Omega = \int_0^t \mathbf{q}\,dt \tag{2.18}$$

where t and q represent time and heat flux respectively.

This model only takes into account the amount of energy delivered and not the duration to deliver the energy. It was later shown that large amount of energy delivered in short durations can severely damage the tissues [26, 27].

2.2.4.2 Arrhenius Burn Integration Approach

Henriques et al. [28] showed that thermal injury can be represented by a Arrhenius rate equation. It was known as Arrhenius burn integration approach. It was proposed that thermal damage can be represented by protein denaturation in the cell or tissue.

2.2.4.2.1 Tissue Damage Model

Tissue damage can be evaluated using Arrhenius function. The rate of tissue injury Ω can be described as [29]:

$$\frac{d\Omega}{dt} = Ae^{-\frac{\Delta E}{R_u T}} \tag{2.19}$$

where

e is constant having value 2.718

A is the frequency factor

ΔE is the tissue activation energy (kJ/mol)

R_u is the universal gas constant [8.31 J/(mol.K)]

T is the absolute temperature (K)

t is the thermal treatment time (s)

Ω = 1 can be attributed to necrosis.

The above model predicts the tissue damage but it is very difficult to conclude that all the cells in the tissue have been destroyed. So a model that can predict the cellular damage is required to be sure of the complete damage to the cells.

2.2.4.2.2 Cellular Damage Model

Cell survival depends on the effective functioning of the organelles in the cell. Hindering of different cell reactions and denaturation chromosomal proteins can cause cell death and each of these reactions follows Arrhenius function [29].

$$k_s = \frac{k_B T}{h} e^{-\frac{\Delta G}{R_u T}} \tag{2.20}$$

where k_s is rate of damage, k_B is the Boltzmann's constant, h is the Planck's constant and ΔG is the Gibbs free energy of activation.

The fraction of the reactions of damaged proteins in the cell can be expressed as followed.

$$F(t) = 1 - e^{-k_s t} \tag{2.21}$$

2.2.4.3 Approach Based on Enzyme Catalyzed Reactions

This relatively new approach to model thermal damage was presented by Xu & Qian [30]. This is very similar in form to Arrhenius model, but the constants have different values based on the experimental data fitting of the data presented by Henriques [28].

The thermal damage Ω can be represented by:

$$\Omega = \int_0^t \frac{Ae^{\gamma z}}{1 + Be^{-\beta z}} dt \qquad (2.22)$$

where γ and β are empirical constants. Following values were obtained by data fitting to the experimental data of Henriques [28]:

γ =100

β =195

A =1.1*10^{-4}

B =8*10^{4}

2.2.4.4 Simplified approach based on the isotherm contour

The models presented above need to be applied for different situations and tissue types. These require tissue specific parameters which are not available most of the time. Hence a simplified approach is adopted in which the boundary of the thermal lesion is defined by the isotherm contour related to a threshold temperature [31]. The threshold temperature value varies according to the nature of therapy i.e., hyperthermic or ablative.

2.3 Taguchi's Design of Experiment Methodology

The performance of a system or a process is evaluated on the basis of experiments. A system or experiment consists of certain input or control parameters and certain

output variables. System performance is indicated by the value of the output or response variables. A crude approach in optimizing the system performance is to vary the input parameters based on the historical performance data in an attempt to achieve better performance. This approach is known as trial and error approach. The inherent drawback of this approach is that it doesn't guarantee the optimum output and efficiency of achieving the output is generally poor. Another primitive approach is to sequentially vary the value of each parameter involved in the process and keeping the other variables constant. It also suffers from the inability of providing the optimum result concomitant by poor performance for large number of parameters [32].

To overcome these issues a systematic and scientific way of designing experiments is known as experimental design. The concept of design of experiments was first presented by Fisher in 1920s [33, 34]. Design of experiment involves carefully designing the experiments with systematic parameter variation to achieve optimum results. Full factorial approach provides a systematic and efficient experimental procedure and explores the full parameter space which contains the parameter effects as well as inter-parameter interactions [35]. However for experiments involving many parameters along with large number of levels, this approach is too cumbersome and becomes inefficient in terms of cost and time required to carry out the analysis. An experiment having n input variables each having k levels, a full factorial design would require k^n experimental runs to fully characterise the system. For 6 parameters with each having 3 levels 3^6=729 experiments are required.

Clearly, for large number of process inputs with multi-levels the number of experimental runs increases enormously.

To overcome these difficulties Taguchi designed the orthogonal arrays (OA) which have fractional factorial characteristics and provide the optimum output utilizing minimum number of experimental with comparable efficiency to that of full factorial design [5, 6, 36]. For example an experiment with 6 parameters each having 3 levels, only 27 experiments are required utilizing L27 orthogonal array.

Orthogonal arrays have many useful properties which give a balanced comparison with minimum number of experimental runs. Each row in the orthogonal array represents an experimental run with respective levels for the included parameters. Each column of the array represents a parameter and for 6 parameters there should be 6 columns each assigned to a parameter. Similarly in a column each parameter level occurs equal number of times. For example, for L27 orthogonal array for parameter 1 in column 1, low, medium and high levels occur equal number of times i.e., 9 times. The orthogonal array results in another array with small number of parameters if some columns of the array are deleted.

2.3.1 Implementation of Taguchi's Methodology

Taguchi analysis has been widely used in manufacturing [37-41], thermal and fluid flow [42, 43], health science [44, 45], biology [46-48], biochemistry [49], ecology [50-52] and for speech recognition [53]. For efficient experimental design based on the Taguchi's orthogonal arrays, following steps are required.

2.3.1.1 Identification of Quality Characteristic to be Optimized

First step in employing the Taguchi's experimental design is to identify the quality characteristic to be optimized. Quality characteristic here means the "output variable of interest" whose value needs to be optimized. For instance, in thermal problems it can be the maximum or minimum temperature depending on the process under consideration. In manufacturing processes it can be the number of defects.

2.3.1.2 Selection of Parameters and Their Respective Levels

It involves the selection of critical parameters regarding the process under consideration. Knowledge about the process is beneficial for parameter selection. After the parameter selection, the respective levels are chosen based on the variation relevant to the process. A parameter can have two or more levels. More number of levels allows the experimenter to explore a larger parameter space in case there is a non linear or quadratic relationship between the input and the response variable. Caution must be exercised as added parameter levels increase the number of experimental runs.

2.3.1.3 Matrix Experiment and Data Collection

After parameter and selection of their levels, the appropriate orthogonal array needs to be selected. Orthogonal array selection is primarily dependent on the number of parameters involved in the experiment. For instance for 6 parameters having 3 levels each L27 orthogonal array is chosen where 27 is number of rows of the orthogonal array or the number of experimental runs. Each parameter resides in a separate column of the orthogonal array.

2.3.1.4 Performance Evaluation

In this step the performance evaluation of the output is made based on the respective changes made in the input or control variables. The performance evaluation is characterized by following regimes based on the nature of interest for output variable.

1. Larger the better

2. Smaller the better

3. Optimal the best

2.4 Radial Basis Collocation Method

In order to overcome the meshing difficulties, various meshless methods have been proposed by researchers [54-60]. Meshless methods hold promise for many applications because of their advantageous features over the conventional methods like FEM or BEM. These methods depend on the point cloud data with no interconnection between the points rendering them more suitable for adaptive mesh refinement. Their point dependency makes them easier to deal with the complex geometries and makes them less sensitive to the dimensionality of the problem. Many meshless methods have been proposed over the course of last two decades which can be broadly classified into two main categories. They are weak formulation and strong formulation depending on the process followed for obtaining the approximate solution of the governing differential equations. Weak formulations like element free Galerkin method (EFGM), method of fundamental solutions (MFS) [61, 62] either require background grid to do the numerical integration of the weak form

or need to solve Helmholtz equations which makes them computationally expensive. Strong methods like radial basis collocation method (RBCM) [63, 64] deal with the original governing differential equations and point collocation is used to satisfy the governing equations in the domain and on the boundary. Strong form meshless methods are 'truly meshless' because they don't require mesh in any form. Multiquadratics are positive definite radial basis functions (RBFs) and have global support. Kansa et al. [65] first used multiquadratics RBFs for the solution of partial differential equations and since then there have been many developments on the properties and application of RBFs [57, 61, 62, 64, 66-70].

2.4.1 Theory of Radial Basis Collocation Method (RBCM) on 2D Heterogeneous Problem

Strong form collocation methods are a form of meshless methods which don't require numerical mesh to solve a problem and no preconditioning is required for the original equations describing a particular phenomenon. They are in strong form as they deal with the original equations describing the phenomenon. For the solution approximation different global RBFs are used. For this research, RBFs known as inverse multi-quadratics will be used. For general description of RBCM, let's consider a problem consisting of open domain Ω and boundary $\partial\Omega$.

The problem can be defined as:

$$\mathbf{L}^{\tau}\mathbf{T}^{\tau} = \mathbf{f}^{\tau} \quad \text{in} \quad \Omega \tag{2.23}$$

$$\mathbf{B}^{\tau}\mathbf{T}^{\tau} = \mathbf{q}^{\tau} \quad \text{on} \quad \partial\Omega$$

Here $\mathbf{T}^{\tau}$ represents the local static temperature, $\mathbf{L}^{\tau}$ denotes the differential operator in Ω, $\mathbf{B}^{\tau}$ is the boundary condition operator. $\mathbf{f}^{\tau}$ is the source term in the open domain whereas $\mathbf{q}^{\tau}$ is related to boundary conditions. τ represents the domain number.

Let $\partial\Omega_g, \partial\Omega_h$ represent the Dirichlet and Neumann boundaries respectively then,

$\mathbf{B}^{\tau}\mathbf{T}^{\tau} = \mathbf{g}^{\tau}$ on Dirichlet boundary (2.24)

$\mathbf{B}^{\tau}\mathbf{T}^{\tau} = \mathbf{h}^{\tau}$ on Neumann boundary

Let's consider a general 2D problem consisting of two homogeneous materials. Strong heterogeneity of material properties is encountered at the interface between the two materials. The two domains are connected by an interface as shown in Figure 2.8.

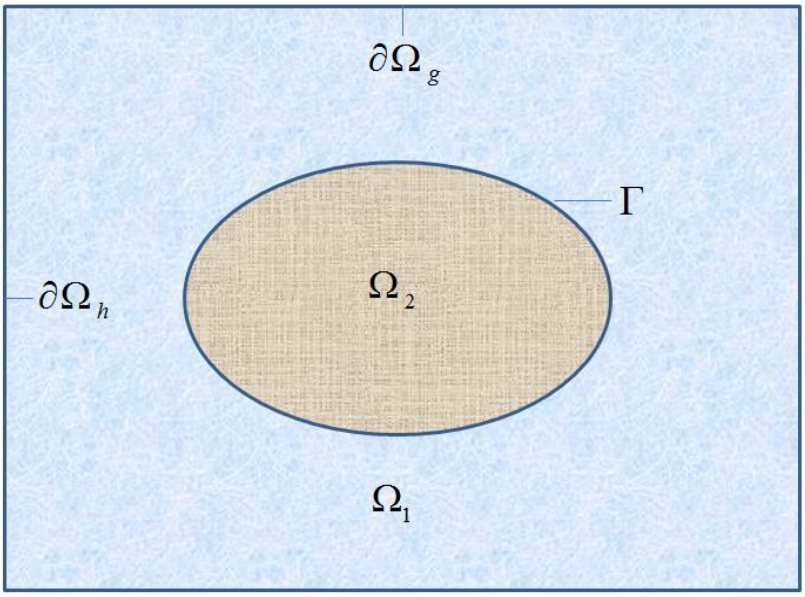

Figure 2.8: Heterogeneous domain problem

For domain 1, Ω^1 :

$$\left.\begin{aligned} \mathbf{L^1T^1} &= \mathbf{f^1} \ \ \mathbf{in} \ \ \boldsymbol{\Omega^1} \\ \mathbf{B_g^1T^1} &= \mathbf{g^1} \ \mathbf{in} \ \ \partial\boldsymbol{\Omega^1} \cap \partial\boldsymbol{\Omega_g} \\ \mathbf{B_h^1T^1} &= \mathbf{h^1} \ \mathbf{in} \ \ \partial\boldsymbol{\Omega^1} \cap \partial\boldsymbol{\Omega_h} \end{aligned}\right\} \tag{2.25}$$

For domain 2, Ω^2 :

$$\left.\begin{aligned} \mathbf{L^2T^2} &= \mathbf{f^2} \ \ \mathbf{in} \ \ \boldsymbol{\Omega^2} \\ \mathbf{B_g^2T^2} &= \mathbf{g^2} \ \mathbf{in} \ \ \partial\boldsymbol{\Omega^2} \cap \partial\boldsymbol{\Omega_g} \\ \mathbf{B_h^2T^2} &= \mathbf{h^2} \ \mathbf{in} \ \ \partial\boldsymbol{\Omega^2} \cap \partial\boldsymbol{\Omega_h} \end{aligned}\right\} \tag{2.26}$$

For Interface Γ :

$$\left.\begin{aligned} \mathbf{T^1 - T^2} &= \mathbf{0} \\ \mathbf{B_h^1T^1 + B_h^2T^2} &= \mathbf{0} \end{aligned}\right\} \tag{2.27}$$

The temperature solution $\tilde{\mathbf{T}}_\mathbf{i}^1$ is calculated separately in each subdomain and can be approximated by evaluating RBFs at collocation points i.e.,

$$\tilde{\mathbf{T}}_\mathbf{i}(\mathbf{x}) = \left\{\begin{aligned} \tilde{\mathbf{T}}_\mathbf{i}^1(\mathbf{x}) &= \mathbf{g}_\mathbf{1}^1(\mathbf{x})\mathbf{a}_{\mathbf{i1}}^1 + \mathbf{g}_\mathbf{2}^1(\mathbf{x})\mathbf{a}_{\mathbf{i2}}^1 + \mathbf{....g}_{\mathbf{N_s^1}}^1(\mathbf{x})\mathbf{a}_{\mathbf{iN_s^1}}^1, \mathbf{x} \in \overline{\boldsymbol{\Omega}}^\mathbf{1} \\ \tilde{\mathbf{T}}_\mathbf{i}^2(\mathbf{x}) &= \mathbf{g}_\mathbf{1}^2(\mathbf{x})\mathbf{a}_{\mathbf{i1}}^2 + \mathbf{g}_\mathbf{2}^2(\mathbf{x})\mathbf{a}_{\mathbf{i2}}^2 + \mathbf{....g}_{\mathbf{N_s^2}}^2(\mathbf{x})\mathbf{a}_{\mathbf{iN_s^2}}^2, \mathbf{x} \in \overline{\boldsymbol{\Omega}}^\mathbf{2} \end{aligned}\right\} \tag{2.28}$$

In Equation (2.28) coefficients $\mathbf{a}_{\mathbf{jI}}$ need to be evaluated at all the collocation points in order to obtain the solution where I contains the source points whereas j represents the collocation point in respective domain. Substituting Equation (2.28) into Equations (2.25)-(2.27), results in an algebraic system of equations which can be easily solved for the coefficients.

For numerical implementation of RBCM, the following steps are involved.

2.4.1.1 Identification of Collocation Points

For ease of implementation, unique set of points in domains, boundaries and interface are identified for each domain. Let τ represent the heterogeneity, $\mathbf{P}^{\tau}$ be the set of collocation points **p** inside the domain, $\mathbf{Q}^{\tau}$ be the set of collocation points **q** on the Dirichlet boundary and $\mathbf{R}^{\tau}$ be the set of collocation points **r** on the Neumann boundary respectively. $\mathbf{S}$ represents the collocation points **s** on the interface.

$$\left.\begin{aligned}
&\mathbf{P}^{\tau} = \left\{(\mathbf{p}_1^{\tau}, \mathbf{p}_{2,\ldots\ldots\ldots}^{\tau}\mathbf{p}_{N_p^{\tau}}^{\tau})\right\} \subseteq \boldsymbol{\Omega}^{\tau},\\
&\mathbf{Q}^{\tau} = \left\{(\mathbf{q}_1^{\tau}, \mathbf{q}_{2,\ldots\ldots\ldots}^{\tau}\mathbf{q}_{N_q^{\tau}}^{\tau})\right\} \subseteq \partial\boldsymbol{\Omega}^{\tau} \cap \partial\boldsymbol{\Omega}_{\mathbf{g}}\\
&\mathbf{R}^{\tau} = \left\{(\mathbf{r}_1^{\tau}, \mathbf{r}_{2,\ldots\ldots\ldots}^{\tau}\mathbf{r}_{N_r^{\tau}}^{\tau})\right\} \subseteq \partial\boldsymbol{\Omega}^{\tau} \cap \partial\boldsymbol{\Omega}_{\mathbf{h}},\\
&\mathbf{S} = \left\{(\mathbf{s}_1, \mathbf{s}_2, \ldots\ldots\mathbf{s}_{N_\tau})\right\} \subseteq \boldsymbol{\Gamma}
\end{aligned}\right\} \qquad (2.29)$$

2.4.1.2 Approximation Function

The next step is to use the approximation function to find the solution. Let $\tilde{\mathbf{T}}^{\tau}$ be the approximate solution being sought, then:

$$\tilde{\mathbf{T}}^{\tau} = \Phi^{\tau^{\mathrm{T}}}\mathbf{a}^{\tau} \qquad (2.30)$$

where

$$\left.\begin{aligned}
&\boldsymbol{\Phi}^{\tau^{\mathrm{T}}} = [\mathbf{g}_1^{\tau}, \mathbf{g}_1^{\tau}\ldots\ldots\mathbf{g}_{N_s^{\tau}}^{\tau}],\\
&\mathbf{g}_{\mathbf{I}}^{\tau} = \mathbf{g}_{\mathbf{I}}^{\tau}\mathbf{I},\\
&\mathbf{a}^{\tau} = [\mathbf{a}_1^{\tau}, \mathbf{a}_2^{\tau}\ldots\ldots\mathbf{a}_{N_s^{\tau}}^{\tau}], \mathbf{a}_{\mathbf{I}}^{\tau} = [\mathbf{a}_{1\mathbf{I}}^{\tau}, \mathbf{a}_{2\mathbf{I}}^{\tau}, \mathbf{a}_{3\mathbf{I}}^{\tau}]^{\mathrm{T}}
\end{aligned}\right\} \qquad (2.31)$$

$\mathbf{g}_\mathbf{I}^\tau$ is the RBF with source point $\mathbf{x}_\mathbf{I}^\tau$ and $\mathbf{I}$ is the identity matrix and $\mathbf{a}_\mathbf{I}^\tau$ is the coefficient matrix required to obtain the solution (superscript T represents transpose). For inverse multiquadratic RBF $\mathbf{g}_\mathbf{I}^\tau$ is given by

$$\mathbf{g_I(x)} = (\mathbf{r_I^2} + \mathbf{sf}^2)^{-1/2}, \quad \mathbf{r_I} = \sqrt{(\mathbf{x} - \mathbf{x_I})^2 + (\mathbf{y} - \mathbf{y_I})^2} \tag{2.32}$$

where $\mathbf{sf}$ is known as the shape factor.

2.4.1.3 RBF Collocation

Next step is to substitute the approximate solution into the original equations. Substituting Equation (2.28) into Equations (2.25)-(2.27) directly and finding the RBF values at all the collocation points in the domain, boundary and interface, Equation (2.25) would result in an over-determined system of discrete equations which can then be solved using method of least squares.

The following system of equations would result where **A** and **b** represent the conductivity and source matrices respectively. Λ is for interface and **a** is the required coefficient matrix as given in Equation (2.30).

$$\mathbf{Aa} := \begin{bmatrix} \mathbf{A}^1 \\ \mathbf{A}^2 \\ \Lambda \end{bmatrix} \mathbf{a} = \begin{bmatrix} \mathbf{b}^1 \\ \mathbf{b}^2 \\ \mathbf{0} \end{bmatrix} =: \mathbf{b} \tag{2.33}$$

The equation system in Equation (2.33) is a global system which consists of the following sub matrices:

$$\mathbf{A}^1 = \begin{bmatrix} \mathbf{A}_L^1 \\ \mathbf{A}_g^1 \\ \mathbf{A}_h^1 \end{bmatrix},\ \mathbf{A}^2 = \begin{bmatrix} \mathbf{A}_L^2 \\ \mathbf{A}_g^2 \\ \mathbf{A}_h^2 \end{bmatrix},\ \mathbf{b}^1 = \begin{bmatrix} \mathbf{b}_L^1 \\ \mathbf{b}_g^1 \\ \mathbf{b}_h^1 \end{bmatrix},\ \mathbf{b}^2 = \begin{bmatrix} \mathbf{b}_L^2 \\ \mathbf{b}_g^2 \\ \mathbf{b}_h^2 \end{bmatrix},\ \mathbf{\Lambda} = \begin{bmatrix} \mathbf{\Lambda}_g \\ \mathbf{\Lambda}_h \end{bmatrix} \tag{2.34}$$

where subscripts **L**, **g** and **h** represent matrices related to domain, Dirichlet and Neumann boundary conditions respectively.

2.4.1.4 Assigning of Weights

Although Equation (2.33) can be solved for coefficients which can be used to find the solution from Equation (2.30) but in strong form collocation, it is imperative to control errors on the material interfaces. This would guarantee exponential convergence of the subdomain RBCM. To accomplish this, the following weights are used as suggested by Hu et al. [71].

$$\sqrt{\omega_g^1} = \sqrt{\omega_g^2} = \sqrt{\overline{\omega}_g} = O(\bar{k}.\bar{N}_s), \sqrt{\omega_h^1} = O(s^1),\ \sqrt{\omega_h^2} = O(s^2),\ \sqrt{\overline{\omega}_h} = O(1) \tag{2.35}$$

where $\bar{k} = \max(k^1, k^2),\ \bar{N}_s = \max(N_s^1, N_s^2),\ s^1 = \dfrac{\bar{k}}{k^1},\ s^2 = \dfrac{\bar{k}}{k^2}$

Introducing the above weights in Equation (2.35), we have

$$\mathbf{A}^1 = \begin{bmatrix} \mathbf{A}_L^1 \\ \sqrt{\omega_g^1}\mathbf{A}_g^1 \\ \sqrt{\omega_h^1}\mathbf{A}_h^1 \end{bmatrix},\ \mathbf{A}^2 = \begin{bmatrix} \mathbf{A}_L^2 \\ \sqrt{\omega_g^2}\mathbf{A}_g^2 \\ \sqrt{\omega_h^2}\mathbf{A}_h^2 \end{bmatrix},$$

$$\mathbf{b}^1 = \begin{bmatrix} \mathbf{b}_L^1 \\ \sqrt{\omega_g^1}\mathbf{b}_g^1 \\ \sqrt{\omega_h^1}\mathbf{b}_h^1 \end{bmatrix},\ \mathbf{b}^2 = \begin{bmatrix} \mathbf{b}_L^2 \\ \sqrt{\omega_g^2}\mathbf{b}_g^2 \\ \sqrt{\omega_h^2}\mathbf{b}_h^2 \end{bmatrix},\ \mathbf{\Lambda} = \begin{bmatrix} \sqrt{\overline{\omega}_g}\mathbf{\Lambda}_g \\ \sqrt{\overline{\omega}_h}\mathbf{\Lambda}_h \end{bmatrix} \tag{2.36}$$

2.4.1.5 Interface Boundary Conditions

Next step will involve the application of proper boundary conditions at the interface. It is shown by Chen et al. [72] that in order to have a continuous solution, both Dirichlet and Neumann boundary conditions need to be enforced at the interface. Otherwise, the errors would grow substantially rendering the solution invalid. The explicit form of the components of matrices in Equation (2.34) is shown below.

$$\mathbf{A}_{\mathbf{L}}^{\mathbf{1}} = \begin{bmatrix} \mathbf{L}^{\mathbf{1}}(\mathbf{\Phi}^{\mathbf{1}^{\mathbf{T}}}(\mathbf{p}_{\mathbf{1}}^{\mathbf{1}})) & \mathbf{0} \\ & \cdot \\ & \cdot \\ \mathbf{L}^{\mathbf{1}}(\mathbf{\Phi}^{\mathbf{1}^{\mathbf{T}}}(\mathbf{p}_{\mathbf{N}_{\mathbf{p}}^{\mathbf{1}}}^{\mathbf{1}})) & \mathbf{0} \end{bmatrix}, \ \mathbf{A}_{\mathbf{L}}^{\mathbf{2}} = \begin{bmatrix} \mathbf{0} & \mathbf{L}^{\mathbf{2}}(\mathbf{\Phi}^{\mathbf{2}^{\mathbf{T}}}(\mathbf{p}_{\mathbf{1}}^{\mathbf{2}})) \\ & \cdot \\ & \cdot \\ \mathbf{0} & \mathbf{L}^{\mathbf{2}}(\mathbf{\Phi}^{\mathbf{2}^{\mathbf{T}}}(\mathbf{p}_{\mathbf{N}_{\mathbf{p}}^{\mathbf{2}}}^{\mathbf{2}})) \end{bmatrix} \tag{2.37}$$

$$\mathbf{A}_{\mathbf{g}}^{\mathbf{1}} = \begin{bmatrix} \mathbf{B}_{\mathbf{g}}^{\mathbf{1}}(\mathbf{\Phi}^{\mathbf{1}^{\mathbf{T}}}(\mathbf{q}_{\mathbf{1}}^{\mathbf{1}})) & \mathbf{0} \\ & \cdot \\ & \cdot \\ \mathbf{B}_{\mathbf{g}}^{\mathbf{1}}(\mathbf{\Phi}^{\mathbf{1}^{\mathbf{T}}}(\mathbf{q}_{\mathbf{N}_{\mathbf{q}}^{\mathbf{1}}}^{\mathbf{1}})) & \mathbf{0} \end{bmatrix}, \ \mathbf{A}_{\mathbf{g}}^{\mathbf{2}} = \begin{bmatrix} \mathbf{0} & \mathbf{B}_{\mathbf{g}}^{\mathbf{2}}(\mathbf{\Phi}^{\mathbf{2}^{\mathbf{T}}}(\mathbf{q}_{\mathbf{1}}^{\mathbf{2}})) \\ & \cdot \\ & \cdot \\ \mathbf{0} & \mathbf{B}_{\mathbf{g}}^{\mathbf{2}}(\mathbf{\Phi}^{\mathbf{2}^{\mathbf{T}}}(\mathbf{q}_{\mathbf{N}_{\mathbf{q}}^{\mathbf{2}}}^{\mathbf{2}})) \end{bmatrix} \tag{2.38}$$

$$\mathbf{A}_{\mathbf{h}}^{\mathbf{1}} = \begin{bmatrix} \mathbf{B}_{\mathbf{h}}^{\mathbf{1}}(\mathbf{\Phi}^{\mathbf{1}^{\mathbf{T}}}(\mathbf{r}_{\mathbf{1}}^{\mathbf{1}})) & \mathbf{0} \\ & \cdot \\ & \cdot \\ \mathbf{B}_{\mathbf{h}}^{\mathbf{1}}(\mathbf{\Phi}^{\mathbf{1}^{\mathbf{T}}}(\mathbf{r}_{\mathbf{N}_{\mathbf{r}}^{\mathbf{1}}}^{\mathbf{1}})) & \mathbf{0} \end{bmatrix}, \ \mathbf{A}_{\mathbf{h}}^{\mathbf{2}} = \begin{bmatrix} \mathbf{0} & \mathbf{B}_{\mathbf{h}}^{\mathbf{2}}(\mathbf{\Phi}^{\mathbf{2}^{\mathbf{T}}}(\mathbf{r}_{\mathbf{1}}^{\mathbf{2}})) \\ & \cdot \\ & \cdot \\ \mathbf{0} & \mathbf{B}_{\mathbf{h}}^{\mathbf{2}}(\mathbf{\Phi}^{\mathbf{2}^{\mathbf{T}}}(\mathbf{r}_{\mathbf{N}_{\mathbf{r}}^{\mathbf{2}}}^{\mathbf{2}})) \end{bmatrix} \tag{2.39}$$

$$\mathbf{\Lambda}_{\mathbf{g}} = \begin{bmatrix} \mathbf{\Phi}^{\mathbf{1}^{\mathbf{T}}}(\mathbf{s}_{\mathbf{1}}) & -\mathbf{\Phi}^{\mathbf{2}^{\mathbf{T}}}(\mathbf{s}_{\mathbf{1}}) \\ & \cdot \\ & \cdot \\ \mathbf{\Phi}^{\mathbf{1}^{\mathbf{T}}}(\mathbf{s}_{\mathbf{N}_{\mathbf{s}}}) & -\mathbf{\Phi}^{\mathbf{2}^{\mathbf{T}}}(\mathbf{s}_{\mathbf{N}_{\mathbf{s}}}) \end{bmatrix} \tag{2.40}$$

$$\Lambda_h = \begin{bmatrix} B_h^1(\Phi^{1^T}(s_1)) & B_h^2(\Phi^{2^T}(s_1)) \\ \vdots & \\ B_h^1(\Phi^{1^T}(s_{N_s})) & B_h^2(\Phi^{2^T}(s_{N_s})) \end{bmatrix} \quad (2.41)$$

$$b_L^1 = \begin{bmatrix} f(p_1^1) \\ \vdots \\ f(p_{N_p^1}^1) \end{bmatrix}, \; b_L^2 = \begin{bmatrix} f(p_1^2) \\ \vdots \\ f(p_{N_p^2}^2) \end{bmatrix} \quad (2.42)$$

$$b_g^1 = \begin{bmatrix} g(q_1^1) \\ \vdots \\ g(q_{N_q^1}^1) \end{bmatrix}, \; b_g^2 = \begin{bmatrix} g(q_1^2) \\ \vdots \\ g(q_{N_q^2}^2) \end{bmatrix} \quad (2.43)$$

$$b_h^1 = \begin{bmatrix} h(r_1^1) \\ \vdots \\ h(r_{N_r^1}^1) \end{bmatrix}, \quad b_h^2 = \begin{bmatrix} h(r_1^2) \\ \vdots \\ h(r_{N_r^2}^2) \end{bmatrix} \quad (2.44)$$

Chapter 3: Parameter Ranking of Capacitive Hyperthermia Using Taguchi Analysis

3.1 Preamble

The basic purpose of the hyperthermia treatment is to raise the tumour temperature above tolerable limits without causing thermal damage to the surrounding healthy tissue. A slight discrepancy in temperature control mechanism could result in irreversible thermal damage to the patient which in the worst case scenario can also cause death.

The motivation behind this research is to rank the parameters that affect the temperature inside the biological tissue. For electromagnetic heating, the maximum achieved temperature depends on the electric field strength inside the biological material. The electric field generated inside the biological material can be calculated using Maxwell's equations. Furthermore, if the wavelength of the radiation is much larger than the size of the object, quasi-static approximation can be used. The electric field strength inside the tissue in a Cartesian domain *X,* can be obtained by evaluating the scalar potential inside the tissue [13, 73] i.e.,

$$-\nabla.\left[(\sigma + j\omega\varepsilon)\nabla\varphi(X)\right] = 0 \tag{3.1}$$

where σ and ε represent electrical conductivity and dielectric permittivity of the material whereas ω is the angular frequency.

Electric field strength E can be evaluated by finding the negative gradient of scalar potential in the tissue $\varphi(\mathrm{X})$.

$$\mathrm{E}(\mathrm{X}) = -\nabla\varphi(\mathrm{X}) \tag{3.2}$$

The electric energy induced in the tissue dissipates in the form of heat. The volumetric generation of heat due to electric field inside the tissue is given by:

$$\begin{aligned} \mathrm{Q_r}(\mathrm{X},\mathrm{t}) &= \frac{\sigma\left|\mathrm{E}(\mathrm{X})\right|^2}{2} \\ &= \frac{\sigma\left[\left|\mathrm{E_x}\right|^2 + \left|\mathrm{E_y}\right|^2 + \left|\mathrm{E_z}\right|^2\right]}{2} \end{aligned} \tag{3.3}$$

It can be seen that the volumetric heat generated in the tissue due to electric field depends on the electrical conductivity σ and electric field strength E inside the tissue.

Electromagnetic heating in the tissue represents an electro-thermal problem. For computation of temperature field in the tissue many thermal models have been proposed [20, 74, 75] but Pennes bioheat model [12] is the most popular one because of its simplicity, ease of application and effectiveness in most cases. Pennes model has been used by many researchers for the heat transfer in biological materials [13-15, 20, 73, 76-78].

The heat transfer inside the tissue can be represented by Pennes Equation:

$$\rho c\frac{\partial \mathrm{T}(\mathrm{X},\mathrm{t})}{\partial \mathrm{t}} = \nabla.\left[\mathrm{k}(\mathrm{X})\nabla\mathrm{T}(\mathrm{X},\mathrm{t})\right] + \rho_b\omega_b c_b\left[\mathrm{T_a} - \mathrm{T}(\mathrm{X},\mathrm{t})\right] + \mathrm{Q}(\mathrm{X},\mathrm{t}) \qquad \mathrm{X} \in \Omega \tag{3.4}$$

As the temperature reaches steady state, the left hand side of the equation containing the transient term vanishes. The temperature of the body is maintained by the metabolic heat generated in the body. The effect of metabolic heat also needs to be considered. In Pennes equation, this effect is accommodated in $Q(X,t)$ which includes the heat generated by external electromagnetic field $Q_r(X,t)$ and metabolic heat $Q_{met}(X,t)$ generated by natural mechanisms of the body. The solution of the system of equations resulting from the application of Pennes bioheat equation in tissue and tumour would result in accurate information about the temperature inside the biological material.

Pennes model is based on the classical Fourier law which assumes that thermal disturbance travels at an infinite speed and small disturbance is felt instantaneously in the body. To incorporate this, non-Fourier models which assume finite propagation speed of thermal disturbance were also presented [20, 21]. Non-Fourier phenomenon has been observed in processes involving very low temperatures, or processes where large amount of energy is deposited in short time scales like laser heating and materials with large heterogeneities neither of which is relevant here. In this context, Pennes bioheat model based on the classical Fourier law is sufficient for this research.

For biological tissues metabolic heat is vital for survival. The energy required for replenishment is generated by the oxidation of the nutrients supplied to the biological tissues. Any decrease in metabolic heat would mean an increase in the input energy to attain hyperthermia and vice versa. Blood perfusion is also an important parameter which is responsible for transfer of energy via convection.

During the electrode based thermal therapy if blood perfusion is increased, it could flush away the supplied energy. Furthermore, the blood escaping out of the treatment zone could cause collateral damage to the peripheral normal tissue and would make it difficult to achieve hyperthermic conditions.

Frequency and applied voltage are also critical to the electrode based thermal therapy as they affect the electromagnetic energy being delivered to the treatment zone. A higher voltage would mean an increased energy input and changes in frequency would result in changes in electrical conductivity and permittivity of the biological material which in turn also affects the heat being delivered as can be seen from Equation (3.3). For hyperthermia treatment different frequencies can be utilized depending on the nature of the problem. The nature of interaction with the material is dependent on the frequency being used. It has been noted that penetration depth and the amount of energy delivered are strong functions of frequency [8, 15, 79, 80]. Varying frequency results in a corresponding change in the electrical conductivity and dielectric properties of the material. Table 3.1 lists the electromagnetic properties of the skin tissue at different frequencies.

Table 3.1: Frequency dependent electromagnetic characteristics of skin tissue [81]

Frequency f (MHz)	Electrical Conductivity σ_1 [S/m]	Dielectric constant ε_1 [$C^2/N.m^2$]
0.001	0.102	$100000\,\varepsilon_0$
0.01	0.114	$50000\,\varepsilon_0$
0.1	0.192	$20000\,\varepsilon_0$
1	0.40	$2000\,\varepsilon_0$
10	0.625	$100\,\varepsilon_0$

where ε_0 is the dielectric constant of the vacuum with $\varepsilon_0 = 0.8538\times10^{-12}$ $C^2/N.m^2$

3.2 Parameters Selection and Ranking Methodology

For current study 6 parameters each having 3 parameters were selected as shown in Table 3.2. The six parameters are: Tissue metabolic rate, tumour metabolic rate, tissue blood perfusion rate, tumour blood perfusion rate, frequency and applied voltage. Each parameter has 3 levels which ensure more comprehensive analysis and utilize larger parametric space. These levels considered are named as low, medium and high respectively. Values at these levels are chosen based on the variation as reported in literature. To obtain reliable results with less number of experiments, Taguchi's orthogonal array can be utilized which possesses fractional factorial characteristics. For this study standard L27 orthogonal array was utilized.

Table 3.2: Parameters with corresponding levels used for ranking analysis

Factor	Units	Level 1(low)	Level 2(medium)	Level 3(high)
Tissue metabolic rate (Q_{met1})	(W/m^3)	800 [12]	1200 [12]	4200 [13]
Tumour metabolic heat source (Q_{met2})	(W/m^3)	700 [82]	42000 [13]	65400 [82]
Tissue blood perfusion rate (ω_{b1})	(1/s)	0.0002 [83]	0.00035 [83]	0.00057 [83]
Tumour blood perfusion rate (ω_{b2})	(1/s)	0.002 [84]	0.007 [83]	0.015 [83]
Frequency (f)	(MHz)	0.1 [73]	1 [73]	10 [73]
Voltage (V)	(V)	5 [13]	10 [13]	15 [13]

3.3 Development of Numerical Model for Hyperthermia Therapy

For this research a numerical model based on finite element method (FEM) was implemented in COMSOL. In order to establish the nature of the effect of each parameter, first the applicability of FEM to obtain desired results needs to be proven. The FEM results were benchmarked against a previous study which acquired solution of the 3D problem utilizing Monte Carlo method [13]. The nature of interaction between the results can only be trusted once the suitability of FEM for carrying out such simulations is established. The geometry of the problem used is shown in Figure 3.1.

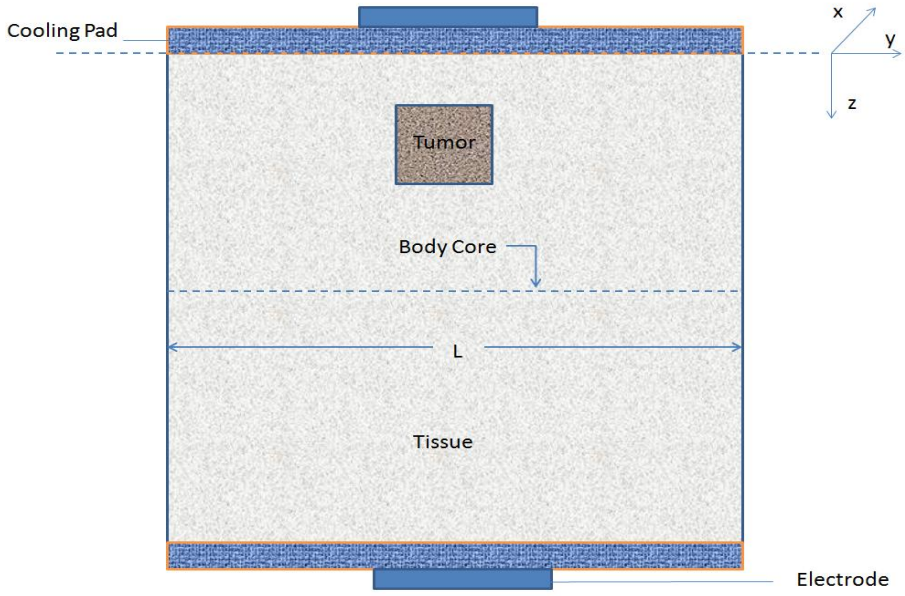

Figure 3.1: 3D hyperthermia system with cooling pads [13]

The numerical domain consists of 0.08 m × 0.8 m × 0.08 m and the heating area is given as:

$$\Omega' \subseteq \left[\mathrm{x} = 0.0, 0.03\,m \le \mathrm{y} \le 0.05\,m, 0.03 \le \mathrm{z} \le 0.05\,m\right] \cup$$
$$\left[\mathrm{x} = 0.016\,m,\ 0.03\,m \le \mathrm{y} \le 0.05\,m,\ 0.03 \le \mathrm{z} \le 0.05\,m\right]$$

The tumour domain is given by:

$$\Omega_2 \subseteq \left[0.02\,m \le \mathrm{x} \le 0.04\,m,\ 0.03 \le \mathrm{y} \le 0.05\,m,\ 0.03 \le \mathrm{z} \le 0.05\,m\right]$$

For steady state the heat transfer inside the tissue can be represented by Pennes Equation:

$$\nabla.\left[\mathrm{k_e}(\mathrm{X})\nabla \mathrm{T_e}(X)\right] + \rho_\mathrm{b}\omega_\mathrm{be}\mathrm{c_b}\left[\mathrm{T_a} - \mathrm{T_e}(X)\right] + \mathrm{Q_e}(X) = 0 \quad X \in \Omega_\mathrm{e} \tag{3.5}$$

Subscript e=1, refers to normal tissue and e=2 refers to tumour.

Cooling pads are often used in the capacitive hyperthermia to prevent overheating of the tissue as shown in Figure 3.1. Cooling pads can be represented by a convection boundary condition on the surface. Body core temperature is assumed in the middle of the domain and thermal insulation boundary condition is applied on the remaining boundaries. Similarly, the electrical and thermophysical properties were taken from Deng et al. [13].

The boundary conditions applied are:

$$\begin{cases} -\mathrm{k}_1 \dfrac{\partial \mathrm{T}_1}{\partial \mathrm{x}} = 0 & x = 0, L \\ -\mathrm{k}_1 \dfrac{\partial \mathrm{T}_1}{\partial \mathrm{y}} = 0 & y = 0, L \\ -\mathrm{k}_1 \dfrac{\partial \mathrm{T}_1}{\partial \mathrm{z}} = \mathrm{h}_\mathrm{w} (\mathrm{T}_1 - \mathrm{T}_\mathrm{w}) & z = 0 \\ \mathrm{T}_1 = \mathrm{T}_\mathrm{o} & z = L \end{cases} \tag{3.6}$$

where h_w is the convective coefficient of the cooling water and T_w is the temperature of the cooling water. T_0 represents body core temperature.

For the 3D analysis, following thermal properties were used.

$\rho_b = 1000\, kg/m^3,\ c_b = 4200\, J/kg.K,$

$T_a = 37\ ^oC,\ k = 0.5\, W/m.^oC,\ L = 0.08\, m,$

$h_w = 100\, W/m^2.^oC,\ T_w = 10^oC.$

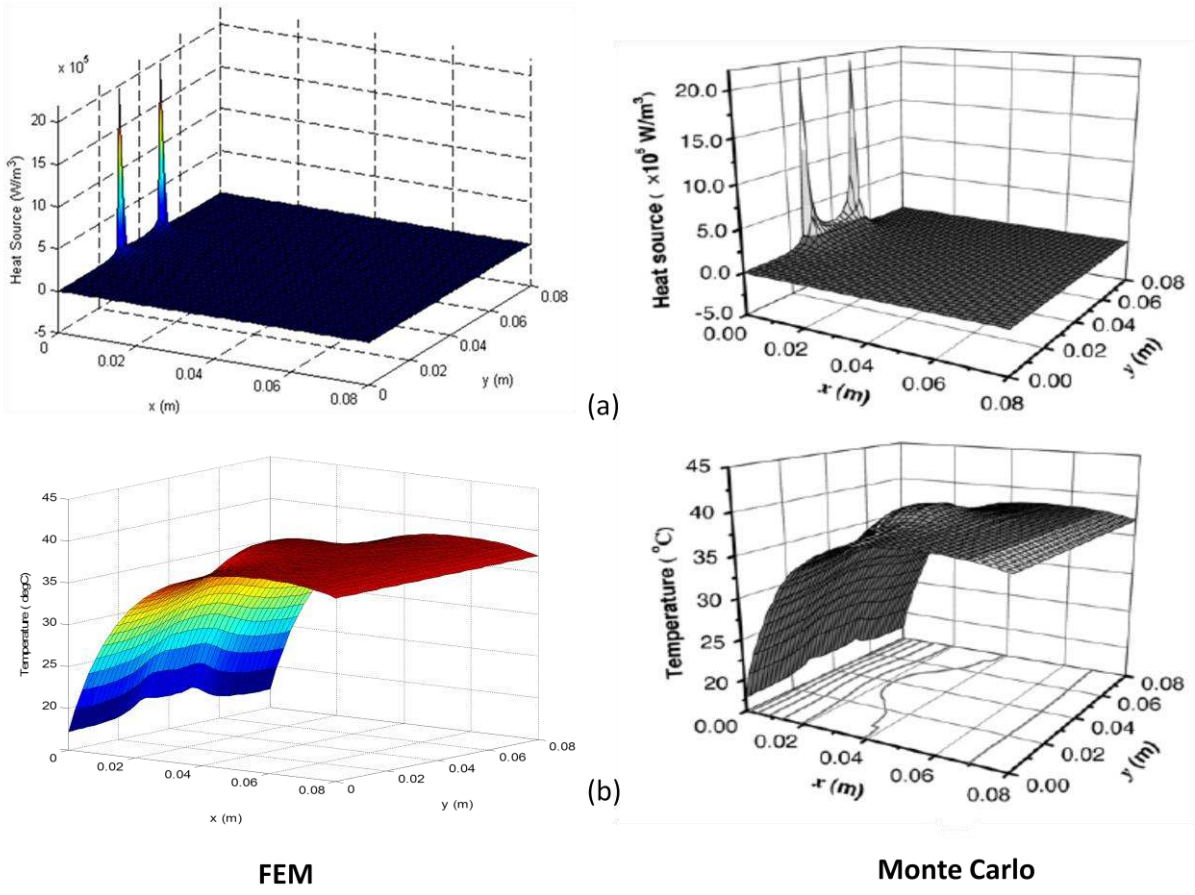

Figure 3.2: 3D Comparison of steady state heat Source (a) and temperature (b) at section z=0.04m for f=1 MHz, U=10 V

As can be seen from Figure 3.2, the results obtained using FEM and Monte Carlo method [13] are very similar and have the same profiles of heat source and temperature for the same treatment conditions. It can also be deduced that the results obtained by FEM are reliable and such bioheat applications involving electromagnetic heating can be successfully simulated using FEM.

As a number of experiments need to be undertaken for this study, which would take longer time to complete, a 2-D analysis is sufficient for this study keeping in view the scope of this study. A 2-D study allows quick acquisition of data needed to perform the Taguchi analysis with milder restrictions on computational resources and memory

requirements. As the tumour in reality is three dimensional in nature, it still needs to be tested whether the 2-D simulation using FEM is sufficient or not. In order to use 2-D configuration, first the results must be validated against some previous study. For two dimensional analysis model used by Ewa et al. [73] was utilized as a benchmark for the current study. Ewa used boundary element method (BEM) to simulate the problem as shown in the Figure 3.3.

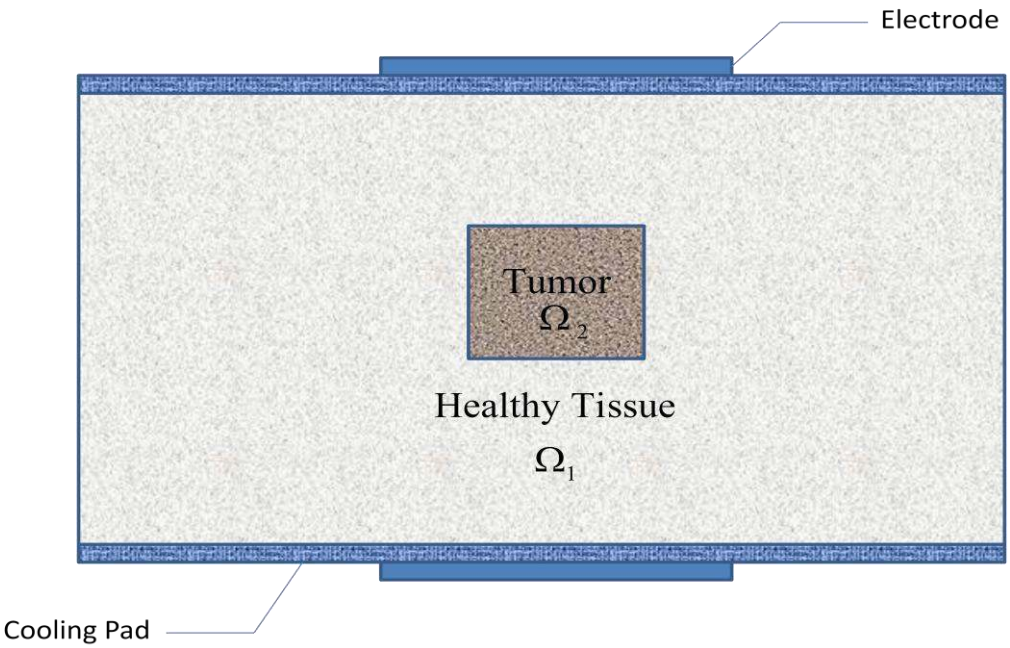

Figure 3.3: Two dimensional hyperthermia system used for analysis [73]

At the interface of healthy tissue and tumour continuity of electric flux and electric potential was assumed. A specified potential U was applied across the electrodes shown in Figure 3.3 while all other boundaries were assumed to be insulated. The computational domain shown in Figure 3.4 is subject to following boundary conditions.

At the interface of skin and tumour, continuity of electric flux and potential is assumed.

$$(x,y)\in\Gamma_c:\begin{cases}\varphi_1(x,y)=\varphi_2(x,y)\\ -\varepsilon_1\dfrac{\partial\varphi_1(x,y)}{\partial n}=-\varepsilon_2\dfrac{\partial\varphi_2(x,y)}{\partial n}\end{cases} \tag{3.7}$$

Electrical potential U is applied across the electrode surfaces.

$$\begin{aligned}&(x,y)\in\Gamma_2:\ \varphi_1(x,y)=U\\ &(x,y)\in\Gamma_5:\ \varphi_2(x,y)=-U\end{aligned} \tag{3.8}$$

Electrical insulation is assumed on all other boundaries i.e.,

$$(x,y)\in\Gamma_1\cup\Gamma_3\cup\Gamma_4\cup\Gamma_6\cup\Gamma_7\cup\Gamma_8:$$

$$-\varepsilon_1\frac{\partial\varphi_1(x,y)}{\partial n}=0 \tag{3.9}$$

This assumption is valid for the surface of the tissue since conductivity of the air or that of the cooling pad filled with distilled water is very low and normal component of electric field at the surface will indeed be negligible. It is also assumed that the side boundaries are far enough and electric field does not penetrate the side boundaries. It is a relevant assumption because the electric field lines start and end at the electrodes.

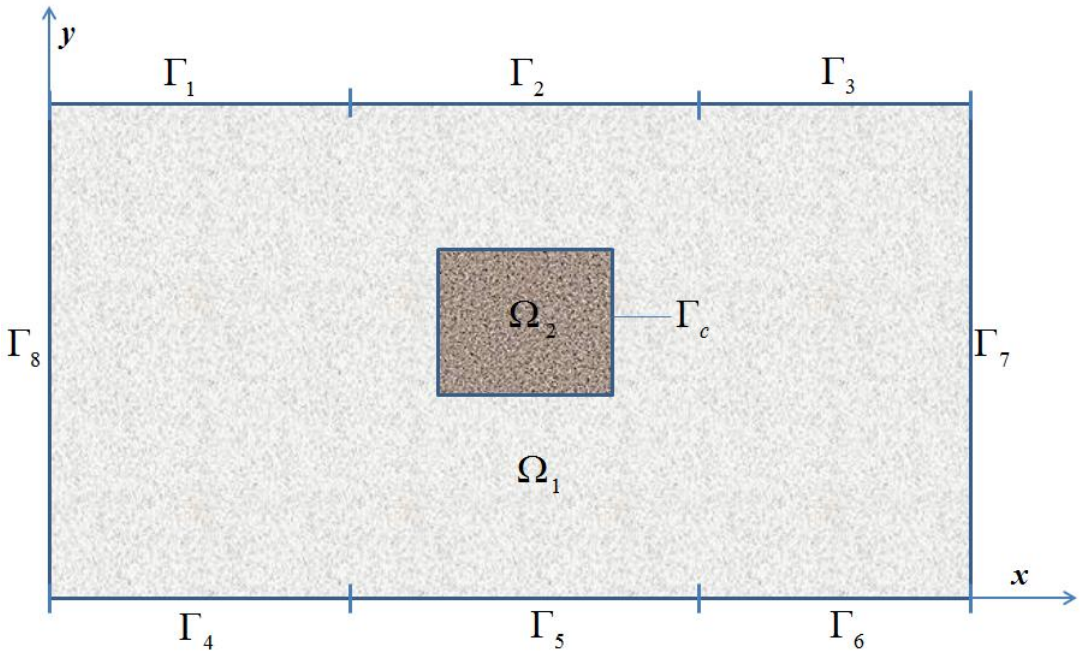

Figure 3.4: Numerical domain with boundary conditions [73]

The bioheat transfer in the specified domain can be described by the Pennes bioheat equation [12]:

$$(x,y)\in\Omega_e : k_e\nabla^2 T_e(x,y)+\rho_b\omega_{be}c_b\left[T_a-T_e(x,y)\right]+Q_e(x,y)=0 \qquad (3.10)$$

And assuming continuity of temperature and heat flux across the interface between healthy tissue and tumour, the boundary conditions are:

$$(x,y)\in\Gamma_c : \begin{cases} T_1(x,y)=T_2(x,y) \\ -k_1\dfrac{\partial T_1(x,y)}{\partial n}=-k_2\dfrac{\partial T_2(x,y)}{\partial n} \end{cases} \qquad (3.11)$$

Negative sign above shows that heat flow is in towards temperature gradient. On far away boundaries (i.e. $\Gamma_7\cup\Gamma_8$) electrical insulation was assumed.

In flat plate electrodes there is a tendency of concentration of electric field near the edges of the electrodes. As a result the tissue near the edges tends to heat up more.

To overcome this problem, cooling pads are used between the electrodes and the tissue. They are useful in preventing the overheating and also help in enhancing the electromagnetic coupling. The thickness and size of the cooling pads varies but pads of thickness 5-10 mm have been used [85]. They are filled with distilled water and enclosed in a thin sheet of PVC. In this study the electrodes were not explicitly modelled rather their effect was quantified by using the proper boundary condition. The effect of cooling pads can be incorporated by using either convective boundary condition [13] between the surface and cooling pad or applying Dirichlet boundary condition [73, 86]. In this study convective boundary condition was applied on the upper and lower surface of the domain to quantify the effect of cooling pads i.e.,

$(x,y) \in \Gamma_1 \cup \Gamma_2 \cup \Gamma_3 \cup \Gamma_4 \cup \Gamma_5 \cup \Gamma_6$ **:**

$$-k_1 \frac{\partial T_1(x,y)}{\partial n} = h_w \left[T_1(x,y) - T_w \right] \tag{3.12}$$

Thermal insulation boundary condition is used on all other boundaries based on the assumption that the side boundaries are far enough so that they are not affected by the temperature field in the middle of the domain [13]. Furthermore, it has been reported that in some situations imposing Dirichlet boundary condition at the distant boundaries may cause numerical simulations to diverge [87].

Frequency has significant effect on the electromagnetic properties of the material. Depending on the frequency being used, EM properties change significantly. Electromagnetic properties used for healthy tissue and tumour are shown in Table 3.3 below.

Table 3.3: Electromagnetic properties used for tissue and tumor domain [73]

S.No	Frequency f (MHz)	Dielectric permittivity [F/m]		Electrical conductivity [S/m]	
		ε_1	ε_2	σ_1	σ_2
1	0.1	$20000\,\varepsilon_0$	$1.2\,\varepsilon_1$	0.192	$1.2\,\sigma_1$
2	1	$2000\,\varepsilon_0$	$1.2\,\varepsilon_1$	0.4	$1.2\,\sigma_1$
3	10	$100\,\varepsilon_0$	$1.2\,\varepsilon_1$	0.625	$1.2\,\sigma_1$

In order to obtain reliable results, a mesh independence study was carried out first. The grid consisted of triangular elements and grid size was progressively refined from coarse to fine. Finally grid consisting of 35680 elements was selected for the current analysis. The calculation domain is 0.08 m × 0.04 m. The tumour region spans $\Omega_2 = \left[\, 0.032\,m \le \mathrm{x} \le 0.048\,m,\ 0.016 \le \mathrm{y} \le 0.032\,m \,\right]$ and heating area is described as: $\Omega' = \left[\{\ 0.032\,m \le \mathrm{x} \le 0.048\,m,\ y = 0\ \},\ \{\ 0.032\,m \le \mathrm{x} \le 0.048\,m,\ y = 0.04\,m\ \}\right]$

Figure 3.5 compares the temperature profile obtained from BEM and FEM. It can be seen that both methods give similar results.

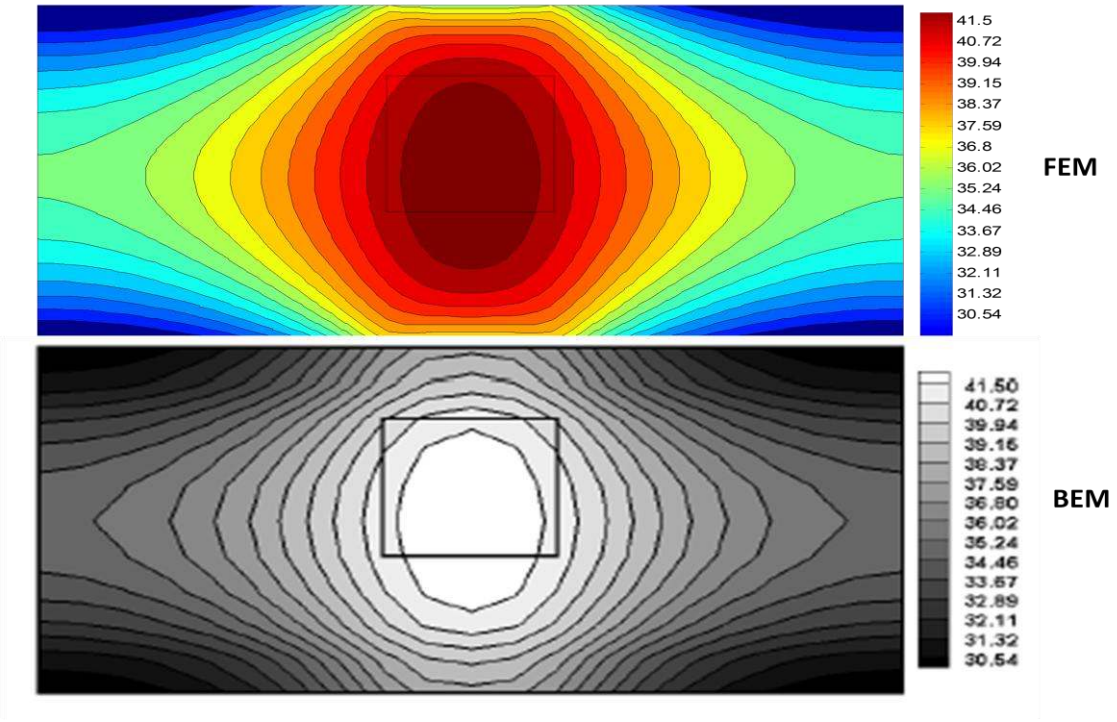

Figure 3.5: Temperature distribution at f=1 MHz and U=10 V

3.4 Numerical Simulation and Data Acquisition for Matrix Experiment

After developing the numerical configuration, Taguchi design of experiment analysis was carried out using Minitab Software [88]. For six parameters having three levels each, standard L-27 orthogonal array was used. For the current analysis, maximum temperature in the domain was chosen as the response variable. Table 3.4 shows the maximum temperature under the influence of varying parameters.

Table 3.4: Taguchi L-27 array with corresponding response values of maximum temperature in the domain [89]

Experiment No.	f (MHz)	V (Volts)	Q_{met1} (W/m^3)	ω_{b1} (1/s)	Q_{met2} (W/m^3)	ω_{b2} (1/s)	Max. Temp. (^oC)
1	0.1	5	800	0.0002	700	0.002	33.307
2	1	10	800	0.0002	700	0.002	40.71
3	10	15	800	0.0002	700	0.002	70.4
4	0.1	5	800	0.00035	42000	0.007	37.229
5	1	10	800	0.00035	42000	0.007	40.484
6	10	15	800	0.00035	42000	0.007	63.305
7	0.1	5	800	0.00057	65400	0.015	37.733
8	1	10	800	0.00057	65400	0.015	39.993
9	10	15	800	0.00057	65400	0.015	59.336
10	0.1	10	1200	0.00035	700	0.015	37.069
11	1	15	1200	0.00035	700	0.015	50.092
12	10	5	1200	0.00035	700	0.015	36.978
13	0.1	10	1200	0.00057	42000	0.002	39.45
14	1	15	1200	0.00057	42000	0.002	52.749
15	10	5	1200	0.00057	42000	0.002	38.929
16	0.1	10	1200	0.0002	65400	0.007	38.683
17	1	15	1200	0.0002	65400	0.007	52.923
18	10	5	1200	0.0002	65400	0.007	38.447
19	0.1	15	4200	0.00057	700	0.007	41.034
20	1	5	4200	0.00057	700	0.007	36.725
21	10	10	4200	0.00057	700	0.007	44.775
22	0.1	15	4200	0.0002	42000	0.015	41.12
23	1	5	4200	0.0002	42000	0.015	37.462
24	10	10	4200	0.0002	42000	0.015	45.388
25	0.1	15	4200	0.00035	65400	0.002	45.074
26	1	5	4200	0.00035	65400	0.002	39.585
27	10	10	4200	0.00035	65400	0.002	49.173

3.5 Results and Discussion

After obtaining the data matrix for L-27 array, Analysis of Variance (ANOVA) was carried out on the data predicted. The main purpose of carrying out ANOVA is to quantify the effect of each of the parameters on the response variable. Details of ANOVA can be found in Refs [90-92]. Results of ANOVA are summarised in Table 3.5.

3.5.1 Quantification of Parameter Influence

Table 3.5 shows the results of ANOVA for the selected parameters.

Table 3.5: ANOVA table for the selected parameters and interactions

Factors	DF	SS	Adj MS	F	P	% Contribution	Ranking
Q_{met1}	2	117.95	58.973	1.52	0.292	6.376	3
Q_{met2}	2	5.4	2.699	0.07	0.934	0.294	5
ω_{b1}	2	4.75	2.373	0.06	0.941	0.252	6
ω_{b2}	2	33.55	16.774	0.43	0.668	1.804	4
f	2	517.07	258.536	6.66	0.03	27.936	2
V	2	1152.12	576.061	14.85	0.005	62.290	1
Q_{met1}×f	4	21.5	5.375	0.14	0.962	0.587	
Q_{met1}×V	4	17.22	4.305	0.11	0.974	0.461	
Residual Error	6	232.83	38.805				
Total	26	2102.38					

Table 3.5 reveals that applied voltage (V) and frequency (f) constitute the major effect on the maximum temperature achieved. Both the parameters account for about 90% of the effect in the response i.e., maximum achievable temperature. Tissue metabolic rate (Q_{met1}) is the third major contributing factor in the response. Furthermore, the selected interactions (Q_{met1}×f, Q_{met1}×V) between the variables are insignificant.

Figure 3.6 shows the main effects plot for Temperature of the six variables selected for Taguchi analysis.

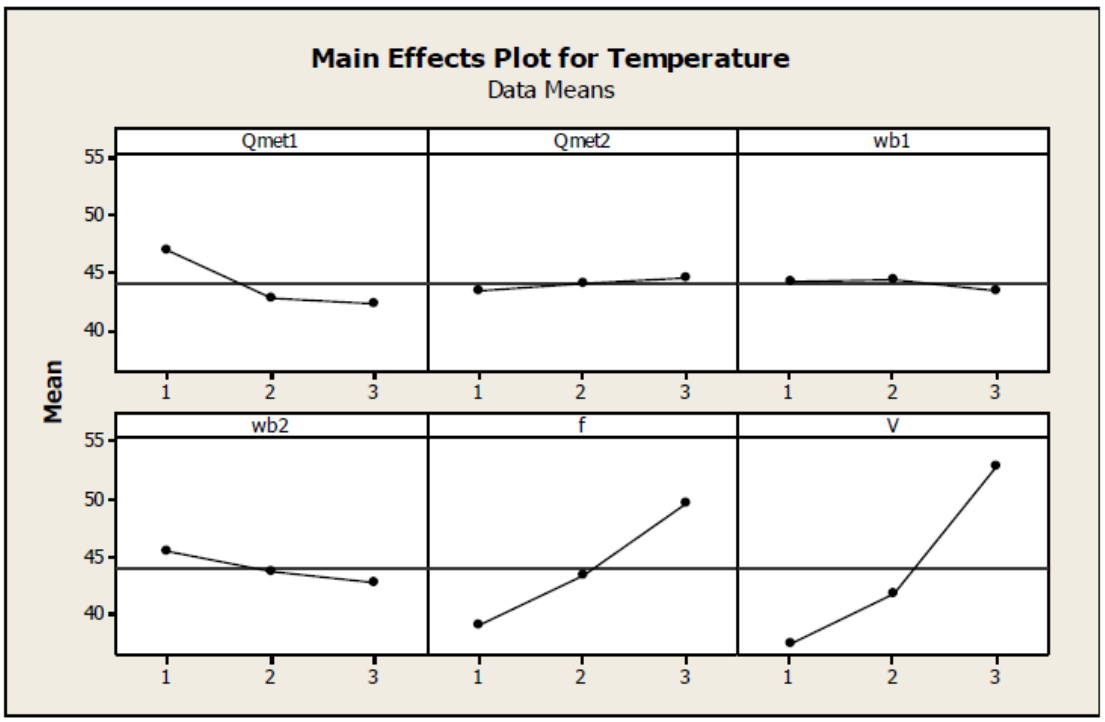

Figure 3.6: Main effects plot for Temperature

Figure 3.6 suggests that the applied voltage (V) and frequency (f) followed by tissue metabolic rate (Qmet1) are the major variables affecting the response. It can also be observed that a linear increase in the input parameters like frequency or voltage doesn't result in corresponding linear increase in temperature. For example, effect of increasing frequency (i.e. 10 times increase) from low to medium is not the same as raising it from medium to high. Although the change intervals are same (Table 3.3) but the corresponding increase in temperature is not the same. This effect can be clearly seen in Figure 3.6 by response having different slopes in each interval.

3.5.2 Optimal Arrangement and Implications

It can be concluded that for the six variables used in analysis each having three levels as shown in Table 3.2, the best arrangement would be to keep Q_{met2}, f and V at high levels and Q_{met1}, ω_{b1} and ω_{b2} at low levels. This also suggests that lower blood perfusion rate would favour a higher achievable temperature. This result can be very

important for proper treatment planning. Tumour is a complex and irregular structure formed by the uncontrolled growth of cells having characteristic behaviour. Most often there is a large vein which supplies blood to the tumour. If before the treatment, that vein is plugged which would cause a reduced supply of blood to the tumour, higher temperature can be achieved with the same treatment arrangement.

Chapter 4: Optimization and Predictive Model for Capacitive Hyperthermia: A Physical Perspective

4.1 Background (Effect of Physical Parameters)

Presently, cancer remains on e of the deadly diseases in the world. There are many treatments that are being used to treat cancer that include chemotherapy, radiation therapy, high intensity focussed ultrasound (HIFU), laser ablation, electroporation and surgery [93-98]. The aim of a treatment is to inflict lethal damage to the cancer cell while shading the normal cells from the harmful effects. Hyperthermia in cancer treatment is a therapeutic procedure in which the temperature of the biological tissue is raised above 42 ^{o}C for certain duration. In therapies like HIFU and laser ablation, the energy can be focussed to a particular area with the help of transducers or lenses. But these therapies suffer from focussing issues due to the presence of bones, air filled viscera and large scattering caused by the hydrated environment. In RFA the energy is delivered at the target site using needle type electrodes. Energy is delivered at high frequencies and can result in charring and carbonization which limits the size of the thermal lesion. In microwave ablation an even higher frequency is used and radiative antennas deliver energy to the target site. Owing to high frequencies used, microwave ablation suffers from limited depth of penetration [23]. Capacitive hyperthermia relies mainly on the heterogeneity of electrical properties and thermal sensitivity of tumour which can be employed to ones advantage for preferential treatment of tumour. In capacitive hyperthermia lower frequencies are

used which also means that higher depth of penetration could be achieved. Simple operation and adjustable position of electrodes favours the heating for various tissues at different angles and sites. Moreover, with different position and customization of electrodes, regional deep heating patterns can be achieved. It can also be used to treat intracavity tumours like cervix, uterus, oropharyngeal and nasopharyngeal cancers.

This research aims to carry out a detailed analysis of the capacitive hyperthermia from a physical perspective. To accomplish this, the geometric dimensions were treated as parameters and were input to the analysis model which subjected these parameters to systematic variation. The primary focus is to quantify the effect of each physical parameter involved that would provide helpful insight for the treatment planning of capacitive hyperthermia. This was accomplished by performing Analysis of Variance (ANOVA) on the data obtained from the experiments. The medical practitioner may need to follow different protocols based on location, orientation or size etc. of the tumour. The obtained results were analyzed with respect to achievement of treatment objective and efficiency of inflicting damage to the tumour. Furthermore, the power delivered to the tissue needs to be regulated. Ideally the heating should only occur in the tumour without causing any harm to the peripheral normal tissue. In practice, certain margin of normal tissue is bound to be destroyed. The extent of this margin depends on many parameters like location, type of tissue and size of the tumour etc. For critical organs such as liver, brain etc., the margin has to be minimal.

4.2 Simulation Setup and Mathematical Modelling for Quantification of Physical and Tunable Parameters

The setup shown in Figure 3.3 and Figure 3.4 for typical capacitive hyperthermia has been used in this study**Error! Reference source not found.** as well with numerical domain of 0.08 m × 0.05 m. For mathematical modelling of coupled electrothermal phenomenon Equations (3.1-3.4) and Equations (3.7-3.12) are still valid for this study. Frequency dependent properties of tissue and tumour as shown previously in Table 3.3 were used. For further details of the capacitive hyperthermia readers are referred to Ref. [99] .

For the current research the following values of the variables were used [13]:

$$k_1 = 0.5\,W/m.K, \quad \omega_{b1} = 0.0005 s^{-1}, \qquad Q_{met1} = 4200\,W/m^3,$$

$$k_2 = 0.6\,W/m.K, \quad \omega_{b2} = 0.002 s^{-1}, \qquad Q_{met2} = 42000\,W/m^3,$$

$$\rho_b = 1000\,kg/m^3, \quad c_b = 4200\,J/kg.K,$$

$$T_a = 37\ ^oC, \quad h_w = 100\,W/m^2.^oC, \quad T_w = 10^oC.$$

4.3 Parameter Selection and Analysis Methodology

By utilizing orthogonal arrays, the number of experiments could be drastically reduced. For 6 factors having 3 levels each, the effect of each parameter can be quantified by utilizing Taguchi's standard L27 array (Table 4.1). For this study, the maximum obtained temperature in the domain was considered as the quality characteristic to be optimized. In this study the physical parameters are scrutinized with respect to their effect on the maximum achievable temperature and thermal damage to the tissue and tumour domain is considered explicitly. Thermal damage is coupled to the respective damage to the tissue or tumour and a detailed two

pronged strategy was formulated and two indices namely treatment index (TI) and damage index (DI) were defined, which were used to analyse the results from the treatment objective point of view and efficiency of tumour killing. This would allow easy acquisition of results owing to less computational resources requirement.

The parameters considered for current analysis are shown in Table 4.2 and Figure 4.1 out of which four are geometric parameters (X_1 to X_4) and two are tunable parameters (X_5 to X_6). The six parameters have three levels each.

Table 4.1 : Data matrix for Taguchi's L27 orthogonal array for physical and tunable parameters

Exp. No.	Side of tumour X1	Position of eletrodes X2	Depth of tumour X3	Size of electrodes X4	Freq. X5	Volt. X6	%age of area damaged Tissue	%age of area damaged Tumour	Tmax	Location of Tmax
1	0.01	-0.02	0.025	0.01	0.1	10	0.00	0.00	32.10	Tumour
2	0.01	-0.02	0.025	0.01	1	15	0.00	0.00	41.09	Normal
3	0.01	-0.02	0.025	0.01	10	20	42.59	56.33	62.04	Normal
4	0.01	0	0.03	0.015	0.1	10	0.00	0.00	33.03	Tumour
5	0.01	0	0.03	0.015	1	15	0.00	0.00	41.07	Normal
6	0.01	0	0.03	0.015	10	20	51.87	100.00	63.68	Normal
7	0.01	0.04	0.035	0.02	0.1	10	0.00	0.00	32.15	Tumour
8	0.01	0.04	0.035	0.02	1	15	0.00	0.00	38.69	Normal
9	0.01	0.04	0.035	0.02	10	20	57.54	100.00	55.79	Normal
10	0.015	-0.02	0.03	0.02	0.1	15	0.00	0.00	37.56	Normal
11	0.015	-0.02	0.03	0.02	1	20	38.73	42.24	59.45	Normal
12	0.015	-0.02	0.03	0.02	10	10	0.00	0.00	41.16	Normal
13	0.015	0	0.035	0.01	0.1	15	0.00	0.00	35.13	Tumour
14	0.015	0	0.035	0.01	1	20	15.79	95.39	47.56	Normal
15	0.015	0	0.035	0.01	10	10	0.00	0.00	36.70	Normal
16	0.015	0.04	0.025	0.015	0.1	15	0.00	0.00	34.61	Tumour
17	0.015	0.04	0.025	0.015	1	20	4.61	0.14	42.99	Normal
18	0.015	0.04	0.025	0.015	10	10	0.00	0.00	35.70	Tumour
19	0.02	-0.02	0.035	0.015	0.1	20	0.00	0.00	41.86	Normal
20	0.02	-0.02	0.035	0.015	1	10	0.00	0.00	36.12	Normal
21	0.02	-0.02	0.035	0.015	10	15	32.56	12.14	51.90	Normal
22	0.02	0	0.025	0.02	0.1	20	0.00	0.00	39.79	Tumour
23	0.02	0	0.025	0.02	1	10	0.00	0.00	36.56	Tumour
24	0.02	0	0.025	0.02	10	15	20.56	100.00	47.25	Normal
25	0.02	0.04	0.03	0.01	0.1	20	0.00	0.00	36.00	Tumour
26	0.02	0.04	0.03	0.01	1	10	0.00	0.00	34.55	tumour
27	0.02	0.04	0.03	0.01	10	15	0.00	0.00	39.54	Normal

Table 4.2: The six independent variables with corresponding levels for effect of physical and tunable parameters

Factor	Units	Level 1(low)	Level 2(medium)	Level 3(high)
Size of the tumour (X_1)	(m)	0.01	0.015	0.02
Rel. position of electrodes (X_2)	(m)	-0.02	0	0.04
Depth of tumour (X_3)	(m)	0.025	0.03	0.035
Size of the electrodes (X_4)	(m)	0.01	0.015	0.02
Frequency (X_5)	(MHz)	0.1	1	10
Voltage (X_6)	(V)	10	15	20

The physical parameters have been varied progressively whereas levels for tunable parameters were taken from Ref [99]. Figure 4.1 labels the parameters considered for analysis.

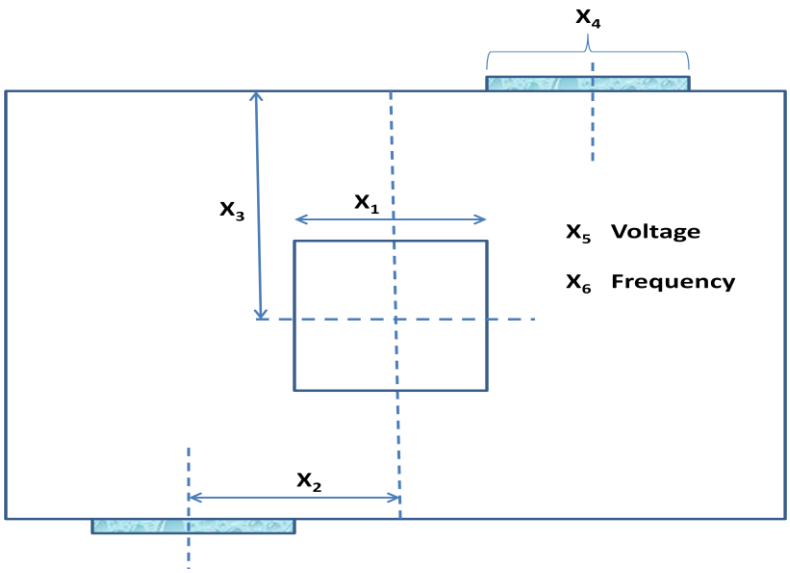

Figure 4.1: Pictorial representation of variables considered for analysis

4.4 Results and Discussion

As stated earlier that the experimental design was carried out using the Taguchi L27 orthogonal array. Experimental matrix was produced and the required data was obtained using the COMSOL multipysics software.

The results obtained from the experimental matrix are shown in Table 4.3. Analysis of Variance (ANOVA) was carried out to categorize each parameter with respect to its effect on the maximum achievable temperature. In Table 4.3, DF is for degrees of freedom, DF is one less than the number of levels. Adjusted mean squares (Adj MS) are the ratio of sum of squares (SS) to degrees of freedom. F-statistic is the ratio of Adj MS of parameter to error and P-value represents the corresponding probability value.

Table 4.3: ANOVA table for L27 orthogonal array with the selected physical and tunable parameters

Factors	DF	SS	Adj MS	F	P	% Contribution	Ranking
X_1	2	80.84	40.42	2.59	0.110	4.139	4
X_2	2	158.74	79.37	5.09	0.022	8.135	3
X_3	2	11.50	5.75	0.37	0.698	0.591	6
X_4	2	32.60	16.30	1.05	0.377	1.678	5
X_5	2	690.87	345.44	22.17	0.000	35.432	2
X_6	2	975.42	487.71	31.30	0.000	50.024	1
Error	14	218.12	15.58				
Total	26	2102.38					

Table 4.3 shows that as expected, tunable parameters i.e., frequency and voltage parameters have substantial impact on the achieved temperature. This is because of the fact that applied voltage (X_6) is indirectly an indicator of the amount of energy supplied to the target area and frequency (X_5) dictates how this supplied energy would interact with the biological matter. It is also noteworthy that relative position of the electrodes (X_2) also affects the response variable considerably followed by the tumour size (X_1).

Main effects plot for the variables selected is shown in Figure 4.2. Voltage and frequency affect the achieved temperature the most as can be seen by their highest gradients. Mean temperature increases by 14 and 12 degrees respectively when voltage and frequency change levels from low to high.

From the analysis, it can also be concluded that for the six variables each having three levels (Table 4.2), the best arrangement would be to keep X_4 , X_5 and X_6 at high levels and X_1, X_2 at low levels whereas X_3 should be at the medium level as indicated by Figure 4.2.

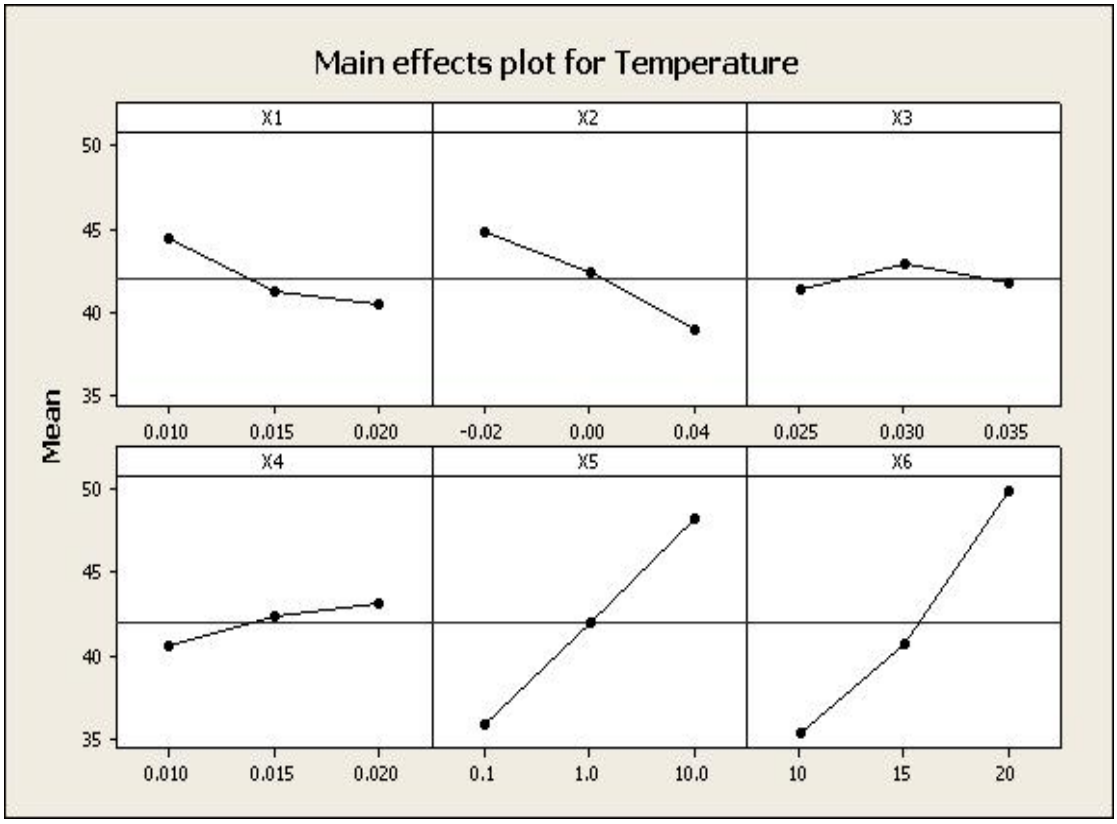

Figure 4.2: Main effects plot of temperature in response to tunable and physical parameters

4.5 Objective Analysis of Therapeutic Outcome

In subsequent sections the result obtained from the Taguchi's analysis are used for further analysis.

It is a well known fact that thermal damage to the biological material is a combination of temperature and exposure time. Tissue damage can be evaluated using Arrhenius function. Thermal damage Ω can be described as [87]:

$$\Omega = A\int_0^t e^{-\frac{\Delta E}{R_u T}} dt \tag{4.1}$$

or

$$\frac{d\Omega}{dt} = Ae^{-\frac{\Delta E}{R_u T}} \tag{4.2}$$

where e is constant having value 2.718, A is the frequency factor, ΔE is the tissue activation energy (J/mol), R_u is the universal gas constant [8.314 J/(mol.K)], T is the absolute temperature (K) and t is the thermal treatment time (s).

$\Omega = 1$ corresponds to a point at which the tissue coagulation first occurs [100]. For the capacitive hyperthermia arrangement, heat generated as a consequence of delivered electromagnetic energy is not uniform and produces a heterogeneous temperature field instead of homogeneous temperature. It can be seen from Equation (4.1) and Equation (4.2) that same exposure will lead to different thermal damage for a varying temperature field.

Moreover, it is also evident from Equation (4.2) that for fixed temperature, the slope of thermal damage is constant with respect to time (w.r.t) i.e.,

$$\frac{d\Omega}{dt} = Ae^{-\frac{\Delta E}{R_u T}} = constant \quad (for\ constant\ T)$$

This means that if the temperature is fixed or steady state has been achieved, thermal damage is linearly related to the exposure time. It has also been observed that at elevated temperatures around 40-41 ^{o}C cells are inactivated. However, this inactivation is temporary and after some time the cells become resistant to the heat due to thermal response of cell via various pathways most notably the release of heat shock protein HSP70 [101, 102]. This phenomenon is known as thermotolerance [103]. Prolonged exposure at temperatures above 41 ^{o}C overcomes the thermotolerance and required biological rationale can be achieved. So for current research, threshold value of 42 ^{o}C has been used. Once the steady state temperature of at least 42 ^{o}C has been achieved, thermal damage becomes a linear function of exposure time only. Similarly, for tissue at temperature above the threshold limit, the slope of thermal damage will be even higher which translates to more swift thermal damage. Figure 4.3 shows the plot of thermal damage against exposure time for a fixed temperature of 42 ^{o}C. Moreover, in clinical practice typical exposure time at 42 ^{o}C is around 60 minutes [22].

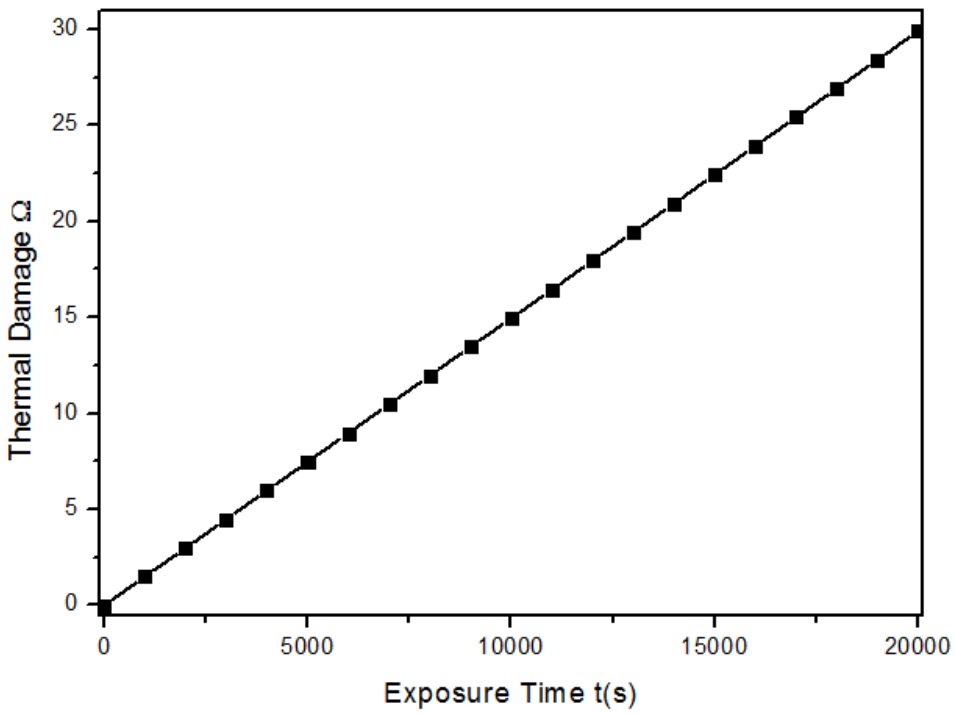

Figure 4.3 : Plot of thermal damage against exposure time for fixed temperature @ 42 ^{o}C with A=7.39e^39 1/s, ΔE=2.577e^5 J/mol

For hyperthermia treatment, the temperature of the tumour needs to be raised to at least 42 ^{o}C. The maximum achieved temperature indicates the efficiency of the energy delivered but it alone doesn't quantify the efficacy of the treatment. For the setup shown in Figure 4.1 and Figure 3.3, the aim of the treatment is to raise the temperature of the tumour above 42 ^{o}C while causing minimum damage to the surrounding normal tissue. An ideal treatment would be one in which the whole tumour is above 42 ^{o}C while all of the normal tissue should preferably be at body temperature. The ideal temperature profile is obviously impossible to achieve but attempt should be made to replicate it as closely as possible.

4.5.1 Analysis Perspectives

The next section will analyze the results from two perspectives.

1. From the treatment objective (complete tumour regression)
2. From the efficiency of tumour killing

4.5.1.1 Efficacy Metric w.r.t Complete Tumour Regression

When a therapy is performed, its main objective is to achieve complete tumour regression. There should be no tumour cells left unharmed, otherwise it would result in recurrence of cancer. For the current research this objective can be accomplished by calculating the percentage of tumour damaged.

4.5.1.1.1 Treatment Index

To quantify the efficacy of therapy with respect to tumour destruction, a treatment index is defined which is given by:

Treatment index = Fraction of tumour at or above hyperthermic temperature

The value of treatment index can vary from 0 to 1. A value of 1 would guarantee complete regression of the tumour while a value of 0 would mean no effect whatsoever. In simple words treatment index only focuses on whether the treatment objective has been achieved or not.

Figure 4.4 shows the graph for treatment index against experiment numbers. The graph reveals that treatment index is 1 for observation number 6, 9 and 24 suggesting that treatment goal has been achieved and is highlighted by circles. Complete tumour regression can be achieved if arrangements in experiments where treatment index of 1 are used.

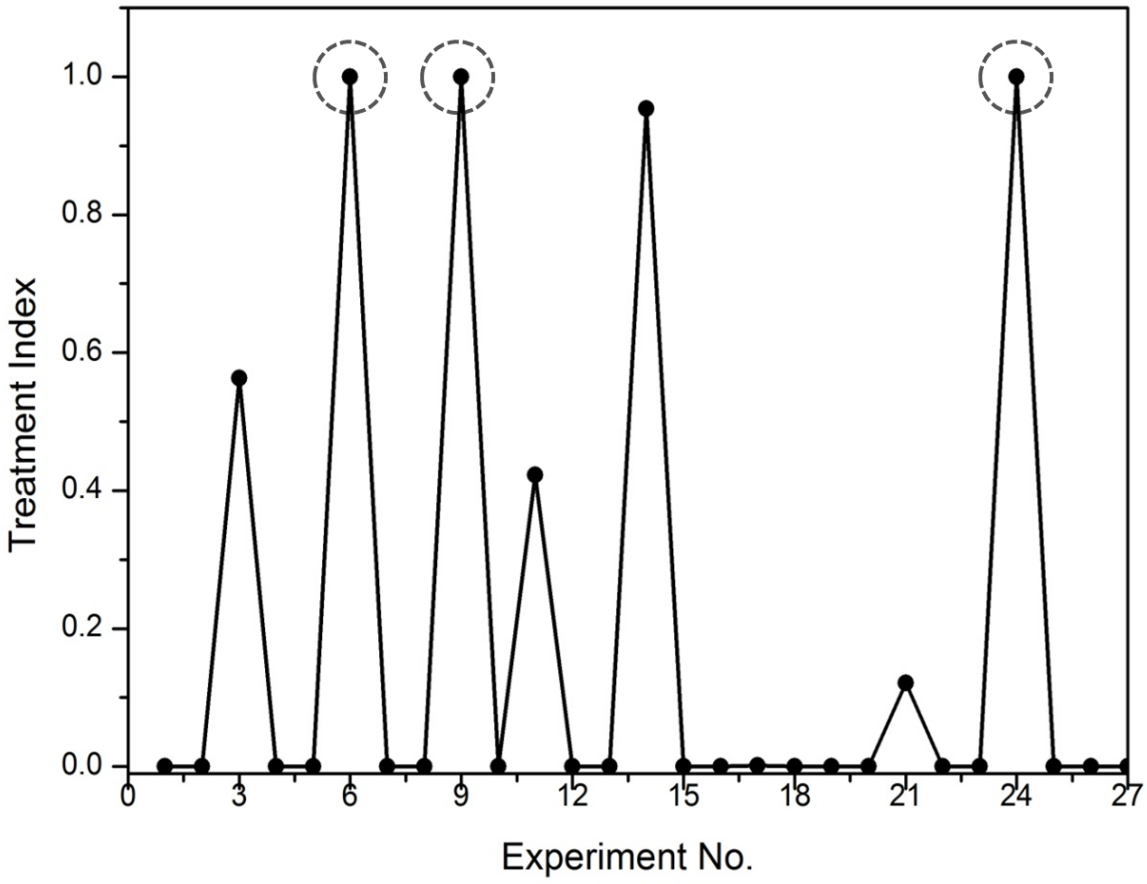

Figure 4.4: Plot of Treatment index corresponding to experiments in Taguchi L27 array for physical and tunable parameters

From Figure 4.4 it is evident that although treatment objective will be achieved for experiments number 6, 9 and 24 but the information contained in Figure 4.4 above is not sufficiently comprehensive because treatment index alone doesn't contain information about the damage caused to the normal tissue. Thus, a treatment index value of 1 doesn't necessarily mean best experimental arrangement or optimum treatment output.

Figure 4.5 further elaborates this point in which the percentage thermal damage to the tumour and surrounding normal tissue is plotted. It is evident that for experiments 6 and 9, the treatment index is 1 but the accompanying thermal damage

to the normal tissue is also very high. Conversely, experiment 24 achieves the high treatment index with corresponding low damage to surrounding normal tissue.

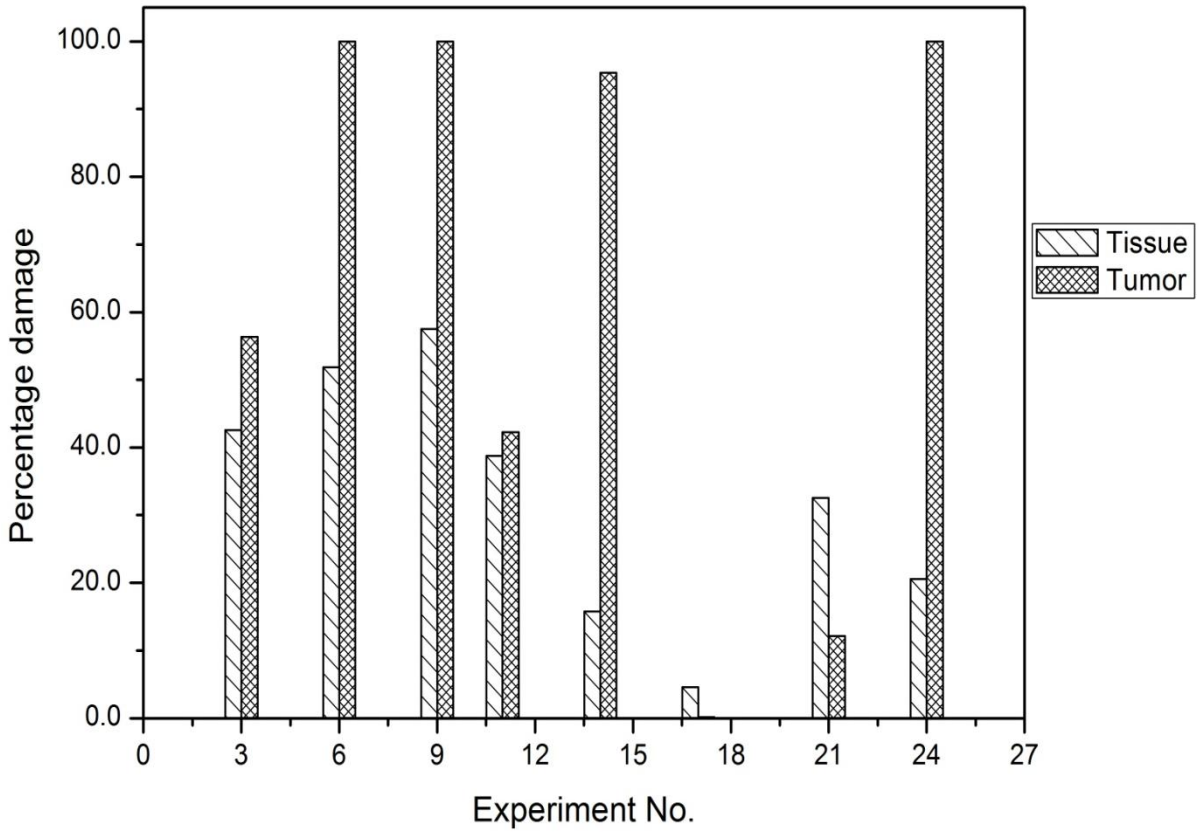

Figure 4.5: Percentage damage to the surrounding healthy tissue and tumor for Taguchi L27 array for physical and tunable parameters

4.5.1.2 Efficacy Metric w.r.t Efficiency of Tumour Killing

Another perspective of analysis can be as to how effectively the tumour damage is achieved. Effectiveness here means incurring maximal damage to the tumour and minimum damage to the normal tissue.

4.5.1.2.1 Damage Index

To accomplish this, damage index is defined which takes into account the thermal damage to the normal tissue as well as thermal damage to the tumour.

Damage index is defined as:

Damage index= Fractional thermal damage to the tumour – fractional thermal damage to the normal tissue

Fractional thermal damage for the tissue is the fraction of tissue above hyperthermic temperature of 42 ^{o}C. Similarly fractional thermal damage for tumour is defined as the fraction of tumour above hyperthermic temperature of 42 ^{o}C. The value of damage index varies from 1 to -1. Ideally the value of damage index should be 1 which would mean complete damage to the tumour with no damage to the peripheral normal tissue. Similarly, a value of -1 means that damage is only incurred by the normal tissue which is the worst case scenario. An attempt should be made to achieve a value of damage index which is close to 1. The damage index describes the protocol which is able to cause maximum damage to the tumour while rendering minimal damage to the normal tissue. In other words it is a measure of how efficiently the tumour is destroyed as a whole.

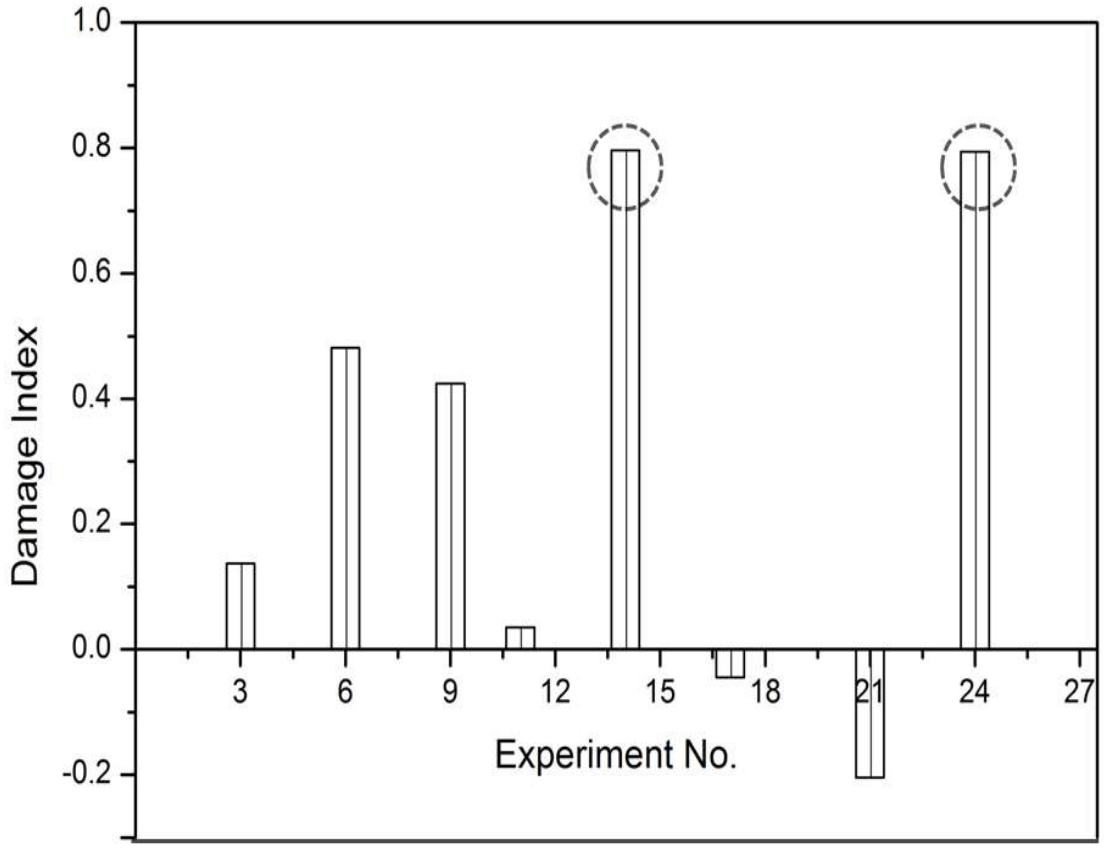

Figure 4.6: Damage index for Taguchi L27 array

Figure 4.6 shows the damage indices for all the 27 experimental combinations which underlines different ranking for damage index than the ranking for treatment index. It can be seen that the damage indices are the highest for experiment number 14 and 24 whereas it is the least for experiment 21. The results suggest that highest killing efficiency for tumour is achieved for experiments 14 and 24 respectively. It is also evident that for experiments 17 and 21 more damage is caused to the normal tissue than to the tumour that is highly undesirable.

Although the best tumour killing efficiency is achieved for experiment number 14 as shown in Figure 4.6 by its highest value of damage index, but this may not be the best option from treatment objective point of view. This can be explained further if we compare Figure 4.4 and Figure 4.6. From Figure 4.4 it is evident that for experiment

number 14, treatment objective is not achieved as its treatment index value is less than 1. As stated earlier, treatment objective is achieved for the experiments 6, 9 and 24 but not all of these have highest damage indices. Out of these experiments, experiment 24 has the highest damage index whereas experiments 6 and 9 have lower damage indices. This suggests that experiments with lower damage index don't kill the tumour efficiently as can be seen from Figure 4.6. It can be seen that experiment number 24 is the best protocol. Firstly, it achieves the treatment objective of incurring complete damage to the tumour as it has a treatment index of 1 (Figure 4.4). Secondly, the treatment objective is achieved with high tumour killing efficiency as well which is signified by high damage index (Figure 4.6). It can be concluded that achievement of treatment objective does not necessarily mean optimum killing efficiency. The best treatment protocol would be the one which has highest treatment index as well as the highest damage index.

4.5.1.3 Importance of Maximum Temperature Location

An important indicator that needs to be taken into consideration is the location of the maximum temperature. Table 4.1 lists the domain in which the maximum temperature is located. To achieve optimum results, maximum temperature should preferably lie inside the tumour region. This arrangement is likely to inflict more damage to the tumour and would shield the normal tissue from the thermal damage. For selective killing of tumour, ideally the hyperthermic condition should only be achieved inside the tumour while normal tissue should be protected from the concomitant thermal damage. This can be further enhanced by injecting the tumour with suitable nanoparticles which can act as thermal localizing agents.

4.6 Statistical Modelling of Capacitive Hyperthermia With Taguchi Based Multiple Regression

The purpose of this research is to devise a multiple linear regression model for capacitive hyperthermia. Knowledge of temperature inside the domain determines the extent of thermal damage in the domain. For the particular case of capacitive hyperthermia, a prediction model based on the regression analysis can be of immense importance in providing a quick and cost effective way to predict approximate temperature that would be achieved inside the computational domain. The regression model based on the physical predictors in an ideal situation, can eradicate the need to solve complex electro-thermal equations for the prediction of temperature. In the first phase, a multiple regression model assuming a linear relationship between six independent variables and maximum achieved temperature as dependent variable or response is considered. A dummy variable was incorporated in the model to categorize the data for tissue and tumour. In order to obtain a better prediction model, regression diagnostics were carried out and a modified model was obtained catering to the inherent nonlinear dependence of some variables on the response variable. Finally, it was revealed that as opposed to simulation software, the proposed regression model presents itself as being cheap, economical and quick alternative which can provide an estimate of the maximum temperature achievable inside the biological tissue.

4.6.1 Multiple Regression Analysis

Success of a research depends on gathering and analysis of data which collectively provide the basis to achieve the ultimate goals of the research. With the advent of

modern equipment and ever increasing computational resources at researcher's disposal, huge amount of data can be collected in short amount of time. Keeping in view the objectives of research and experimental design, a set of data is collected at the end of the measurement. Regression is a statistical tool used to describe the experimental data with set of parameters by establishing a certain relationship between dependent and independent variables. Dependent variable also known as response variable is the variable whose value is to be found. Independent variable also known as predictor variable is the one whose value is varied in order to find out its functional relationship with the dependent variable. The choice of independent variables and their respective levels are decided by the researcher in the experimental design stage.

Regression analysis has previously been applied in biochemistry [49, 104], biology [50, 51], environmental science [105, 106], and nanomedicine [107, 108] etc. As can be seen from Equations (4.1)-(4.7), in order to find out the maximum temperature inside the tissue, complex mathematical equations need to be solved which requires personal effort as well as computational resources. In this scenario, multiple regression analysis can prove to be of great value if it can be used to predict the maximum temperature inside the tissue rendering itself as an easy and inexpensive alternative to the complex and time consuming numerical simulations.

In linear regression model, linear relationship is assumed between the predictors and the response. The mathematical equation that best describes the obtained data is known as regression equation or fitting function. The aim is to select the model that best fits the data between response and predictors. The functional relationship

between the dependent and independent variables is established mathematically by employing the parameters in the regression equation. Parameters are the coefficients of independent variables in the regression equation and have same values at each data point. If the regression equation involves only one independent variable, the analysis is called simple regression. Regression involving more than one independent variable is known as multiple regression.

Regression is said to be linear if the parameters in the regression equation are linear and equation needs not be linear in terms of independent variables. The linear model can be described by following equation.

$$\hat{T} = \beta_0 + \beta_1 X_1 + \beta_2 X_2 + \ldots\ldots\ldots\ldots\ldots\ldots + \beta_k X_k \qquad (4.3)$$

where hat "^" on T indicates that it is a predicted value of T and Xs are the predictors or regressors, β represents the regression coefficients or parameters and k is total number of predictor variables.

Regression analysis is widely used in statistics for analyzing multivariable or multifactor data. Once the relationship between the response variable and the independent variables is established, it can be used for making predictions about the response variable.

Residual ε is the difference between the observed and predicted values. The aim of regression is to fit the line on the data in such a way that results in minimum error between observed and fitted data.

$$\varepsilon = \sum_{i=1}^{n} (T_i - \hat{T}_i) \qquad (4.4)$$

where n is the number of observations.

By analyzing Equation (4.4) it is clear that cumulative sum of the residuals will not indicate the error of prediction. This is because residual can be negative or positive and their cumulative sum can hence result in underestimation of errors.

To overcome this problem, Sum of Squared Error (SSE) is used.

$$SSE = \sum_{i=1}^{n} \varepsilon_i^2 = \sum_{i=1}^{n} (T_i - \hat{T}_i)^2 \qquad (4.5)$$

Equation (4.5) allows an unbiased estimate of the error. So the best fitting function will be the one which would result in least squares of errors.

In multiple regression the quality of fit can be measured by a quantity known as coefficient of determination which is represented by R^2. R^2 represents the proportion of total variability in the response variable that can be explained by all the dependent variables. R^2 is given by [109];

$$R^2 = \frac{SSR}{SST} = 1 - \frac{SSE}{SST}$$

$$SST = \sum_{i=1}^{n} (T_i - \overline{T})^2 \qquad (4.6)$$

$$SSR = \sum_{i=1}^{n} (\hat{T}_i - \overline{T})^2$$

where $\overline{T}$ represents the average of the observed values. SST stands for total sum of squared deviations in Y, and SSR is sum of squares due to regression. Value of R^2 can

be between 0 and 1. R^2 value of 1 represents perfect fit and value of 0 implies no predictive power at all.

As explained above that linear regression analysis assumes linear relationship between the response and the predictors. In order to have reliable results, first the assumption of the linear relationship needs to be checked. This is accomplished by carrying out residual diagnostics. One of the plots that is used is known as partial residual plot or residual plus component plot [110].

Partial residual plot for predictor X_j is a scatter plot of

$$(\varepsilon' + \beta_j X_j) \ versus \ X_j$$

where ε' represents the ordinary least squares residual and β_j is the coefficient of X_j in the full model i.e., regression model that includes all predictors.

Partial residual plot can be insightful in assessing linearity between the response and predictors. If the partial residual plot for a predictor is linear, the relationship between predictor and response is likely to be linear.

For regression analysis, 6 predictors each having 3 levels were chosen as shown in Table 4.4.

Table 4.4: Six independent predictors with corresponding levels used for regression analysis

Factor	Units	Level 1(low)	Level 2(medium)	Level 3(high)
Size of the tumour (X_1)	(m)	0.01	0.015	0.02
Rel. position of electrodes (X_2)	(m)	-0.02	0	0.04
Depth of tumour (X_3)	(m)	0.025	0.03	0.035
Size of the electrodes (X_4)	(m)	0.01	0.015	0.02
Frequency (X_5)	(MHz)	0.1	1	10
Voltage (X_6)	(V)	10	15	20

4.6.2 Results and Discussion

Before applying the multiple linear regression to electrode based thermal therapy, the location of the maximum temperature also needs to be considered. Depending on the adopted treatment protocols, the location of the maximum temperature can change.

Table 4.5:Taguchi L-27 table of observed values for physical and tunable parameters

Exp. No.	Size of tumour X_1	Position of electrodes X_2	Depth of tumour X_3	Size of electrodes X_4	Freq. X_5	Vol. X_6	Max. Temp T	Location of Max. T
1	0.01	-0.02	0.025	0.01	0.1	10	32.102	Tumour
2	0.01	-0.02	0.025	0.01	1	15	41.09	Normal
3	0.01	-0.02	0.025	0.01	10	20	62.038	Normal
4	0.01	0	0.03	0.015	0.1	10	33.027	Tumour
5	0.01	0	0.03	0.015	1	15	41.067	Normal
6	0.01	0	0.03	0.015	10	20	63.676	Normal
7	0.01	0.04	0.035	0.02	0.1	10	32.152	Tumour
8	0.01	0.04	0.035	0.02	1	15	38.692	Normal
9	0.01	0.04	0.035	0.02	10	20	55.792	Normal
10	0.015	-0.02	0.03	0.02	0.1	15	37.5565	Normal
11	0.015	-0.02	0.03	0.02	1	20	59.446	Normal
12	0.015	-0.02	0.03	0.02	10	10	41.164	Normal
13	0.015	0	0.035	0.01	0.1	15	35.133	Tumour
14	0.015	0	0.035	0.01	1	20	47.555	Normal
15	0.015	0	0.035	0.01	10	10	36.698	Normal
16	0.015	0.04	0.025	0.015	0.1	15	34.612	Tumour
17	0.015	0.04	0.025	0.015	1	20	42.987	Normal
18	0.015	0.04	0.025	0.015	10	10	35.695	Tumour
19	0.02	-0.02	0.035	0.015	0.1	20	41.855	Normal
20	0.02	-0.02	0.035	0.015	1	10	36.116	Normal
21	0.02	-0.02	0.035	0.015	10	15	51.9	Normal
22	0.02	0	0.025	0.02	0.1	20	39.794	Tumour
23	0.02	0	0.025	0.02	1	10	36.559	Tumour
24	0.02	0	0.025	0.02	10	15	47.248	Normal
25	0.02	0.04	0.03	0.01	0.1	20	36.004	Tumour
26	0.02	0.04	0.03	0.01	1	10	34.551	Tumour
27	0.02	0.04	0.03	0.01	10	25	39.54	Normal

Table 4.5 shows the location of maximum temperature for the observed data. It is important to categorize the effect of proposed predictors for normal tissue and tumour in order to eliminate any inherent bias in the data. For this purpose a dummy variable X_7 with coefficient β_7 can be added to the regression model to signify whether the maximum temperature lies in normal tissue or tumour. Dummy variable is assigned a value of 1 for tumour and 0 otherwise.

$$\left.\begin{aligned} T = \beta_0 + \beta_1 X_1 + \beta_2 X_2 + \beta_3 X_3 + \beta_4 X_4 + \beta_5 X_5 + \beta_6 X_6 + \varepsilon \quad & For\ Tissue \\ T = \beta_0 + \beta_1 X_1 + \beta_2 X_2 + \beta_3 X_3 + \beta_4 X_4 + \beta_5 X_5 + \beta_6 X_6 + \beta_7 + \varepsilon \quad & For\ Tumor \end{aligned}\right\} \qquad (4.7)$$

As can be clearly seen from Equation (4.7) that the effect of adding a dummy variable is that the slope of regression changes which would subsequently provide an intuition about the effect of proposed predictors for healthy tissue and tumour.

4.6.2.1 Initial or Original Predictive Model

Regression analysis was performed using Microsoft Excel software. Table 4.6 shows the results of initial linear regression model which will be referred to as original regression model here forth and corresponding coefficients. Based on the results obtained, the equation of the model is given by:

$$T = 18.92 - 395.11*X_1 - 93.27* X_2 + 24.90* X_3 + 257.59*X_4 + 1.00*X_5 + 1.43*X_6 - 0.51*X_7 \qquad (4.8)$$

From Equation (4.8) the R^2 value is 0.821 which is closer to 1. This indicates that the current equation is able to describe approximately 82 percent of the variation in the response variable. While a higher R^2 value suggests that this equation explains most of the variation in the response variable, this however doesn't guarantee the

appropriateness of linear model. Further diagnostics are therefore required before the decision for appropriateness of the model can be made.

Table 4.6: Predictors' values for Original multiple linear regression model

Source	*Coefficients*	*Standard Error*	*t Stat*	*P-value*
Intercept	18.92	10.24	1.85	0.08
X_1	-395.11	214.73	-1.84	0.08
X_2	-93.27	39.09	-2.39	0.03
X_3	24.90	230.12	0.11	0.91
X_4	257.59	214.73	1.20	0.25
X_5	1.00	0.23	4.39	<0.0001
X_6	1.43	0.24	5.91	<0.0001
X_7	-0.51	2.63	-0.19	0.85
	R^2= 0.821	R^2 adj=0.755		

The t-statistic in Table 4.6 is equal to the ratio of respective standard error to the coefficient value and it tests the significance of individual regression coefficients for a specified confidence interval (typically 95 %). Under the normality assumption, for n number of observations, t-statistic follows student's t-distribution with (n-2) degrees of freedom. The t-test is carried out by comparing the observed t-statistic with the appropriate critical value obtained from the standard student's t-distribution table which is readily available in any statistics text. Alternatively, critical value of t-statistic can also be found out by using TINV function in Excel which comes out to be 2.06. For a preset confidence level, an observed t-value greater than the critical t-value indicates that the respective regression variable has a significant effect on the response variable. Greater the t-value than the critical value, greater is the influence of that coefficient on the regression model. As can be seen that X_6 coefficient has the strongest effect on the regression model followed by X_5 coefficient. P-value in Table

4.6 is the probability that for a particular confidence level, a random variable having a student's t-distribution with (n-2) degrees of freedom is greater than absolute value of observed t-statistic and hence significant. Equivalently, we can use the P-value to explain the significance of the individual factors. This translates into saying that the parameter is statistically significant if P-value is less than 0.05 (i.e. 95 % confidence level). Moreover, a negative coefficient indicates an inverse relationship with the response variable and vice versa.

For testing whether the original multiple regression model gives any useful information about the response variable or not, standard hypothesis testing was carried out using Analysis of Variance (ANOVA).

$$\left.\begin{aligned} &H_0 : T = \beta_0 + \varepsilon \\ &H_a : T = \beta_0 + \beta_1 X_1 + \beta_2 X_2 + \beta_3 X_3 + \beta_4 X_4 + \beta_5 X_5 + \beta_6 X_6 + \beta_7 X_7 + \varepsilon \end{aligned}\right\} \qquad (4.9)$$

Null hypothesis H_0 states that the current model doesn't give any useful information about the response variable and predictor variables have no explanatory power. Alternative hypothesis H_a states that regression parameters provide useful information about the response variable. Table 4.7 below summarizes the result of ANOVA.

Table 4.7: Table for Analysis of Variance (ANOVA) for original regression model

Source	DF	Sum of squares	Mean squares	F	P
Model	7	1781.18	254.45	12.50	<0.0001
Error	19	386.92	20.36		
Corrected Total	26	2168.10			

Computed against model $T = \overline{T}$

In Table 4.7 DF represents the degrees of freedom and F-statistic is the ratio of mean squares due to regression model and error. F-statistic is used to test the significance of regression model for a specified confidence level (typically 95 %). The F-test is carried out by comparing the observed F-statistic with the appropriate critical value obtained from the standard F-distribution table. For a preset confidence level, if the observed F-value for a regression model is greater than the critical F-value, it shows that regression model has statistically significant predictive capability. Critical value of F for the original regression model can be found out from standard F distribution table by F (7, 19, 0.05) = F (DF for Model, DF for error, 95 % confidence interval). Alternatively, critical value can also be found out by using FINV function in Excel, which comes out to be 2.54. As can be seen that the observed F-value 15.308 > 2.54, it can be concluded that regression model is statistically significant and the last column of Table 4.7 shows the corresponding probability value P (F). It can be deduced that the regression model has statistically significant predictive capability if P-value is less than 0.05 (i.e. 95 % confidence level). It can be seen from Table 4.7 that the P-value is less than 0.0001 which suggests that with 95% confidence level (i.e. $P < 0.05$), null hypothesis H_0 is rejected. So it can be concluded that we can accept the alternative hypothesis H_a with 95% confidence level that the current regression model reveals useful information about the response.

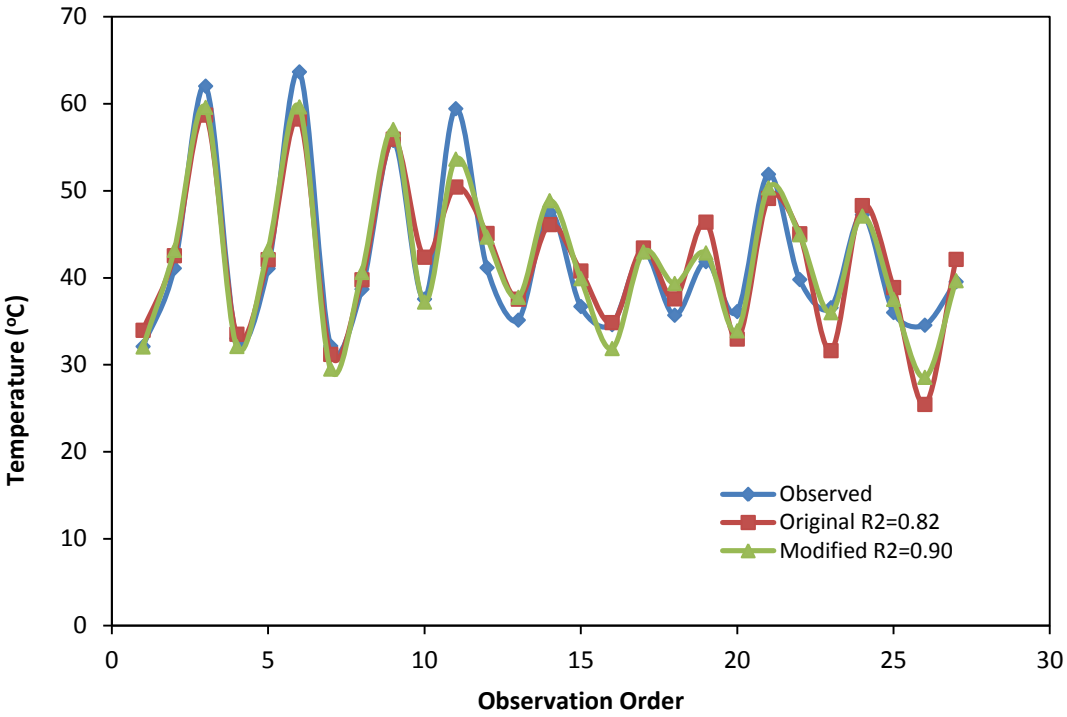

Figure 4.7: Comparison of original and modified linear regression model with observed data

Figure 4.7 shows the comparison of observed and original linear regression models. The original model closely fits the observed values except at observations 11 and 26 where there is large difference between the observed and fitted model. This may be the result of inability of the original model to explain completely the observed data. This is also highlighted by the fact that original model is able to explain approximately 82 % of the variation in the observed values as indicated by the R^2 value. The predicted values and residuals for this model are listed in Table 4.8.

Table 4.8: Table of predictions and residual for original and modified models

Exp. No	T	Original	Residual (orig.)	Std. Residual (orig.)	Modified	Residual (mod.)	Std. Residual (mod.)
1	32.102	33.963	-1.861	-0.482	32.046	0.056	0.020
2	41.090	42.541	-1.451	-0.376	43.157	-2.067	-0.739
3	62.038	58.710	3.328	0.863	59.593	2.445	0.874
4	33.027	33.510	-0.483	-0.125	32.103	0.924	0.330
5	41.067	42.088	-1.021	-0.265	43.213	-2.146	-0.767
6	63.676	58.257	5.419	1.405	59.650	4.026	1.439
7	32.152	31.191	0.961	0.249	29.506	2.646	0.945
8	38.692	39.769	-1.077	-0.279	40.617	-1.925	-0.688
9	55.792	55.938	-0.146	-0.038	57.053	-1.261	-0.451
10	37.557	42.366	-4.809	-1.247	37.208	0.349	0.125
11	59.446	50.435	9.011	2.336	53.644	5.802	2.073
12	41.164	45.096	-3.932	-1.019	44.683	-3.519	-1.257
13	35.133	37.540	-2.407	-0.624	37.754	-2.621	-0.936
14	47.555	46.118	1.437	0.372	48.864	-1.309	-0.468
15	36.698	40.779	-4.081	-1.058	39.903	-3.205	-1.145
16	34.612	34.848	-0.236	-0.061	31.866	2.746	0.981
17	42.987	43.426	-0.439	-0.114	42.977	0.010	0.004
18	35.695	37.578	-1.883	-0.488	39.342	-3.647	-1.303
19	41.855	46.396	-4.541	-1.177	42.859	-1.004	-0.359
20	36.116	32.957	3.159	0.819	33.898	2.218	0.793
21	51.900	49.126	2.774	0.719	50.334	1.566	0.560
22	39.794	45.060	-5.266	-1.365	44.950	-5.156	-1.842
23	36.559	31.622	4.937	1.280	35.989	0.570	0.204
24	47.248	48.300	-1.052	-0.273	47.100	0.148	0.053
25	36.004	38.878	-2.874	-0.745	37.517	-1.513	-0.541
26	34.551	25.440	9.111	2.362	28.556	5.995	2.142
27	39.540	42.118	-2.578	-0.668	39.667	-0.127	-0.045

4.6.2.2 Regression Diagnostics

In order to make any predictions based on the original linear regression model, some regression diagnostics must be carried out. To ascertain the relationship between response and predictors, partial residual plots for each of the predictors are shown in Figure 4.8.

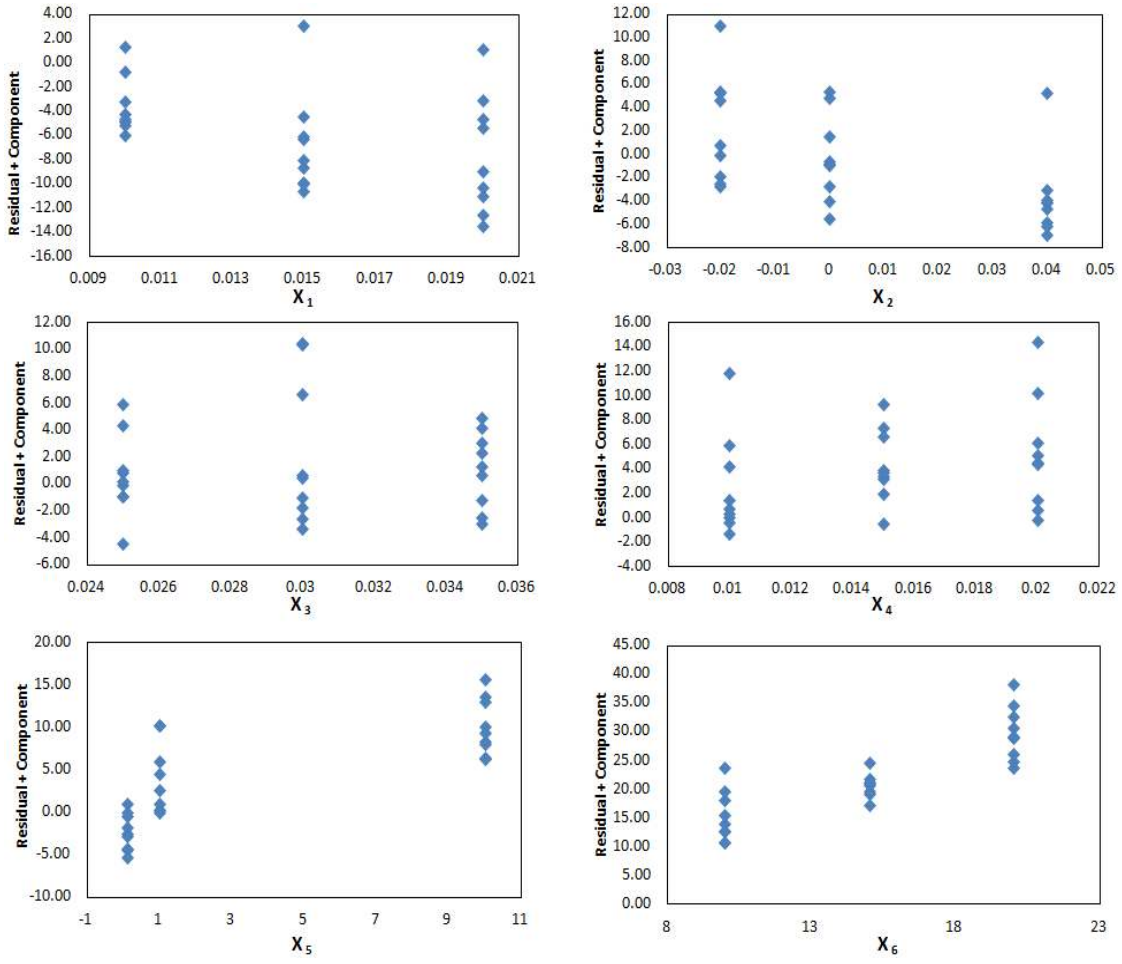

Figure 4.8 : Partial residual plots for all the six independent variables in the original regression model

From the plot of frequency (X_5) in Figure 4.8 it can be seen that the relationship between X_5 and response is nonlinear. The response initially increases with increasing frequency (X_5) and subsequently approaches an asymptotic value suggesting a logarithmic relationship between the frequency and response.

4.6.2.3 Improved or Modified Predictive Model

Hence in order to better fit the data, instead of using linear relationship for X_5, a logarithmic relationship can be used for the component part i.e.,

$$\beta_5 \ln(X_5) \quad instead \quad of \quad \beta_5 X_5$$

The full model equation would be:

$$\hat{T} = \beta_0 + \beta_1 X_1 + \beta_2 X_2 + \beta_3 X_3 + \beta_4 X_4 + \beta_5 \ln(X_5) + \beta_6 X_6 + \beta_7 X_7 \qquad (4.10)$$

It should also be noted that the dependence of response on the predictor X_5 is nonlinear but the equation above is still linear in terms of regression coefficients and linear regression can still be utilized to draw results. Similarly $\ln(X_5)$ can be replaced say by a new variable X_5' and the regression model thus obtained will here forth be called modified regression model.

$$\hat{T} = \beta_0 + \beta_1 X_1 + \beta_2 X_2 + \beta_3 X_3 + \beta_4 X_4 + \beta_5 X_5' + \beta_6 X_6 + \beta_7 X_7 \qquad (4.11)$$

Furthermore, this nonlinearity is highlighted more by the scatter plot of observed and predicted values. The closer the set of points to a straight line, the stronger is the linear relationship between response and predictors. It can be seen from Figure 4.9 that some points sway away from the straight line. This could be the result of nonlinearity inherent in X_5 in the regression equation.

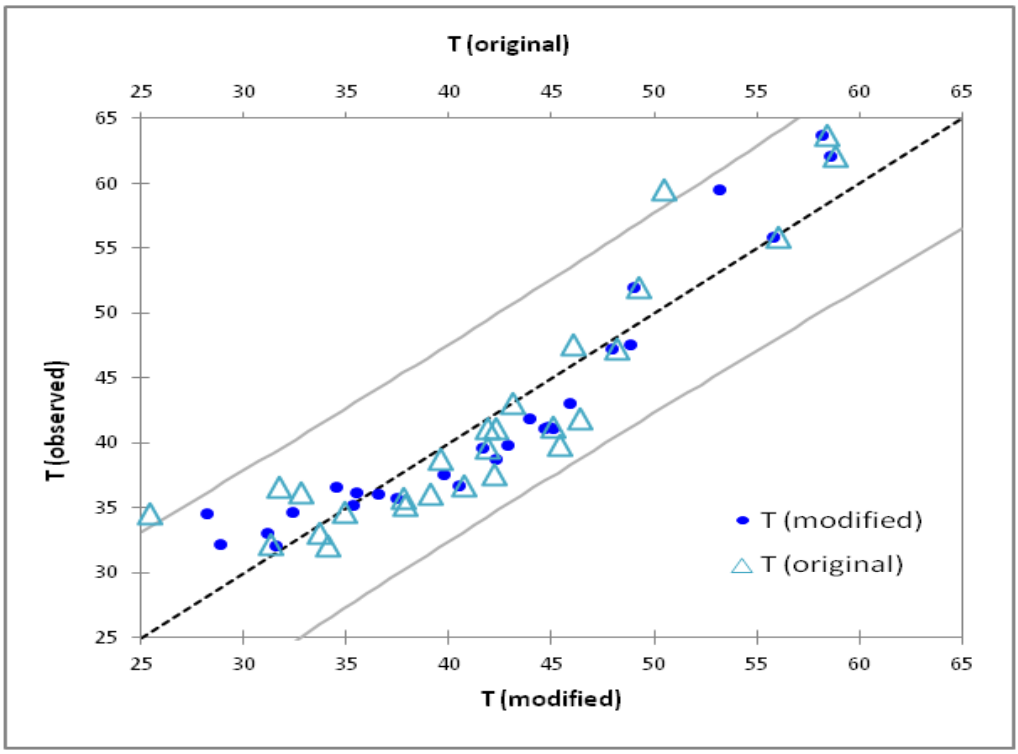

Figure 4.9: Scatter plot of Observed versus Original and Modified regression models

Table 4.9 shows the parameters in the modified regression model. It can be seen that a higher R^2 value has been achieved from the modified model. It is able to explain 90.6 % of the variation as compared to 82 % variation obtained by the original model. This means that modified model is able to explain more variation in the response variable which ultimately would result in higher reliability of prediction regarding the response variable.

Table 4.9: Parameters values for modified regression model

Source	*Coefficients*	*Standard Error*	*t Stat*	*P-value*
Intercept	11.00	7.67	1.43	0.17
X_1	-459.94	156.42	-2.94	0.01
X_2	-132.63	29.63	-4.48	<0.0001
X_3	219.39	172.27	1.27	0.22
X_4	322.42	156.42	2.06	0.05
X_5	3.46	0.47	7.33	<0.0001
X_6	1.69	0.19	9.15	0.00
X_7	5.33	2.30	2.32	0.03
	R^2=0.906	R^2 adj=0.871		

The equation for the modified model is given below.

$$\hat{T} = 11.00 - 459.94*X_1 - 132.63*X_2 + 219.39*X_3 + 322.42*X_4 + 3.46*X_5 + 1.69*X_6 + 5.33*X_7 \quad (4.12)$$

It can be seen from Equation (4.12) that in case of tumour, the slope of regression is different than the tissue. The repercussion of this result is that in case of tumour, the prediction of temperature will be different. For the current model it can be deduced that maximum temperature for tumour is higher than the maximum temperature in tissue because of the difference in gradient of regression. This fact is consistent with the available information keeping in view the higher electrical conductivity of the tumour.

ANOVA is also carried out for the modified model with the null hypothesis that modified model doesn't provide any useful information and alternate hypothesis that it gives useful information about the response variable. The results of ANOVA for the modified model are shown in Table 4.10.

Table 4.10 : Table of ANOVA for modified regression model

Source	DF	Sum of squares	Mean squares	F	P
Model	7	1964.46	280.64	26.18	<0.0001
Error	19	203.63	10.72		
Corrected Total	26	2168.10			

Computed against model $T = \overline{T}$

It can be seen from the ANOVA Table 4.10 above for the modified model that P value is less than 0.0001 which suggests that with 95% confidence interval (i.e. P < 0.05) modified model is statistically significant and provides useful information about the response variable which translates into accepting the alternate hypothesis.

Figure 4.7 shows the comparison of modified and original models with the observed data for the maximum temperature. It is evident from the plot that modified model closely correlates with the observed values and is able to predict values with better accuracy than the original model. An obvious improvement can also be seen in Figure 4.9 which shows the scatter plot of original and modified model against observed values. It is evident that modified model has resulted in further linearization of the original model and proposed changes in the original model resulted in improved performance which would ultimately translate to better predictive capability of the regression model. Predicted values and residuals for the modified model are shown in Table 4.8.

Chapter 5: Application of Meshless Radial Basis Collocation Method (RBCM) to Heterogeneous Conduction and Bioheat Transfer

5.1 Preamble

Accurate measurement of temperature in the biological tissues is very important since most of the thermal therapies like, hyperthermia, hypothermia require precise information about the temperature field inside the tissues and their outcome depends on the final achieved temperature. To obtain the temperature field inside the body is a complex problem because of the presence of inherent heterogeneous structures such as veins, arteries and accompanying blood perfusion. Complexity, non uniformity and health restrictions make it difficult to use experimental procedures to measure the temperature or the variable of interest in vivo. To prevent thermal damage, boundary of the isotherm that represents the critical temperature needs to be known. For clinical purposes the inherent limitation of computerized tomography (CT), ultrasound and magnetic resonance imaging (MRI) make it difficult to capture the boundary of thermal damage. For this purpose numerical simulations offer a relatively inexpensive and easy option which can be used effectively for multitude of situations. Traditionally conventional methods such as Finite Element Method [87, 111] (FEM), Finite Difference Method (FDM) [112], Monte Carlo Method (MCM)[13] and Boundary Element Method (BEM) [75] have been used for such simulations. These methods are well established and have been developed over the course of many decades. The common characteristic of all these is that they all require mesh to

discretize the domain under consideration. In certain cases, the effort required to create a numerical mesh is more than the calculation of solution itself [75, 111, 112] . The physics and complexity of the geometries may require extremely fine mesh which could result in very skewed elements leading to large errors that would hinder in obtaining an accurate and stable solution.

In order to overcome the meshing difficulties, various meshless methods have been proposed by researchers [54-60]. Meshless methods hold promise for many applications because of their advantageous features over the conventional methods like FEM or BEM. These methods depend on the point cloud data with no interconnection between the points rendering them more suitable for adaptive mesh refinement. Their point dependency makes them easier to deal with the complex geometries and makes them less sensitive to the dimensionality of the problem. Many meshless methods have been proposed over the course of last two decades which can be broadly classified into two main categories namely weak formulation or strong formulation depending on the process followed for obtaining the approximate solution of the governing differential equations. Weak formulations like element free Galerkin method (EFGM), method of fundamental solutions (MFS) [61, 62] either require background grid to do the numerical integration of the weak form or need to solve Helmholtz equations which makes them computationally expensive. Strong methods such as Radial Basis Collocation Method (RBCM) [63, 64] deal with the original governing differential equations and point collocation is used to satisfy the governing equations in the domain and on the boundary. Strong form meshless methods are 'truly meshless' because they don't require mesh in any form.

Multiquadratics are positive definite radial basis functions (RBFs) and have global support. Kansa et al. [65] first used multiquadratics RBFs for the solution of partial differential equations and since then there have been many developments on the properties and application of RBFs [57, 61, 62, 64, 66-70].

In this research RBCM has been utilized to simulate the bioheat transfer problem in the two dimensional domain. Approximation function is developed using inverse multiquadratic (IMQ) RBF. The aim of this research is firstly to demonstrate the effectiveness of the RBCM for simulating the heterogeneous heat conduction problem and secondly to apply the said method to bioheat transfer problem for accurate prediction. The research objectives were successfully achieved and the results presented in the later sections are indicative of the appropriateness of RBCM. For this research only steady state problem is considered which can easily be extended to unsteady case. Unsteady analysis can be carried out by discretizing the time derivative and the problem can be solved at each time step similar to the steady problem.

5.2 Implementation of RBCM for 2D Heterogeneous Conduction

In this section the RBCM has been applied to simulate the 2D heterogeneous conduction problem. The theory of RBCM has already been discussed in literature review in Chapter 2.

5.2.1 Benchmark Problem (Material Heterogeneity)

To demonstrate the effectiveness of RBCM in simulating 2D heat conduction in heterogeneous media, RBCM has been coded in Matlab to simulate a benchmark problem, analyzed by Fang et al. [113] and is shown in Figure 5.1. This problem

represents a material heterogeneity and consists of two domains having different material properties. The problem under consideration consists of a square having dimensionless length 1. Outer material has thermal conductivity k_2 and contains an inclusion in the form of square of dimensionless length 0.5. The inclusion has a thermal conductivity k_1.

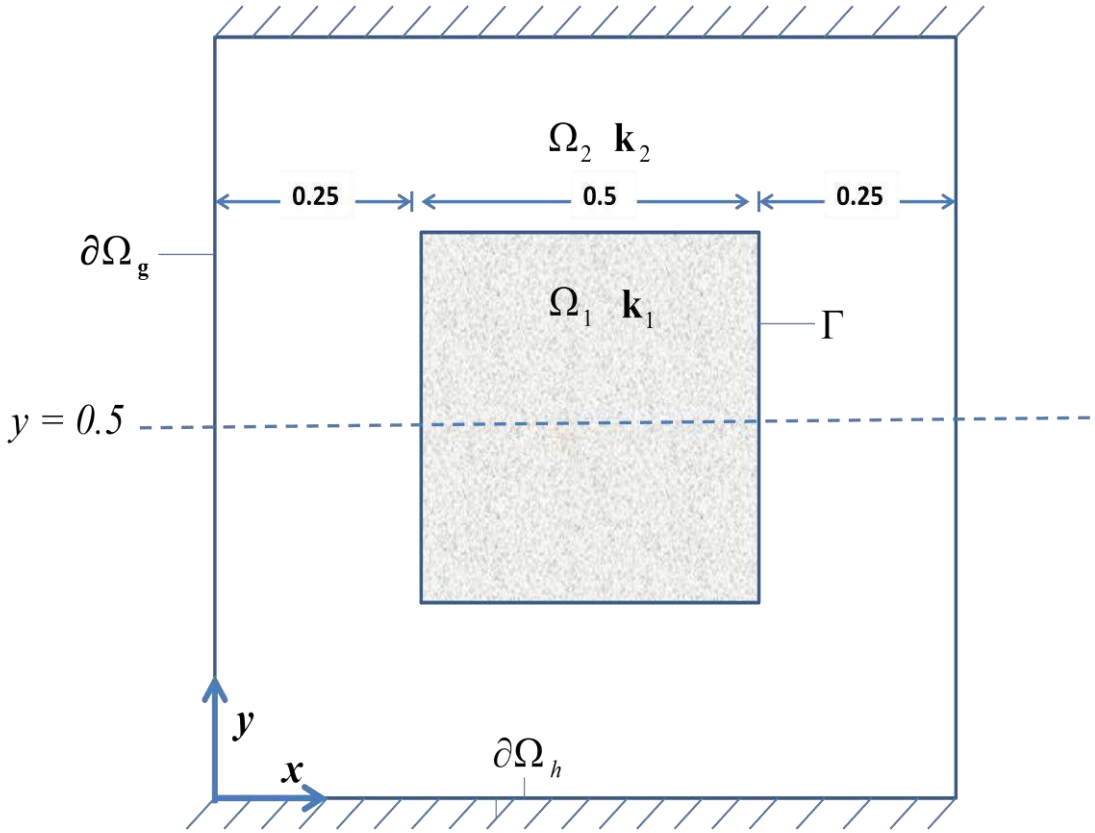

Figure 5.1: Two dimensional heat conduction problem with k_1/k_2=0.01 [113]

Conduction in a two dimensional problem can be represented in dimensionless form as:

$$\frac{\partial}{\partial x}\left(k\frac{\partial T}{\partial x}\right)+\frac{\partial}{\partial y}\left(k\frac{\partial T}{\partial y}\right)=Q$$

$k = k_1,\ Q = Q_1$ for inner domain (5.1)

$k = k_2$, $Q = Q_2$ for outer domain

with boundary conditions:

$T - T_b = 0$ on Dirichlet boundary (5.2)

$k\frac{\partial T}{\partial n} - q = 0$ on Neumann boundary (5.3)

where k, Q, T_b, q represent thermal conductivity, heat source, prescribed temperature at the Dirichlet boundary and normal heat flux respectively. Subscripts 1 and 2 represent the domain number.

Here

$Q_1 = 0$

$Q_2 = 0$

k_1=0.01

k_2=1

$T(0, y) = 0$

$T(1, y) = 1$

$k\frac{\partial T}{\partial n}$=0 on insulated edges (upper and lower edges of domain 2 as shown in Figure 5.1)

For the calculation of temperature in the heterogeneous media, source points and collocation points were used. For sufficient accuracy, the number of collocation

points should be more than the source points as suggested by Hu et al. [114, 115] . For the current analysis number of collocation points used was twice the number of source points. Figure 5.2 shows the arrangement of collocation and source points in the domain. For the RBCM collocation point-cloud consisted of equally spaced points with a grid of 33 × 33.

It is important to note in Figure 5.2 that the approximate solution in each domain is calculated from the points present in the respective domain. There is no need for the additional points outside the boundary or the ghost points as are needed in some of the other methods such as MFS-RBF [61].

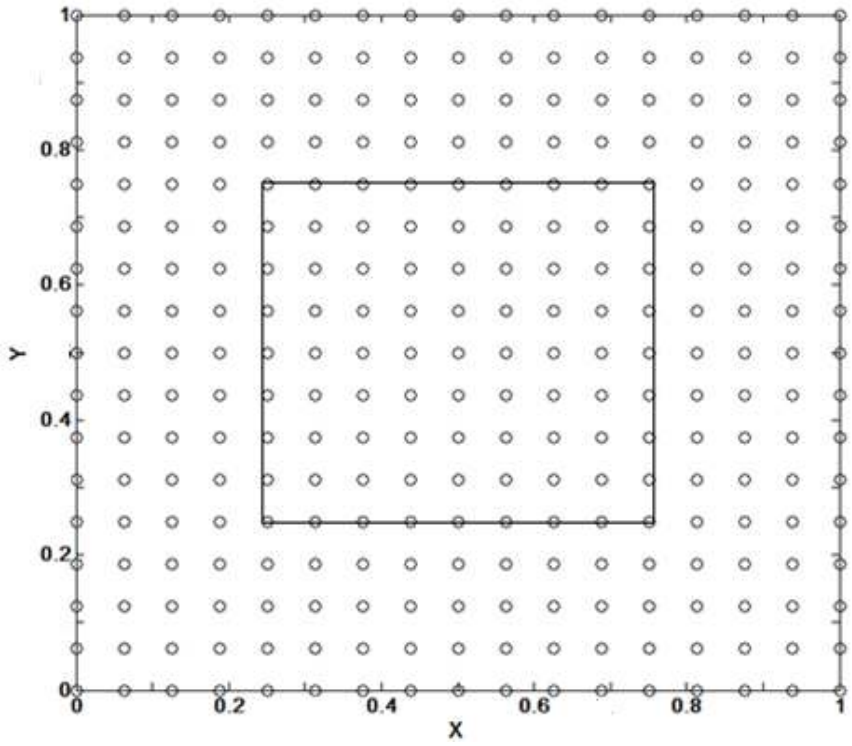

(a) Source Points

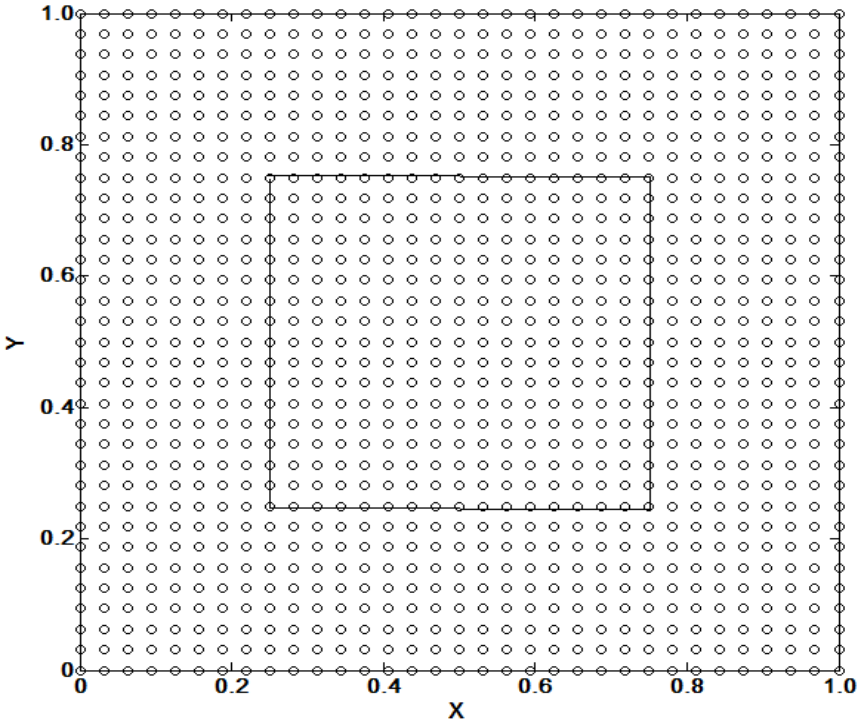

(b) Collocation points

Figure 5.2: Distribution of source points (a) and collocation points (b) in the domain

Fang et al. [113] used the same geometry as shown in Figure 5.1 for comparing the performance of two meshless point collocation methods (MPCM) with FEM. He compared his newly developed meshless point collocation method (MPCM2) with the meshless point collocation method of Sadat et al. [60] (MPCM1) and FEM using regular grid of 41 × 41. Figure 5.3 shows the results obtained from RBCM versus the results published by Fang et al. [113] along a horizontal line at y=0.5.

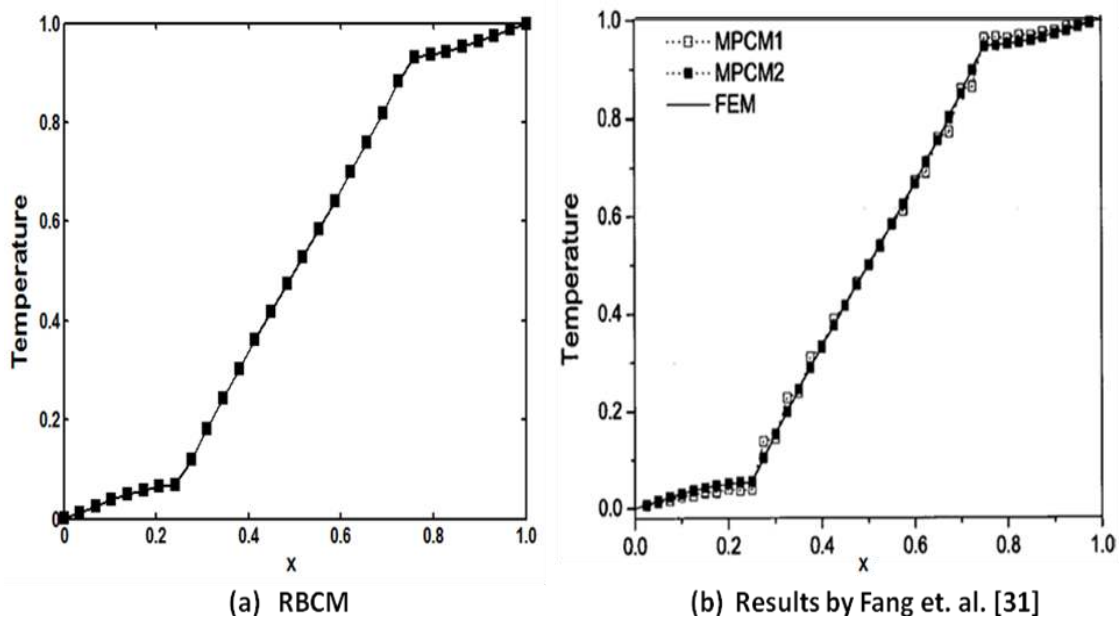

Figure 5.3: Temperature plots using RBCM using Matlab (a) and results published by Fang et al.[113] (b) for k_1/k_2=0.01, Q_1=Q_2=0 at a section y=0.5 (as indicated in Figure 5.1)

As can be seen from Figure 5.3 that the RBCM has been able to obtain comparable results to those of MPCM1, MPCM2 and FEM. Furthermore, the current test problem represents a case of strong variation in thermal conductivity (i.e. 100 times) though may not be applicable for certain situations because the change in material properties normally is not that large order of magnitude. It is also evident that RBCM is still able to deal with such strong heterogeneity by keeping the errors at the interfaces small and produces accurate results. Moreover, RBCM has been able to

obtain accurate results with even less number of points due to the global nature of the RBF being used.

5.2.2 Source Heterogeneity

To quantify the effectiveness of RBCM for simulating the problems having heat source, FEM analysis was carried out using COMSOL Multiphysics software [116]. Regular grid (41× 41) consisting of 1681 grid points was generated and steady state solution was obtained using direct PARDISO solver recommended for such type of problems.

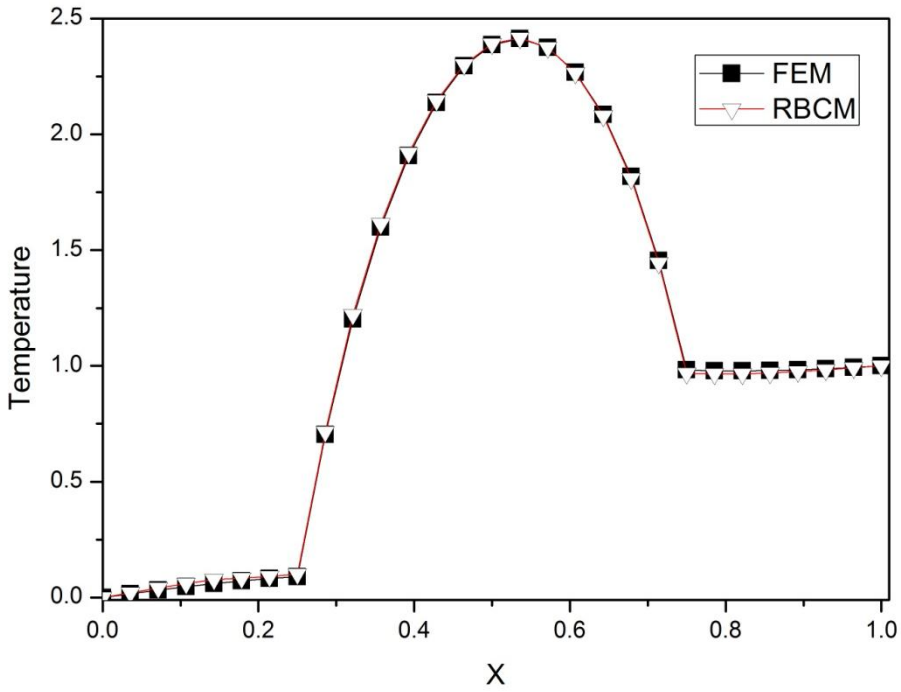

Figure 5.4: Temperature line plots for RBCM using Matlab and FEM using COMSOL for k_1/k_2=0.01, Q_1=1 at section y=0.5 (as indicated in Figure 5.1)

Temperature profile obtained for the heterogeneous problem with Q_1=1 and k_1/k_2=0.01 using RBCM and FEM at a section y=0.5 have been presented in Figure 5.4. Owing to lower thermal conductivity and heat generation term, temperature in domain 1 changes significantly and subsequently results in higher gradients at the

interface. It is also evident that despite such large gradients RBCM has been able to perform really well and provides accurate results.

Figure 5.5 compares the surface plots obtained from FEM and RBCM for Q_1=1 and k_1/k_2=0.01. The weighted RBCM has been able to control errors at both the boundaries and interface. Using assigned weights ensure that errors at the boundaries are not allowed to grow exorbitantly large and the error at the boundaries remains within the acceptable limits (< 5%).

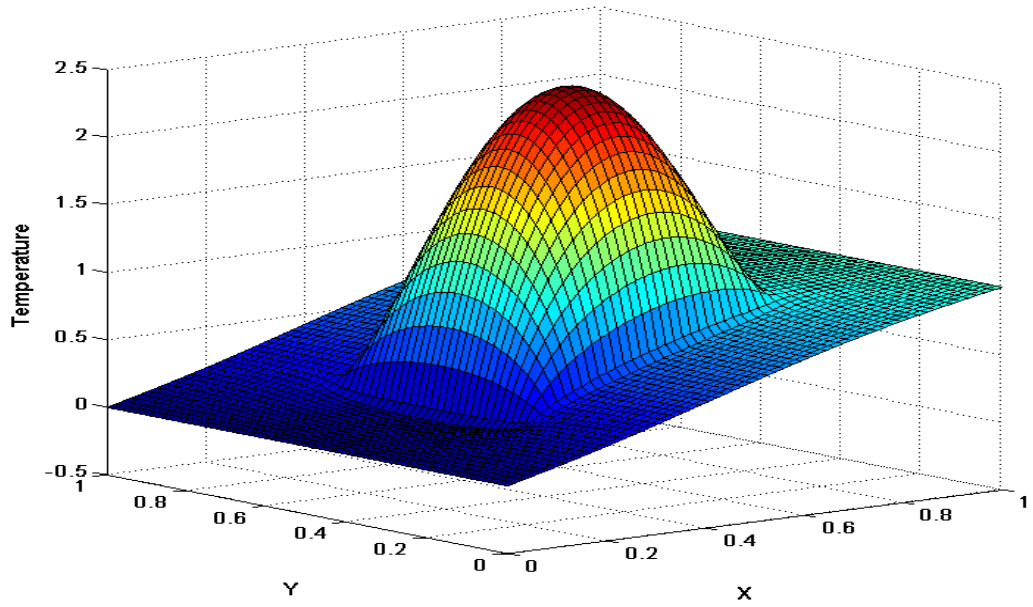

(a) RBCM

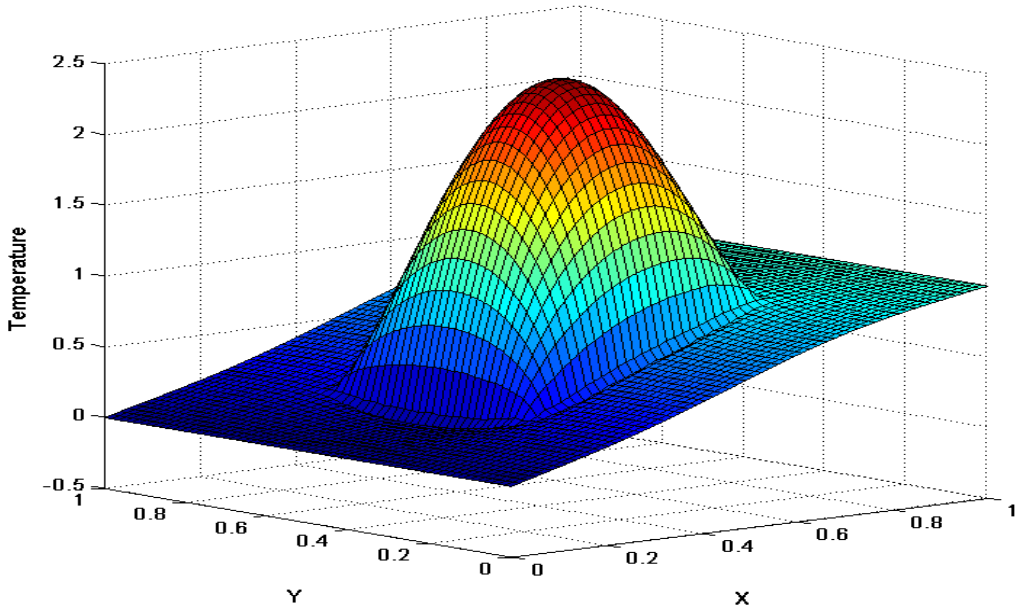

(b) FEM

Figure 5.5: Temperature surface plots using RBCM using Matlab (a) and FEM using COMSOL (b) for k_1/k_2=0.01, Q_1=1, Q_2=0

5.2.3 Extreme Material Heterogeneity

For the heterogeneous problem, the errors stem from the mismatch of properties at the interfaces and if not controlled properly can grow so large as to make the problem unstable. Figure 5.6 shows the temperature plot of the results obtained for the case of k_1/k_2=0.001 which represents extreme thermal conductivity variation

(1000 times). It is clear that despite the extreme heterogeneity, the RBCM has been able to obtain accurate results.

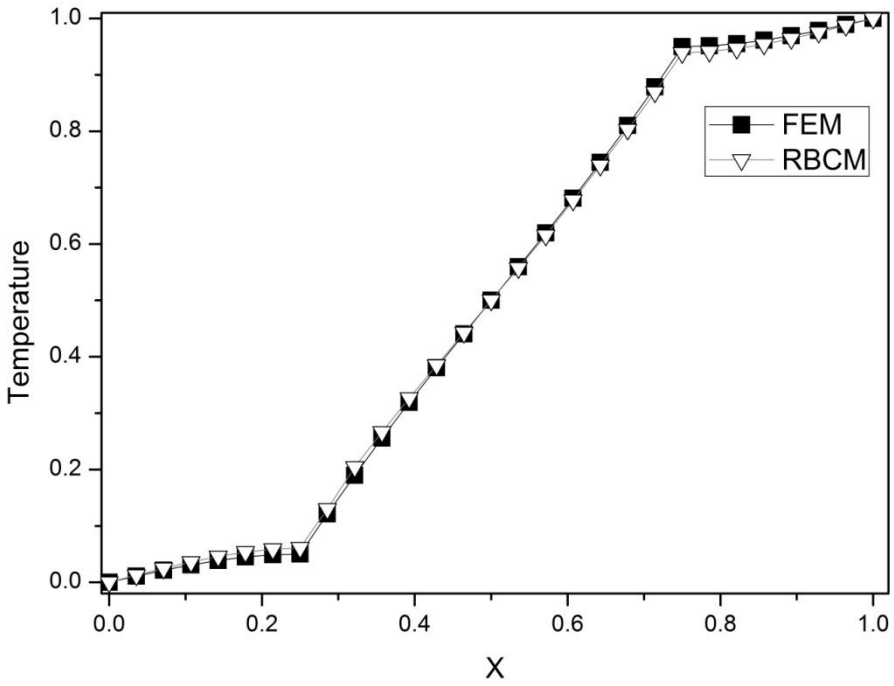

Figure 5.6: Temperature line plots for RBCM and FEM for $k_1/k_2=0.001$, $Q_1=Q_2=0$ using COMSOL at section y=0.5 (as indicated in Figure 5.1)

5.3 Study of RBCM for Bioheat Transfer Problem

A novel meshfree method Radial basis collocation method (RBCM) was used to implement the Pennes bioheat equation. The details of the method have already been discussed earlier in section 2.4 of chapter 2.

5.3.1 Benchmark Homogeneous Bioheat Problem

The geometry used to manifest the suitability of RBCM for bioheat problem was used in [61] and is shown in Figure 5.7. It consists of a rectangular area of skin tissue. The left boundary (skin surface) is at a prescribed temperature and right boundary is

considered to be at the body core temperature. Thermal insulation is considered at the remaining boundaries.

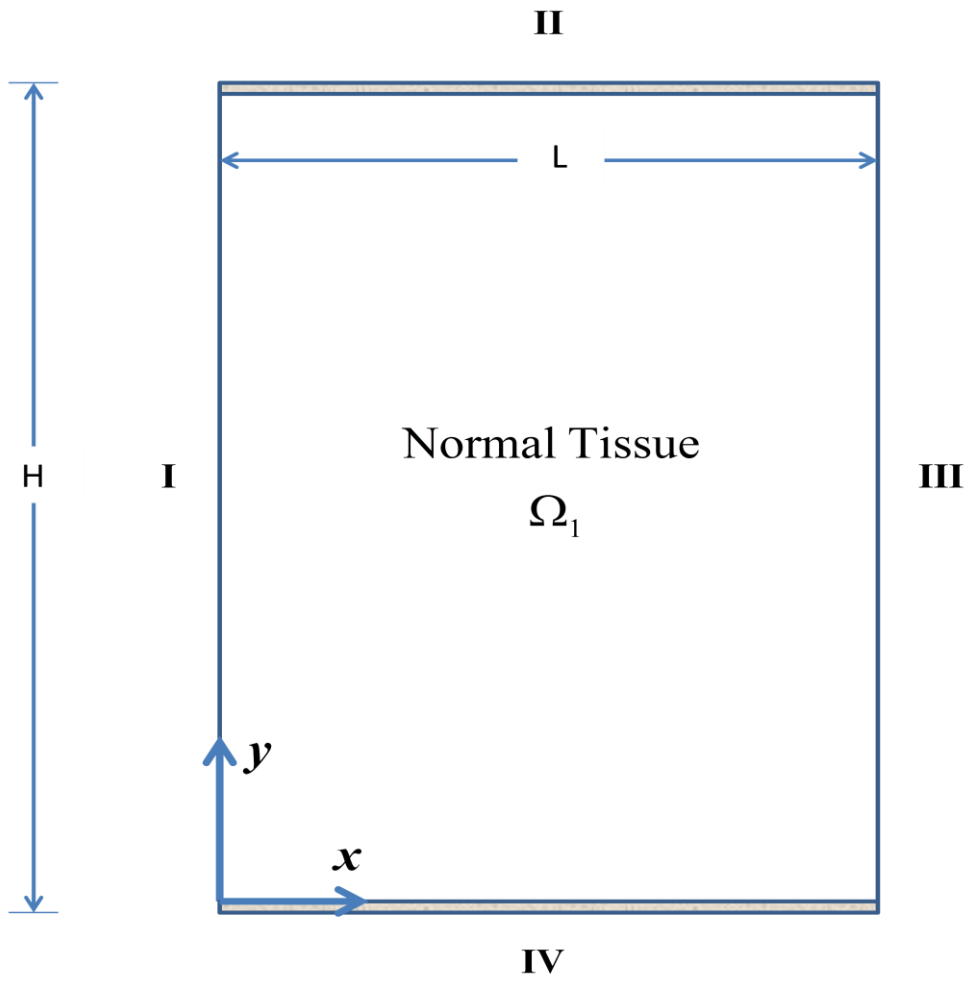

Figure 5.7: Domain used for analysis of skin tissue [19]

Bioheat transfer in the domain as shown in Figure 5.7 can be represented by Pennes bioheat equation.

The following parameters were used in the analysis of bioheat problem.

L = 0.03 m

H = 0.08 m

$$\rho = \rho_b = 1000\ \mathrm{kg/m^3}$$

$$c = c_b = 4000\ \mathrm{J/(kg.^0C)}$$

$$k = 0.5\ \mathrm{W/(m^0C)}$$

$$T_a = T_c = 37\ ^{o}\mathrm{C}$$

The boundary conditions involved were:

$$T(x,y) = 45\ ^{o}\mathrm{C} \qquad (x,y) \in \mathrm{I}$$

$$q(x,y) = 0 \qquad (x,y) \in \mathrm{II, IV}$$

$$T(x,y) = 37\ ^{o}\mathrm{C} \qquad (x,y) \in \mathrm{III}$$

The analytical solution of the skin tissue bioheat problem without metabolic heat source has the form of:

$$T(x) = T_a + \frac{(T_s - T_a)\mathbf{sinh}\left[\mu(L-x)\right] + (T_c - T_a)\mathbf{sinh}(\mu x)}{\mathbf{sinh}(\mu L)} \tag{5.4}$$

with $\mu = \sqrt{\frac{\omega_b \rho_b c_b}{k}}$

5.3.1.1 Response to Varying Blood Perfusions

Results obtained from RBCM for the bioheat problem with different values of blood perfusion rate have been presented in Figure 5.8. Inverse multiquadratic RBF with sf=3.5 was used for the analysis and 31*31 collocation grid with equally spaced points in x and y directions were used.

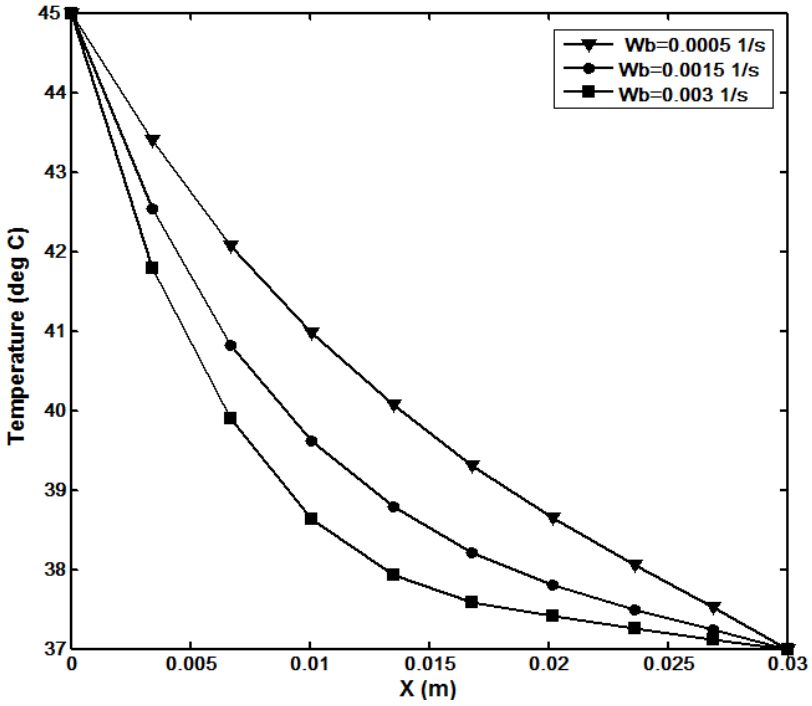

Figure 5.8: Temperature Distribution in 2-D domain using RBCM (sf=3.5) along the x-axis

Figure 5.8 reveals that as the perfusion rate increases, the temperature profile becomes more parabolic. This is because of the fact that higher perfusion rate would result in greater loss of heat energy to the surrounding tissue. The surface plot of temperature for blood perfusion rate (ω_b) value of $0.0005s^{-1}$ is shown in Figure 5.9. It can also be seen that the temperature profile remains stable in the domain and at the boundaries.

Exact solution for the homogeneous bioheat transfer problem as shown in Figure 5.7 can be obtained inside the domain by utilizing Equation 5.26. Figure 5.10 shows the absolute error plot (difference between exact and obtained temperature) for the RBCM solution. It is evident from Figures 5.8-5.10 that RBCM performs really well and the error in the domain doesn't grow large and remains less than 5%. This underlying effectiveness of the RBCM is evident from the fact that the calculated errors are small when RBCM is used to simulate the steady state bioheat transfer problems.

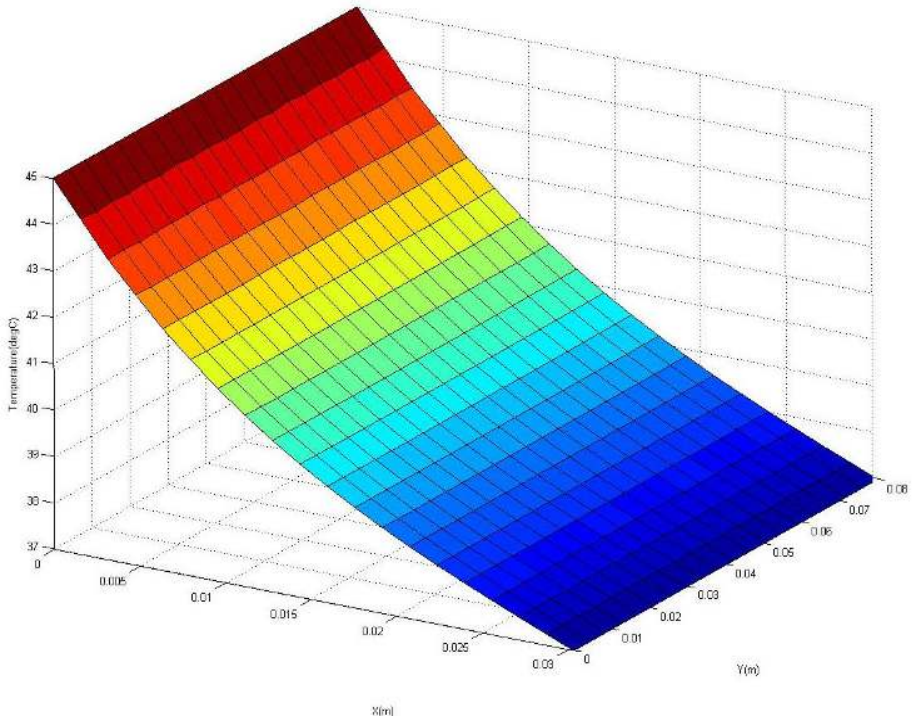

Figure 5.9: Surface plot of Temperature (isotherm) in 2-D domain with w_b=0.0005 s^{-1}

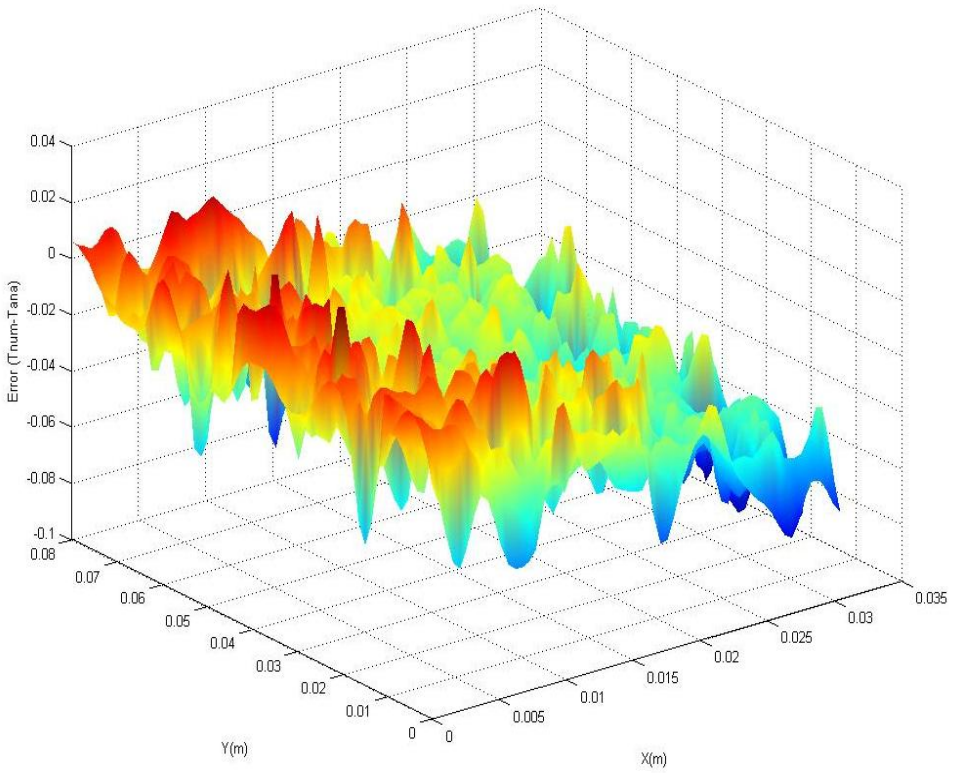

Figure 5.10: Surface error plot over the 2-D domain with w_b=0.0005 s^{-1}

The average relative error (ARE) for the whole domain can be computed as:

$$ARE = \sqrt{\frac{\sum_{i=1}^{N_c} \left(T - T_{ana}\right)_i^2}{\sum_{i=1}^{N_c} \left(T_{ana}\right)_i^2}} \tag{5.5}$$

The ARE for RBCM for different values of blood perfusion rate was also evaluated and has been tabulated in Table 5.1. It shows that ARE doesn't grow large even for the whole domain and solution remains stable.

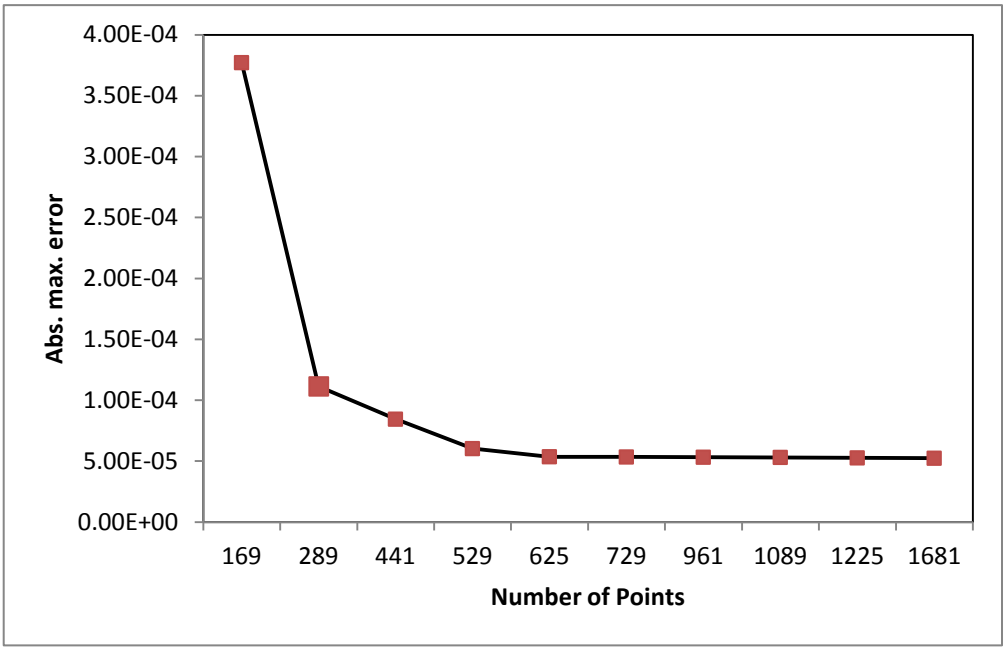

Figure 5.11: Absolute maximum error plot for bioheat problem at w_b=0.0005 s^{-1}

Figure 5.11 shows the effect of number of points on the absolute maximum error. It can be seen that as the number of points increases, the accuracy of the computation also increases with corresponding decrease in absolute maximum error. This is due to

the fact that higher number of points means more points for the interpolation which results in accurate prediction of temperature.

5.3.1.2 Application of RBCM to Heterogeneous Bioheat Problem

Next, the RBCM was extended for the simulation of steady state heterogeneous bioheat transfer problem. For this purpose, same geometry as shown in Figure 5.1 was used and was modelled in COMSOL. Following parameters were used for the heterogeneous bioheat problem:

$k_1 = 0.65\ \mathrm{W/(m^0C)}$
$k_2 = 0.5\ \mathrm{W/(m^0C)}$

$\omega_{b1} = 0.002\ \mathrm{s^{-1}}$

$\omega_{b2} = 0.0005\ \mathrm{s^{-1}}$

$Q_1 = 100000\ \mathrm{W/m^3}$

$Q_2 = 0$

Dirichlet boundary condition was used on the boundaries i.e.,

$$T(x, y) = 37^0\mathrm{C} \qquad (x, y) \in \mathrm{I} - \mathrm{IV}$$

Thermal conductivity and blood perfusion rate values used for domain 1 are representative of tumour embedded with nanoparticles in magnetic fluid hyperthermia [13]. In magnetic fluid hyperthermia tumour is injected with magnetic nanoparticles and subsequently application of electromagnetic field results in heating to cause necrotic death of tumour cells. Tumour has a higher perfusion rate and injection of nanoparticles in the tumour results in higher cumulative thermal

conductivity. Furthermore, heat source used in domain 1 is of the same order of magnitude as is encountered in the magnetic fluid hyperthermia treatment which is localized to tumour region only [13].

Figure 5.12 shows the comparison of temperature line plots obtained from RBCM and FEM in COMSOL for the heterogeneous bioheat transfer problem. It is evident that RBCM gives congruent results to that of FEM (COMSOL) and the heterogeneous boundary is captured appropriately.

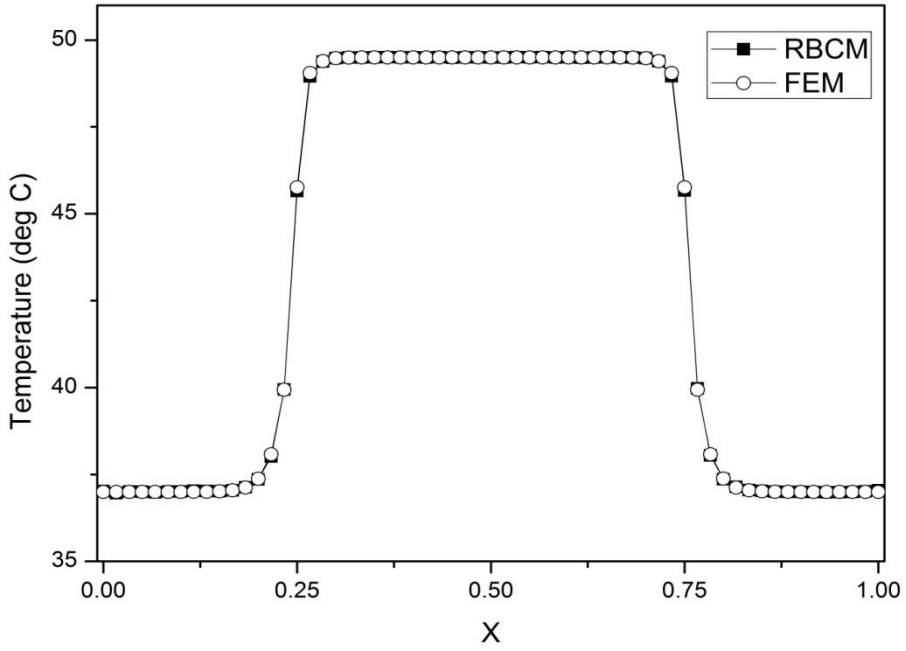

Figure 5.12: Temperature line plots comparison for 2D heterogeneous bioheat transfer problem using RBCM (sf=5.5) in Matlab and FEM in COMSOL at section y=0.5

Surface plot of temperature by RBCM for the heterogeneous bioheat transfer problem is shown in Figure 5.13.

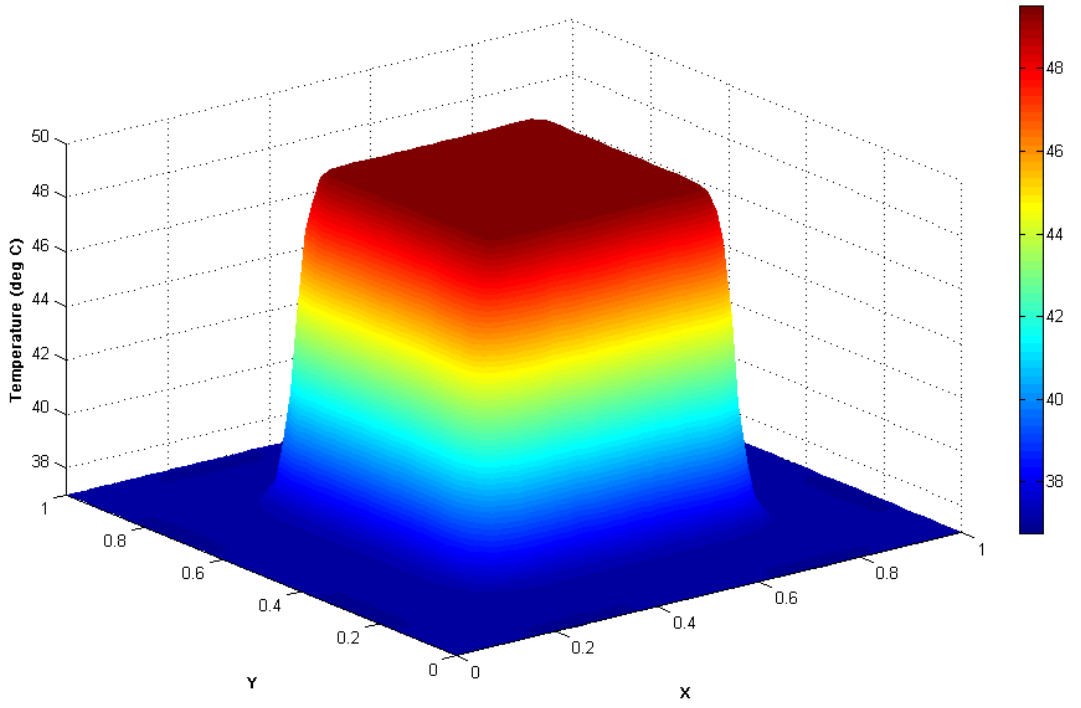

Figure 5.13: Temperature surface plot by RBCM for 2D heterogeneous bioheat transfer problem

5.4 Influence of Number of Points

Figure 5.14 shows the comparison of solution time versus number of points for the RBCM and FEM. It can be seen that with increasing number of points, the solution time is affected significantly for RBCM. It is evident that RBCM performs better for smaller number of points and for large number of points the FEM does well in terms of solution time. It should also be emphasized here that as being meshless method requiring no prior treatment of governing equations, the computational time is less with the reduced effort and time needed in meshing. Generally it is expected that for unsteady problems or problems with heavy point density, the collocation methods can become cumbersome and the size of the collocation matrix becomes increasingly large which requires large memory, making it difficult to solve [117, 118]. It is also known that the shape factor can also affect the RBF collocation which can be accounted for by utilizing the golden section search algorithm [69]. Furthermore, to

deal with the large number of points, strategies like local collocation and domain decomposition can be used which can result in comparable solution times as that of FEM and can offset the accompanying disadvantages for large or unsteady problems by restoring the accuracy and quick solution time that are forte of RBCM.

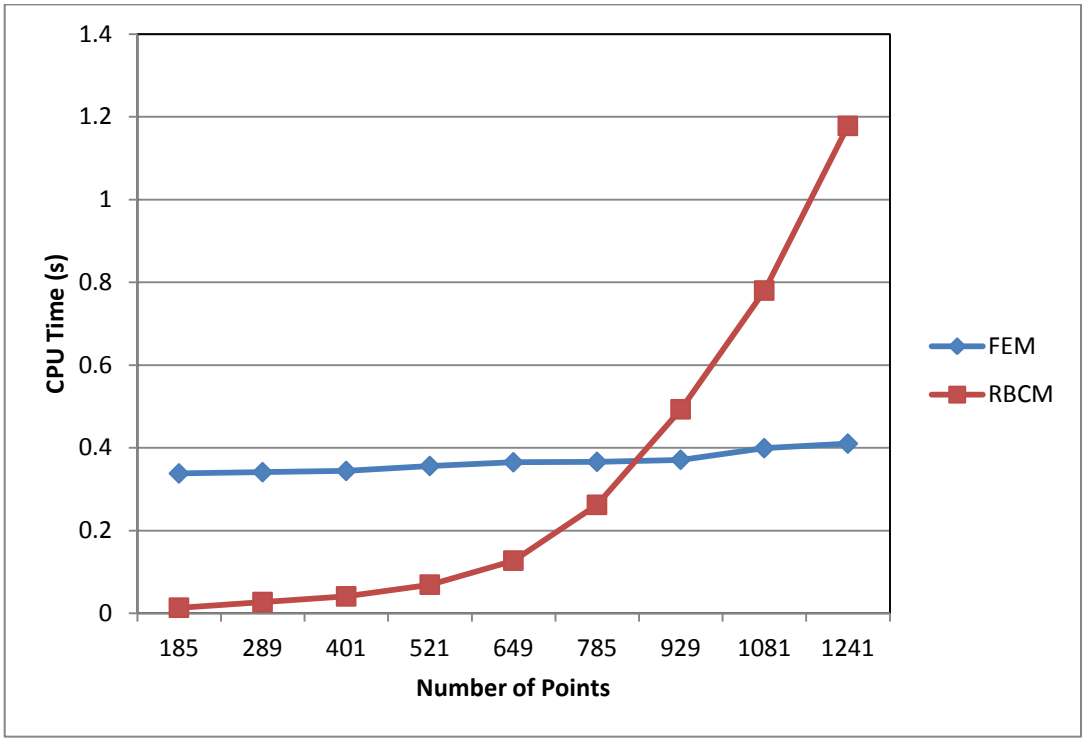

Figure 5.14: CPU solution time versus number of points comparison between FEM and RBCM

It is evident from the results presented in this research that RBCM has been successfully applied to solve steady state problems like heterogeneous conduction and heterogeneous bioheat transfer problems and can be easily extended to unsteady and 3D problems with little effort.

Table 5.1: Comparison between the RBCM and Exact [61] (Equation 5.26) Temperature Solution for various Blood Perfusion Rates

ω_b (1/s)	x (m)	0.000	0.003	0.007	0.010	0.014	0.017	0.020	0.024	0.027	0.030	ARE for whole domain
	RBCM	45.000	43.391	42.072	40.981	40.076	39.309	38.643	38.058	37.517	37.000	
0.0005	**Exact**	45.000	43.387	42.064	40.972	40.060	39.288	38.620	38.026	37.479	37.000	7.16E-05
	Error (Abs)	0.000	0.005	0.008	0.009	0.015	0.021	0.023	0.032	0.039	0.000	
	RBCM	45.000	42.540	40.823	39.621	38.796	38.209	37.809	37.485	37.242	37.000	
0.0015	**Exact**	45.000	42.524	40.808	39.616	38.783	38.196	37.774	37.458	37.205	37.000	6.69E-05
	Error (Abs)	0.000	0.017	0.015	0.005	0.013	0.013	0.035	0.027	0.037	0.000	
	RBCM	45.000	41.786	39.901	38.639	37.930	37.587	37.408	37.258	37.113	37.000	
0.003	**Exact**	45.000	41.748	39.817	38.670	37.987	37.580	37.333	37.179	37.076	37.000	1.50E-04
	Error (Abs)	0.000	0.039	0.085	-0.030	-0.057	0.008	0.075	0.078	0.037	0.000	

Chapter 6: Parametric Sensitivity Analysis and Simplified Prediction Models for Radiofrequency Ablation

6.1 Background

Thermal medicine is the field of medicine in which the curative effect of heat is used for treatment. Depending on the treatment type heat can flow in and out of the body. In treatments like cryoablation the temperature is decreased to -50 ^{o}C and heat flows out of the system [22]. In hyperthermia and heat ablation therapies temperature is increased to above 42 ^{o}C and 45 ^{o}C respectively and excessive energy is thus delivered in to the system [31]. In these therapies the lethal effect of heat is harnessed and temperature of the tissue is raised above a threshold to cause lethal effects. Juxtaposedly, the lethal consequence of heat has a remedial effect for cancer and results in death of cancer cells. Mild temperatures (>42 ^{o}C) known as hyperthermic cause cell death by apoptosis [119]. Mostly these are used as an adjunct therapy to increase the effectiveness of other therapies like radiation therapy and chemotherapy [120, 121]. Temperatures above 45^{o}C are known as thermoablative. Prolonged exposure at such high temperature destroys the cells via coagulation necrosis [122].

RFA has been used for treatment of cancer in many tissues such as liver, lung, heart bone and kidney [123-127]. It has been frequently used for hepatocellular carcinoma (HCC) with non resectable tumours in achieving locoregional treatment objective [128, 129]. Survival rate can be enhanced by surgical removal. Surgical removal presents itself as an attractive alternative but more often than not it is not achievable

because of location and advanced cancer stage. Goetz et al used RFA to treat painful non-treatable metastatic tumours to relieve pain [130]. Bitsch et al. studied the effect of vascular perfusion on the lesion size in bovine livers [131]. Berjano et al. simulated RFA for atrial tissue using finite element model [125]. Yoon et al. reported that efficacy of RFA can be increased with renal artery occlusion for treatment of VX2 tumours [132]. Steinke treated large tumours in lung metastases [133]. It was shown that large tumours are associated with high risk of recurrence owing to difficulty in achieving complete ablation.

In RFA the electrode is inserted in the body utilizing image guidance modalities like MRI and CT scan [129, 134]. The degrees of freedom of the electrode depend on the method and location of the nodules. RFA can cause seeding along the needle track when the tumour is punctured by the needle [135]. RFA administration can be open, percutaneous, laparoscopic, or thoracoscopic depending on the limitations i.e., accessibility, vasculature, available hepatic reserve and case history etc. [136-139].

The voltage is applied to the active part of the electrode and a dispersive or grounding pad is placed at another location in the body to complete the electric circuit [140]. The current flows through the body and energy is dissipated in the form of heat. The tissue adjacent to the electrode incurs the lethal effect directly from the electrode surface whereas the tissue far away from the electrode gets heated via conduction of heat away from the electrode. After a finite time the tissue is destroyed progressively and as a result, a thermal lesion or ablation zone evolves owing to lethal thermal dose. The lethal effect of thermal dose is multifaceted. It causes denaturation of cellular proteins to incur necrosis; tissue structures are

irreversibly damaged and cause stasis of tissue vasculature. The cumulative effect of all the aforementioned effects leads to thermal lesion with complete necrosis. The zone incurring the direct thermal damage is termed as lethal zone. The peripheral tissue exposed to lower lethal dose gets destroyed within 2-3 days [141]. The tissue which is exposed to non lethal hyperthermic dose experiences physiological effects like increased perfusion, oxygenation and porosity [142]. These changes sensitize the tissue for the other adjunct treatments like chemotherapy and radiotherapy. To obtain optimum results, an ablation margin surrounding the tumour also needs to be destroyed. This fact is based on the clinical experience and previously reported studies which suggest that tumour microvasculature permeates into the peripheral tissue and is undetectable because of the limited resolution of imaging modalities [129].

The outcome of the RFA is strongly dependent on the properties of the biological tissues. Biological tissues vary in terms of electrical conductivity, thermal conductivity and blood perfusion as shown in Table 6.1. Bone and fat have lesser blood perfusion while kidney is the one with highest perfusion. Fat has lowest thermal conductivity while liver has the highest thermal conductivity of the tissues analyzed. Similarly, muscle tissue has the highest electrical conductivity and fat is the one with lowest electrical conductivity. This variation encountered in the properties of different tissues is bound to have varied repercussions for the output of the therapy.

The power deposition is regulated with the help of control algorithm. Moreover, the control algorithm which ensures to prevent charring and overheating of the tissue also responds differently to this variation. This is due to the fact that each tissue

behaves differently in terms of temperature increase and evolution of ablation volume to the external impetus provided by the RFA system. Apart from many factors involved that may contribute towards selection of a particular therapy from a large pool of therapies available, the efficacy of RFA can be assessed by the ablation volume/lesion size produced in the tissue.

6.2 Parametric Sensitivity of RFA to Surrounding Tissue Properties: Combined Effect and Implications for Various Tissues

Based on the heterogeneity of electrothermal properties encountered in biological tissues, the aim of this study was firstly to see the effect of critical parameters like thermal conductivity, electrical conductivity and blood perfusion on the RFA. This quantification is studied under fixed temperature control where enough voltage is applied so that the temperature doesn't increase above the threshold limit. In addition to the independent variation, the changes in parameter values across the various tissues are simultaneous. Further analysis was thus carried out to evaluate the cumulative effect of these parameters in various tissues. Ablation volumes for RFA were obtained in bone, fat, lung, liver, kidney, muscle and heart (myocardium) tissues.

6.2.1 Mathematical Modelling of RFA for Various Tissues

RFA represents a coupled electrothermal problem and applies electromagnetic energy to heat the required target. Thus, the determining factor for RFA is how the electromagnetic field interacts with the biological tissue. This interaction is dependent on the size and frequency of the electromagnetic field [23]. Frequency determines the wavelength of the stimulating field and size of the object is crucial for

the nature of interaction. The electromagnetic field theory is numerically coded to study the respective magnitudes of field variables which subsequently determine the amount of heat produced. Maxwell's equations that form the basis of the electromagnetic field theory are used for the determination of field variables inside the biological domain and are applicable over the whole frequency range. In full Maxwell's equations the electric and magnetic fields are coupled and call for solution of more equations requiring enhanced numerical resources. For low frequencies as are used in RFA (460 kHz), a simplified approach for Maxwell's equation known as quasi static approach can be used. It has been reported that quasi static approach for lower frequencies is much less rigorous in giving similar results as those by full Maxwell's equations without compromising accuracy. At lower frequencies the electric and magnetic fields are decoupled and electromagnetic field behaves in the same way as a static field does. Using the quasi static formulation, the electric field intensity E (V/m) inside the tissue can be calculated as [143]:

$$\nabla.[\sigma \nabla V] = 0 \tag{6.1}$$

$$E = -\nabla V \tag{6.2}$$

$$J = \sigma.E \tag{6.3}$$

$$Q = J.E \tag{6.4}$$

where V is the voltage (V), σ is the electrical conductivity (S/m), J is the current density (A/m^2) and Q is the volumetric heat generation rate (W/m^3) due to electromagnetic heating.

For the simulation of bioheat transfer inside the domain, Pennes bioheat equation can be utilized with Equation (6.4) as external source term.

6.2.2 Simulation Setup for Fixed Temperature RFA Control

The setup used for current research is shown in Figure 6.1(a). Radionics cool-tip RF single needle type ablation electrode with diameter of 2mm was modelled and rotational symmetry was utilized to minimize the memory usage [87, 144]. Noticing the rotational symmetry (Figure 6.1(a)), only half of the geometry was modelled. A 2D axisymmetric model was used in lieu of 3D geometry as shown in Figure 6.1(b). These electrodes are minimally invasive and are planted to the desired location under image guidance from CT or MRI. In RFA the electrode is inserted to the desired location and a dispersive pad is placed elsewhere in the body which acts as ground. Voltage is applied on the active part of the electrode and desired power is delivered to avoid overheating or charring of the tissue. Application of voltage makes current flow through the tissue and energy is dissipated in the form of heat. Constant voltage boundary condition is applied on the active part of the electrode (1.5 cm tip length) whereas right (II) and lower (III) boundaries were considered as ground. Electric insulation is assumed on the remaining boundaries. For thermal modelling, body temperature was assumed at the far away boundaries (I-III) whereas thermal insulation was applied on the non active electrode surface. The gradients in the area adjacent to the electrode are high which require finer mesh to resolve those

gradients. For the simulation of bioheat transfer processes many numerical methods have been used that include Finite Element Method (FEM) [89] , Boundary Element Method (BEM) [75], Finite Difference Method (FDM) [112], Monte Carlo Method (MCM) [13], Radial Basis Collocation Method (RBCM) [145] etc. But for this simulation study, Finite Element Method has been used. Mesh consisted of three zones with varying level of resolution. Total mesh is segmented in 3 zones with zone adjacent to electrode containing the extremely fine while zone far away from the electrode was coarsely meshed to save the time and memory. In zone 1 the maximum mesh size was set to 0.2 mm while zone 2 has slightly coarser mesh of maximum size 0.3 mm. The final mesh used in the study is shown in Figure 6.1(b) which consisted of 63611 mesh elements.

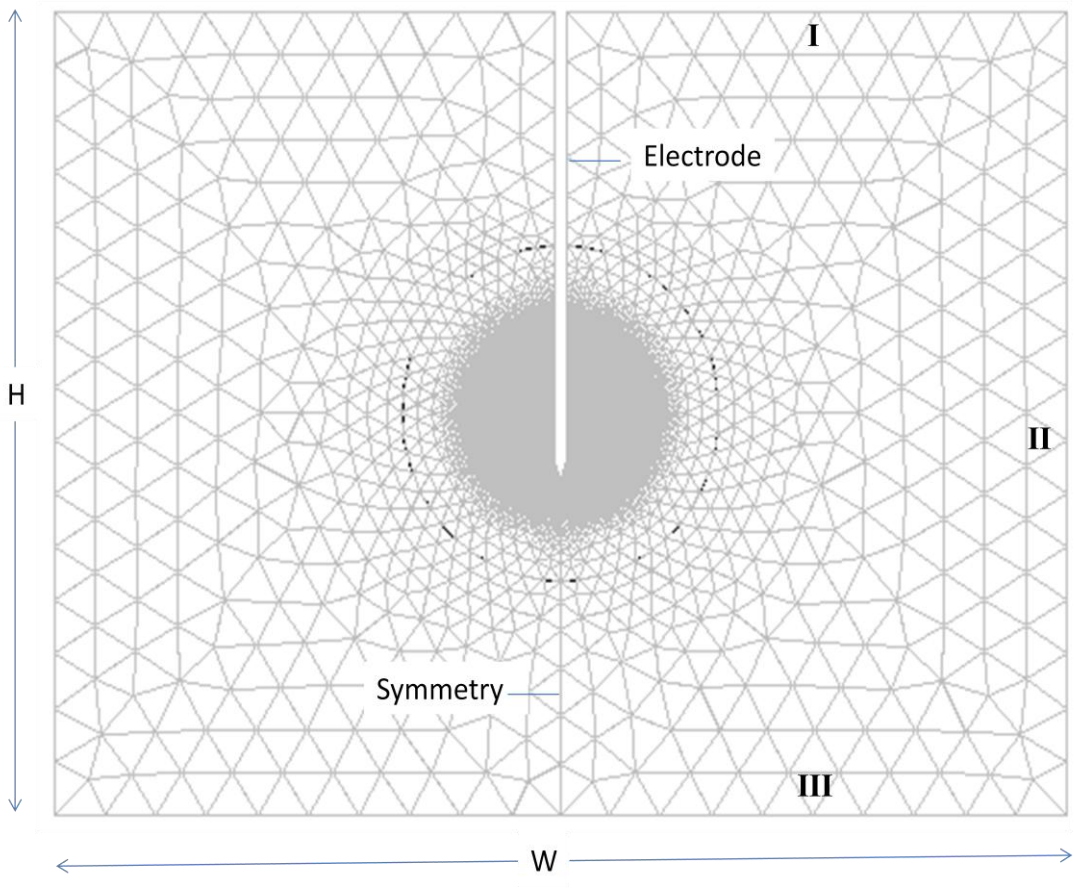

(a)

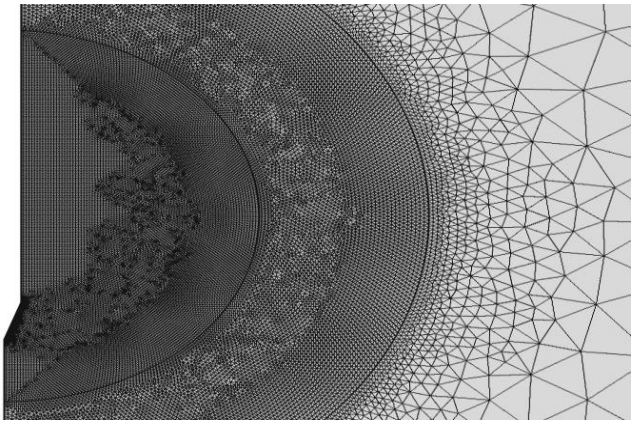

(b)

Figure 6.1: Simulation setup utilizing axial symmetry (a) with W/2=0.08m and H/2=0.06m, extremely fine mesh around the RFA electrode to resolve the high gradients (b)

An important aspect that needs to be considered is the temperature dependence of these properties. As the temperature increases the electrothermal properties of the tissue also change. Thermal conductivity changes by a factor of 0.0012 per ^{o}C and electrical conductivity was varied by 1% per ^{o}C [146, 147]. Moreover, as the temperature rises about a threshold limit, cells die via necrotic pathway. The extraneous energy causes enzymic failure and microvasculature responsible for blood perfusion also gets destroyed. The threshold limit for this study was set at 50 ^{o}C above which the blood perfusion stops [148].

Table 6.1: Electrical and thermal properties of various tissues used for analysis

Parameter	Bone	Fat	Lung	Liver	Kidney	Muscle	Heart (myocardial)
Electrical Conuctivity σ [S/m]	0.022	0.01998	0.122	0.148	0.226	0.3	0.541
Thermal Conductivity k [W/(m.K)]	0.4	0.22	0.302	0.564	0.54	0.49	0.531
Blood Perfusion rate [1/s]	0.000833	0.00035	0.0033	0.0167	0.0667	0.00045	0
Density ρ [kg/m^3]	1990	888	260	1050	1050	1060	1060
Heat capacity c [J/(kg.K)]	1300	2387	2500	3600	3890	3900	3111
Reference	[127]	[149]	[127]	[127]	[149]	[150]	[151, 152]
Ablation volume V_i [m^3]	8.74E-05	1.08E-04	5.66E-05	3.44E-05	1.85E-05	1.02E-04	1.17E-04
Applied Voltage V [V]	31.8	25.5	12.4	15.5	13.15	9.4	7.15

As the power is delivered systematically, temperature of the biological tissue increases progressively. Biological tissues have water content and as the temperature approaches 100 ^{o}C, tissue boiling could occur which is highly undesirable for two reasons. Firstly, the higher temperature surrounding the electrode causes vaporization and creates a plume of steam having very low electrical conductivity which hampers the current flow path. Secondly this phenomenon is accompanied by poor resolution in CT or MRI which in turn limits the assessment capabilities of the radiologist. Sufficient voltage is applied so that the temperature of the tissue at any point is not allowed to increase above 100 ^{o}C.

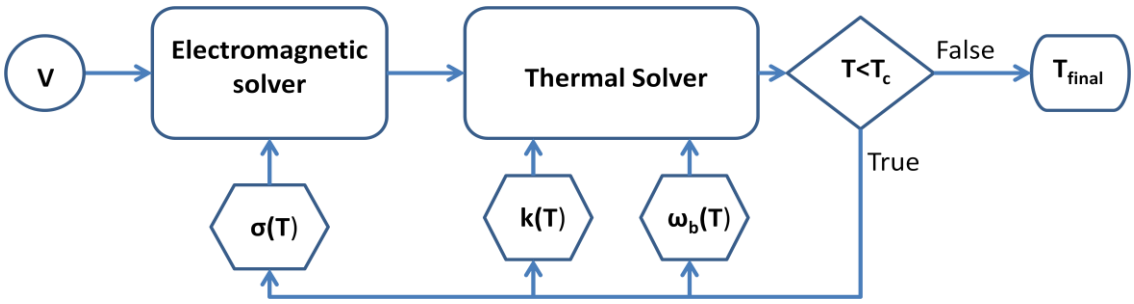

Figure 6.2: Flow chart for fixed temperature RFA control simulation

Assimilating all these factors, a coupled electrothermal mathematical model (Figure 6.2) was formulated to obtain the desired results. The model was implemented in COMSOL multiphysics software [116].

6.2.3 Parametric Analysis Approach for Fixed Temperature RFA Control

Taguchi designed orthogonal arrays (OA) are derived from the classical experimental design [4-6] and require least number of experiments to obtain the results. Taguchi's methodology has been successfully applied in many fields for process improvement [44, 89, 153-155]. For the current research Taguchi's L9 standard orthogonal array was used that requires 9 experiments. Taguchi's arrays are systematically designed.

Each column represents a variable while each row represents the combination of parameters for experimental run. Moreover, within a column each parameter level occurs equal number of times which ensures a balanced analysis [156].

Table 6.2: Selected parameters for fixed temperature RFA control with their respective levels

Parameter Level	Electrical conductivity σ [S/m]	Thermal conductivity k [W/(m.K)]	Blood Perfusion rate ω_b [1/s]
Low	0.02 [149]	0.22 [127]	0.000833 [127]
Medium	0.148 [127]	0.302 [127]	0.0167 [127]
High	0.3 [150]	0.564 [127]	0.0667 [149]

For this research the objective is to maximize the ablation volume or larger the better. For such situations the output from each experiment is converted to Signal-to-Noise (S/N) ratio as outlined in Taguchi's methodology.

$$\frac{S}{N} = -10 \log \left[\frac{1}{V_i^2} \right] \tag{6.5}$$

where V_i refers to the output value for experiment i.

Three parameters namely electrical conductivity, thermal conductivity and blood perfusion rate were considered and the effect of each parameter on the ablation volume was quantified utilizing Taguchi's experimental design. As shown in Table 6.2 each parameter has been assigned levels of low and high depending on the values found in the literature for various tissues. Three levels are used to provide greater parameter space and allowing any quadratic parameter effect.

6.2.4 Discussion of Results

The results for temperature controlled system using Taguchi L9 orthogonal arrays are tabulated in Table 6.3. Figure 6.3 shows the means effects plot for S/N for the three variables considered.

6.2.4.1 Effect of Electrical Conductivity

Furthermore, as the electrical conductivity increases, the general trend is that for constant voltage application the ablation volume increases slightly (Figure 6.3 (a)). As the electrical conductivity is increased progressively from level 1 to level 3, the ablation volume tends to marginally increase. Additionally, for tissue with higher electrical conductivity, critical temperature is reached with the application of low voltage that limits the application of voltage value.

6.2.4.2 Effect of Thermal Conductivity

As can be seen from Figure 6.3(b), higher the thermal conductivity, higher will be the ablation volume. This is because of the fact that tissue near the electrode gets heated directly but in order to disseminate the heat away from the electrode into the surrounding tissue, thermal conductivity plays an important role. Excessive heat is conducted through the tissue and higher conductivity discourages the overheating phenomenon adjacent to the electrode.

Table 6.3: Taguchi's L9 Orthogonal Array for fixed temperature RFA control

Experiment No.	σ (S/m)	k [W/(m.K)]	ω_b [1/s]	Ablation Volume V_i [m^3]	Applied Voltage V [V]
1	0.02	0.22	0.000833	9.71E-06	34.3
2	0.02	0.302	0.0167	1.16E-06	54.5
3	0.02	0.564	0.0667	5.57E-07	81
4	0.148	0.22	0.0167	9.32E-07	18.2
5	0.148	0.302	0.0667	3.20E-07	24.1
6	0.148	0.564	0.000833	1.56E-05	17.6
7	0.3	0.22	0.0667	2.46E-07	15.4
8	0.3	0.302	0.000833	1.13E-05	9.85
9	0.3	0.564	0.0167	1.84E-06	17.4

6.2.4.3 Effect of Blood Perfusion Rate

It has been observed that higher blood perfusion rate tends to decrease the ablation volume. As the perfusion rate increases, more energy is lost due to the blood with convection which ultimately is counterproductive in achieving a higher ablation volume. Another important aspect to observe is that blood perfusion has the largest effect on the ablation volume as can be seen in Figure 6.3 (c) which shows the highest gradient in S/N with varying blood perfusion.

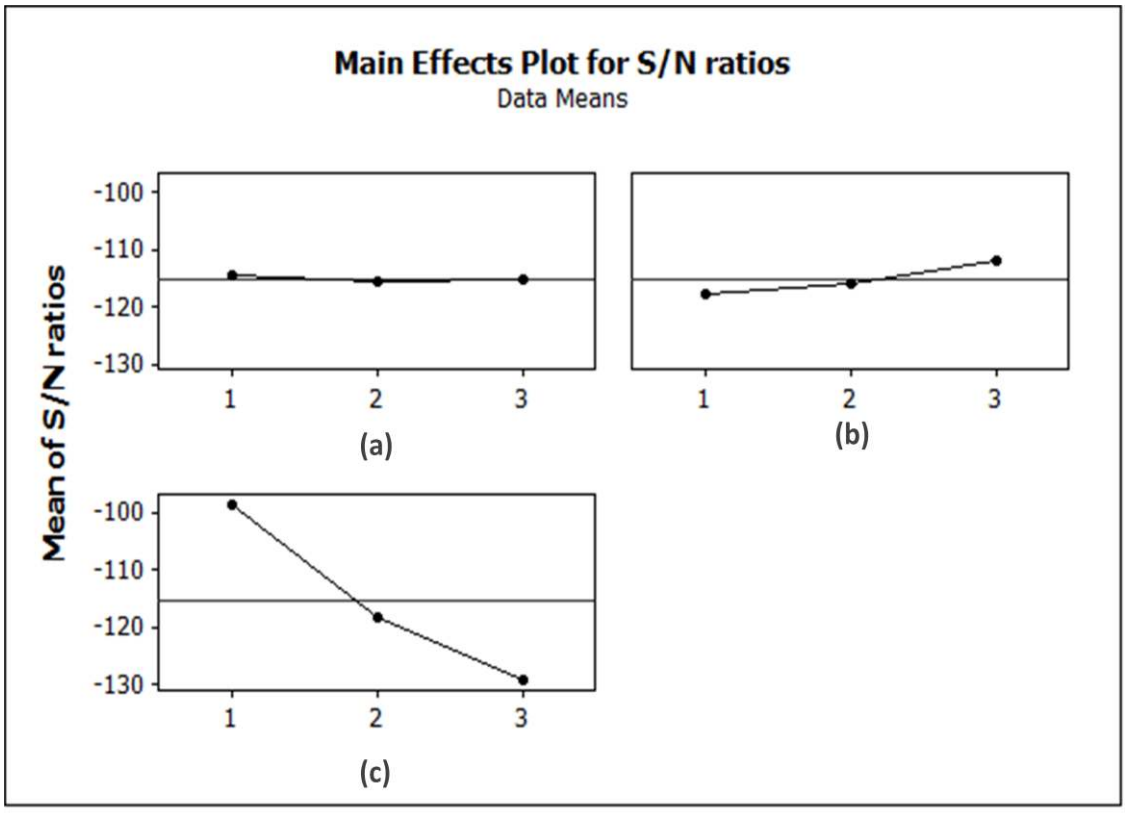

Figure 6.3: Main effects plot for S/N of electrical conductivity (a), thermal conductivity (b) and blood perfusion rate (c) respectively for fixed temperature RFA control

6.2.4.4 Combined Effect of Parameters and Implications for Various Tissues

Although the effect of individual factors has been quantified, in reality these parameters don't change individually. For every tissue, electrical and thermal properties change collectively. In further analysis, the objective would be to observe the cumulative effect of change in properties. For this purpose RFA has been applied to different tissue types using their characteristic electrical and thermal properties. These include fat, bone, lung, liver, kidney, muscle and heart tissues in which the least perfused tissue is bone and the highly perfused tissues is kidney. Heart has higher electrical conductivity whereas bone and fat are electrically less conductive

tissues. Similarly liver has highest thermal conductivity while fat offers lowest thermal conductivity.

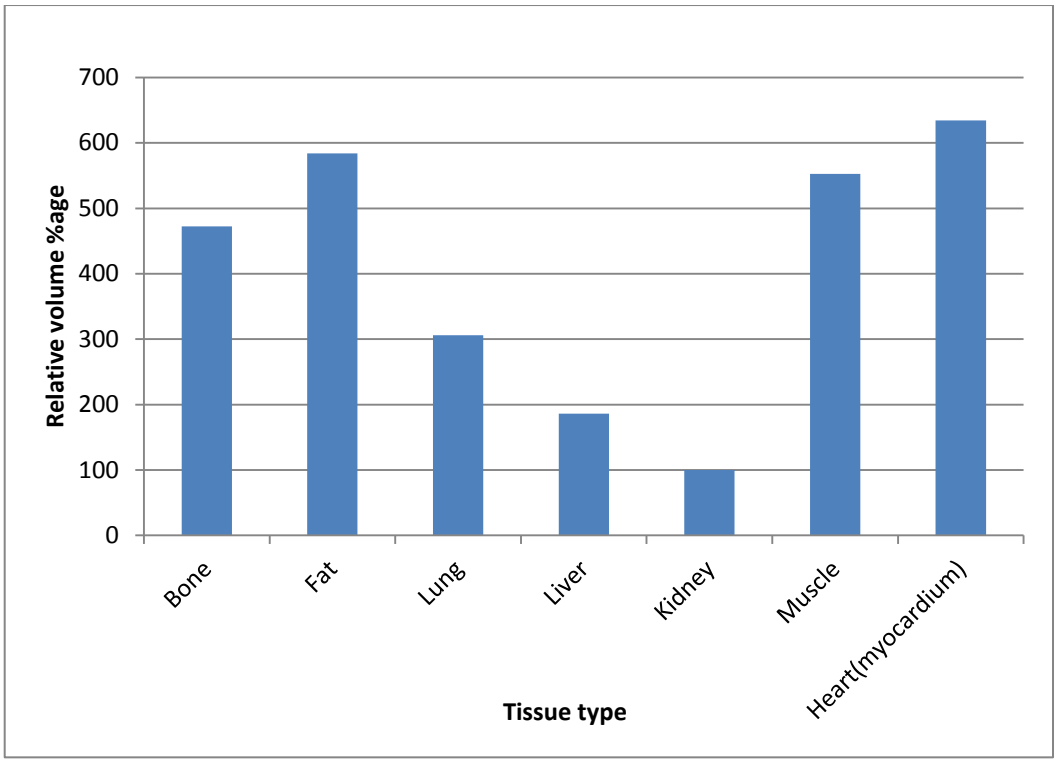

Figure 6.4: Ablation volume for various tissues as relative percentage of ablation volume produced in kidney tissue as baseline for fixed temperature RFA control

The ablation volume produced in different types of tissue is shown in Figure 6.4 as relative percentage of smallest ablation volume produced. The focus of this research is to quantify the ablation volume and draw logical conclusions and implications of RFA for different type of tissues. Instead of dealing with tedious and less insightful magnitude of ablation volume, the final results were normalized with the smallest ablation volume (i.e., ablation volume in kidney as baseline) to give a more insightful quantitative comparison.

It is evident from Figure 6.4 that depending on the tissue type the efficacy of RFA and ablation volume produced varies greatly. The smallest ablation volume is produced in

the kidney. Higher electrical conductivity along with high thermal conductivity amplifies the ablation volume. Despite higher electrical conductivity which allows more current to flow through the kidney tissue, less voltage is required to attain limiting temperature of 100 ^{o}C. Moreover, for kidney another incapacitating factor to the maximized ablation volume is its higher blood perfusion. Kidney is highly perfused tissue which aggravates the evolution of ablation volume. Higher perfusion takes the heat out of the treatment zone and convects it to the surrounding tissue. This debilitating factor has been accommodated in the Pennes bioheat model as a heat sink term. Higher the perfusion rate, greater is the heat sink and the more difficult it is to produce larger ablation zone.

Bone and fat produce ablation volumes of 4.5 to 5.75 times that of ablation volume produced in kidney. Bone and fat have almost similar electrical conductivity but bone has higher thermal conductivity (0.4 W/m.K compared to 0.22 W/m.K) which favours higher ablation volume. This fact is undermined by higher perfusion in bone (2.38 times to that of fat) which ultimately results in lesser ablation volume in bone compared to fat.

Likewise, ablation volumes produced in lung and liver are respectively 3 and 1.8 times the volume achieved in kidney. Both have similar electrical properties (0.122 S/m for lung compared to 0.148 S/m for liver) and liver has higher thermal conductivity (0.564 W/m.K compared to 0.302 W/m.K) which increases ablation volume. But this fact is counterbalanced by much higher perfusion (5 times) in liver as compared to lung which is mainly responsible for smaller ablation volume in liver.

Similarly, in muscle and heart (myocardial) tissues, the ablation volumes produced are respectively 5.5 and 6.3 times that of volume produced by kidney. This can be attributed to their higher electrical and thermal conductivities accompanied by lower perfusion rates which contribute towards higher achieved ablation volume.

Another factor that needs to be considered is the applied voltage in achieving the critical temperature as shown in Table 6.1. As can be seen from Equation 6.3 and Equation 6.5 that heat generated and heat dissemination depend on the electrical properties and thermal properties of the tissue. From Table 6.1 it is evident that applied voltage varies for various types of tissues. For example the applied voltage for heart is 7.15 V as opposed to 31.8 V for bone. For example, 1 V change in applied voltage would result in higher temperature rise in heart than bone. This clearly leads to different level of sensitivity required for control system of heart and bone. This heterogeneity in tissue properties leads to different system response for each tissue under the external stimulus which should be accounted for in the control algorithm design.

It can be seen that depending on the tissue properties, the efficacy of the RFA system is affected considerably. It has been observed that higher thermal and electrical conductivity favour the expanded ablation volume whereas higher perfusion rate is detrimental to RFA. These findings are not only important for applying RFA in different tissue types but may also be beneficial for optimal control design of RFA power delivery system. One would require different power delivery strategy and sensitivity for different types of tissues.

6.3 Quantification of Electrothermal Parameters Effect on RFA for Concentric Tumour Model Under Automatic Temperature Control

The scope of this research is also to quantify the effect of the tumour as well as the surrounding normal tissue properties such as thermal conductivity, electrical conductivity and blood perfusion rate on the ablation volume utilizing Taguchi's experimental design. For this purpose a concentric tumour model was utilized in which the tumour is surrounded by the normal. This study was done under automatic temperature control that was achieved by utilizing the PID controller. The underlying extended objective is to observe how the ablation volume corresponds to changes in size of the tumour and parameter values. It also aims to critically analyze if there are any size associated changes in the effect of the respective parameter.

6.3.1 Mathematical Modelling of Concentric Tumour Model

A concentric tumour model has been considered in which tumour is surrounded by normal tissue. The heat transfer inside the biological tissues is expressed by Pennes bioheat equation and for electromagnetic heating Equations (6.1-6.4) apply. Tissues possess heterogeneous electrical and thermal properties and for concentric tumour model these equations need to be solved separately in tissue and tumour domains along with proper boundary conditions based on the respective properties.

In RFA the ultimate objective is to maximize the ablation volume in order to produce larger thermal lesions. Ablation volume in this study is defined as the volume contained within the 50 ^{o}C isotherm contour [122]. This is imperative because of the fact that complete ablation guarantees the achievement of treatment objective and prevents recurrence. For the same reasons, larger tumours (>5cm) require multiple

electrodes and have higher recurrence rate owing to some of the microvasculature left unharmed. The purpose of this study is to quantify the effect of each parameter on the attainable ablation volume. For the thermal damage assessment the 50 ^{o}C isotherm has been used as the boundary of thermal damage [31]. A control algorithm via PID controller has been implemented which limits the temperature to 100 ^{o}C to prevent overheating.

6.3.2 Simulation Setup for Concentric Tumour Model Under Automatic Temperature Control

The domain used to obtain the simulation results is shown in Figure 6.5. The needle type electrode having 2mm diameter is inserted in the middle of the nodule surrounded by normal tissue [87, 144]. The rotational symmetry of the domain was utilized and a 2D axisymmetric geometry was modelled instead of full 3D geometry which allowed finer mesh to be used for analysis. Modelling was done in COMSOL modelling interface and mesh was generated in COMSOL's built in mesh generator [116]. COMSOL uses finite element method (FEM) to solve this coupled problem. FEM discretizes the problem into small tetrahedral parts or elements via mesh generator and solves the governing equations on the points that relate to the elements. The physics of the current problem requires a finer mesh near the electrode surface. This is owing to the fact that the thermal gradients close to the electrode are extremely high and a finer mesh is required to assure the stability of the numerical scheme and to obtain accurate results. For this purpose the finite element mesh was striated into 3 zones (Figure 6.6) to use finer mesh where required. To obtain any meaningful results the grid optimization study needs to be carried out first. For this purpose, the grid was progressively refined to obtain the

optimum results. Grid Convergence Index (GCI) is a grid quality metric that signifies the amount of discretization error in the grid solution relative to the converged numerical solution [157, 158]. Three grids namely coarse, medium and fine were generated which consisted of 5022, 13795 and 43546 mesh elements respectively. A successive mesh refinement from coarser to medium and from medium to fine yielded GCI indices of 0.5% and 0.2% respectively which are well within the acceptable limits (<<5%). Based on the grid optimization studies, fine grid consisting of 43546 elements was selected to carry out further numerical simulations as it yielded the least error. Zone 1 is adjacent to the electrode and consisted of extremely fine mesh of maximum size 0.2 mm while zone 2 consisted of slightly coarser mesh of maximum size 0.3 mm. Zone 3 was meshed using a default extra fine setting with element growth rate of 1.2 which yielded maximum element size of 4.8 mm.

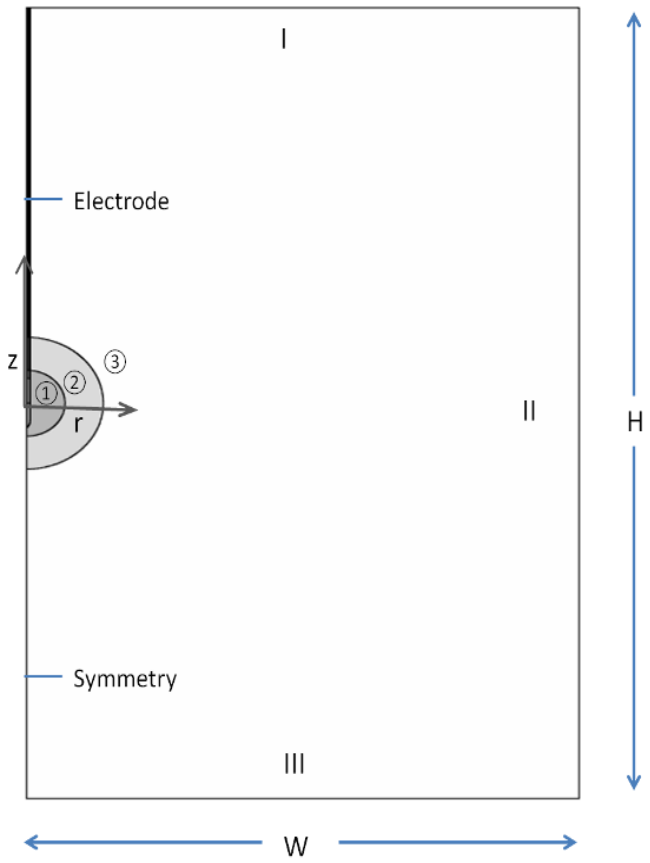

Figure 6.5: Numerical domain used the current study with W=0.07 m, H=0.12 m

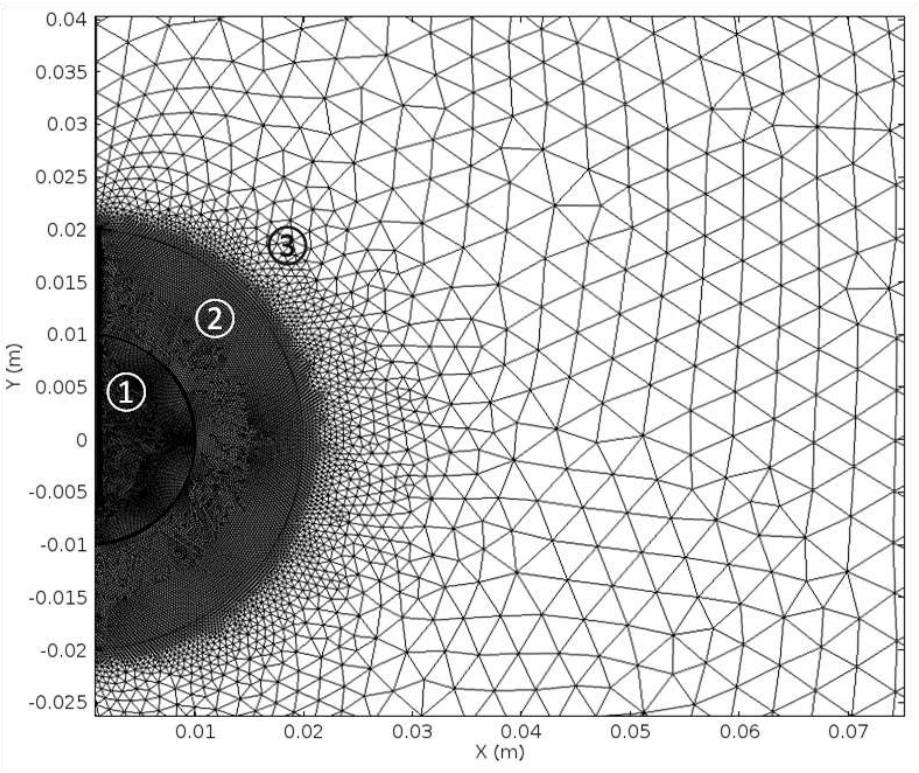

Figure 6.6: Mutli-zonal grid used for the axisymmetric model

To avoid overheating and charring that entail poor image resolution and drastic decrease in electrical and thermal conductivities owing to tissue vaporization known as steam pop [159, 160], the temperature of the tissue needs to be controlled and should not be allowed to increase beyond a specified limit. To guard against these adverse effects, a Proportional-Integral-Derivative (PID) controller has been designed to limit the temperature to a set point as shown in Figure 6.7. PID controller is characterized by the following equation:

$$V(t) = K_p e(t) + K_i \int_0^t e(\tau)\, d\tau + K_d \frac{d}{dt} e(t) \tag{6.6}$$

where V is the applied voltage, e is the error and K_p, K_i, K_d are the proportional, integral and derivative gains. For this study the values used for K_p, K_i and K_d are 0.02, 0.01 and 0.001 respectively.

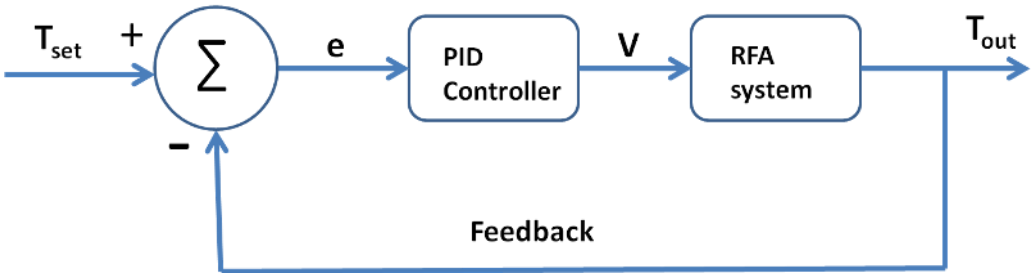

Figure 6.7: PID controller coalesced in the RFA system with continuous feedback

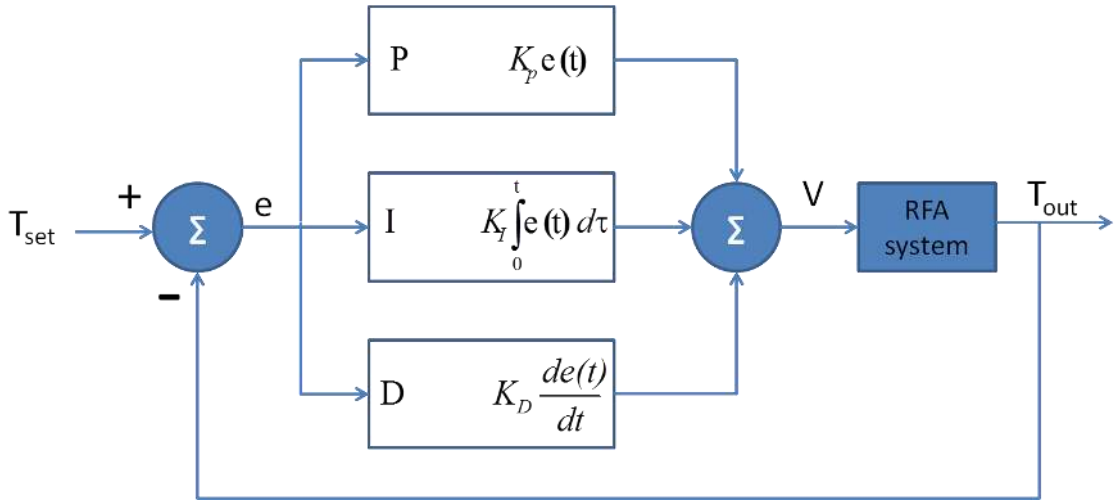

Figure 6.8: Structure of the PID controller for error control of the RFA system

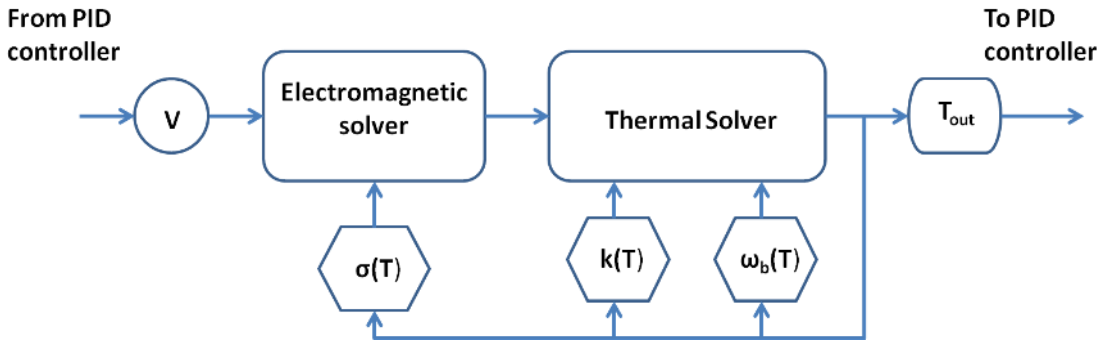

Figure 6.9: Flow chart representation of the simulation setup

PID controllers are widely used in many applications because of their easy control and simple operation. For this research the temperature in the domain is not allowed to increase above 100 ^{o}C. As shown in Figure 6.8 the error between measured output and desired output is continuously fed back to the controller. The controller gauges the error and modulates the required input voltage for the system accordingly. This cycle continues until the error vanishes and the desired output is achieved.

Voltage is applied on the active part of the electrode (Figure 6.5) whose length L is 0.75 times the diameter of the tumour D i.e. L = 0.75*D. Right and lower boundaries

of the domain (II and III) are considered as ground and electric insulation boundary condition is applied on the remaining boundaries. For thermal modelling far away boundaries (I-III) were considered at body temperature as they are not affected by the heating stimulus whereas remaining boundaries were treated as thermally insulated. Another aspect that needs to be considered is the temperature dependence of the electrical and thermal properties. Thermal conductivity varies as 0.0012 per ^{o}C whereas electrical conductivity variation of 1% per ^{o}C was incorporated in the model [146, 147]. Similarly at ablative temperatures the extreme heat causes necrotic failure of the cells and destroys the associated microvasculature which results in interruption of blood supply. The threshold limit at which the vasculature gets destroyed and the blood perfusion stops was set at 50 ^{o}C [148]. The thermoregulatory response in terms of increased perfusion was however not considered due to the absence of the specific data for the modelled tissues. Figure 6.9 shows the complete work flow chart during the simulation.

6.3.3 Experimental Design Methodology

Designing an experiment includes carefully designing the experiments with systematic parameter variation to achieve optimum results. The experimental design can be enhanced based on experience, expertise and knowledge about the process. The number of experiments increases dramatically with number of parameters and associated levels. For this study Taguchi's L27 orthogonal array (OA) is utilized. Taguchi's methodology has found application in many fields [44, 89, 153-155].

Table 6.4 represents the L27 orthogonal array used for this study. Orthogonal arrays have many useful properties which give a balanced comparison with minimum

number of experimental runs. Each row in the orthogonal array represents an experimental run with respective levels for the included parameters. Each column of the array represents a parameter and for 6 parameters there should be 6 columns each assigned to a parameter. Similarly in a column each parameter level occurs equal number of times. For example, for L27 orthogonal array for parameter 1 in column 1, low, medium and high levels occur equal number of times i.e., 9 times. The orthogonal array results in another array with small number of parameters if some columns of the array are deleted.

Table 6.4: Taguchi's L27 orthogonal array for RFA with automatic temperature control for concentric tumour model

Exp. No.	σ_1 (S/m)	k_1 [W/(m.K)]	ω_{b1} (1/s)	σ_2 (S/m)	k_2 [W/(m.K)]	ω_{b2} (1/s)	$Vi_{2cm@L=0.75}$ (mm^3)	$Vi_{3cm@L=0.75}$ (mm^3)
1	0.01998	0.22	0.000833	0.01998	0.22	0.000833	15.3569	25.2292
2	0.01998	0.22	0.000833	0.01998	0.302	0.0167	19.5295	30.2582
3	0.01998	0.22	0.000833	0.01998	0.564	0.0667	29.0321	8.39784
4	0.01998	0.302	0.0167	0.148	0.22	0.000833	9.47059	11.3257
5	0.01998	0.302	0.0167	0.148	0.302	0.0167	12.4585	12.7594
6	0.01998	0.302	0.0167	0.148	0.564	0.0667	18.4272	8.96382
7	0.01998	0.564	0.0667	0.3	0.22	0.000833	3.65273	8.79919
8	0.01998	0.564	0.0667	0.3	0.302	0.0167	5.34179	8.12757
9	0.01998	0.564	0.0667	0.3	0.564	0.0667	11.9739	6.01079
10	0.148	0.22	0.0167	0.3	0.22	0.0167	4.87146	7.13654
11	0.148	0.22	0.0167	0.3	0.302	0.0667	6.6302	3.30838
12	0.148	0.22	0.0167	0.3	0.564	0.000833	10.6514	19.939
13	0.148	0.302	0.0667	0.01998	0.22	0.0167	2.38155	5.25802
14	0.148	0.302	0.0667	0.01998	0.302	0.0667	1.74102	2.43907
15	0.148	0.302	0.0667	0.01998	0.564	0.000833	3.62456	8.49615
16	0.148	0.564	0.000833	0.148	0.22	0.0167	6.83717	7.91824
17	0.148	0.564	0.000833	0.148	0.302	0.0667	10.2892	3.00548
18	0.148	0.564	0.000833	0.148	0.564	0.000833	21.1903	37.0678
19	0.3	0.22	0.0667	0.148	0.22	0.0667	1.64981	2.26948
20	0.3	0.22	0.0667	0.148	0.302	0.000833	3.0757	8.05318
21	0.3	0.22	0.0667	0.148	0.564	0.0167	4.40713	8.06188
22	0.3	0.302	0.000833	0.3	0.22	0.0667	3.66882	2.56812
23	0.3	0.302	0.000833	0.3	0.302	0.000833	17.0895	28.7649
24	0.3	0.302	0.000833	0.3	0.564	0.0167	27.5884	48.8763
25	0.3	0.564	0.0167	0.01998	0.22	0.0667	1.49274	1.91988
26	0.3	0.564	0.0167	0.01998	0.302	0.000833	2.95851	7.82159
27	0.3	0.564	0.0167	0.01998	0.564	0.0167	4.29439	7.83867

For this research a generic model consisting of concentric tissue and tumour was utilized which served as the test case for the relevant changes to be made in the aforementioned electrical and thermal parameters. For current study 6 parameters each having 3 levels was selected and the underlying statistic used for comparative evaluation was volume of the ablation zone. Parameters include thermal conductivity, electrical conductivity and blood perfusion of tumour and normal tissue surrounding the tumour respectively. The value of these parameters varies depending on the type of tissue and low, medium and high levels were selected based on the variation as reported in literature (Table 6.5). The experiments were carried out in an organized manner as per the L27 orthogonal arrays and results were collected after simulation time of 3600 seconds. The results were converted to signal-to-noise (S/N) ratio for "Larger-the-better" framework as given by Equation 6.5.

The effect of a parameter "n" at a particular level "m" is given by [156]:

$$\overline{\eta}(m,n) = \frac{s}{N} \sum_{i,OA(i,n)=m} \eta_i \qquad (6.7)$$

where s is the number of levels of parameter "n", N is the total number of experiments or rows of the orthogonal array, i is the experiment index, m is the level of parameter "n" at which its effect needs to be calculated. The results of the Taguchi's orthogonal array were analyzed in Minitab statistical software.

Table 6.5: Parameters with their selected levels for RFA with automatic temperature control for concentric tumour model

Factor	Units	Level 1(low)	Level 2(med)	Level 3(hig)
Tissue electrical conductivity (σ_1)	S /m	0.01998 [149]	0.148 [127]	0.3 [150]
Tissue thermal conductivity (k_1)	W/(m.K)	0.22 [149]	0.302 [127]	0.564 [127]
Tissue blood perfusion rate (ω_{b1})	1/s	0.00083 [127]	0.0167 [127]	0.067 [127]
Tumour electrical conductivity (σ_2)	S /m	0.01998 [149]	0.148 [127]	0.3 [150]
Tumour thermal conductivity (k_2)	W/(m.K)	0.22 [149]	0.302 [127]	0.564 [127]
Tumour blood perfusion rate (ω_{b2})	1/s	0.00083 [127]	0.0167 [127]	0.067 [127]

For this study tumour size of 2cm and 3cm was considered. As mentioned earlier, for tumours of larger size multiple insertions are required. A coupled electrothermal mathematical model was formulated and all the aforementioned factors were incorporated in the model to obtain the desired results. The model was implemented in COMSOL multiphysics software.

6.3.4 Results and Discussion

6.3.4.1 Effect of Electrical Conductivity

Figure 6.10 and 6.11 show the effect of electrical conductivity for tumour diameters of 2 cm and 3 cm in terms of variation in mean ablation volume and S/N ratio respectively.

For both tumour sizes of 2 cm and 3 cm diameter, it has been observed that as the tumour electrical conductivity is increased progressively, S/N ratio and ablation volume also increase. Notably the quantitative effect of this increase is different for

different tumour size. For example, the ablation volume for 2cm tumour is more sensitive to electrical conductivity than tumour of 3cm. This can be seen by different gradient in S/N ratio for both the sizes. For 3 cm tumour, the same increase in electrical conductivity results in smaller increase in S/N ratio as compared to 2cm tumour. This means that for a larger tumour, the ablation volume is mildly affected by the electrical conductivity as compared to a smaller tumour.

However, an increase in surrounding tissue electrical conductivity has a detrimental effect on the final achievable ablation volume. As the tissue electrical conductivity is increased the S/N ratio decreases which is undesirable. Conclusively, surrounding tissue with higher electrical conductivity would however result in a smaller ablation volume.

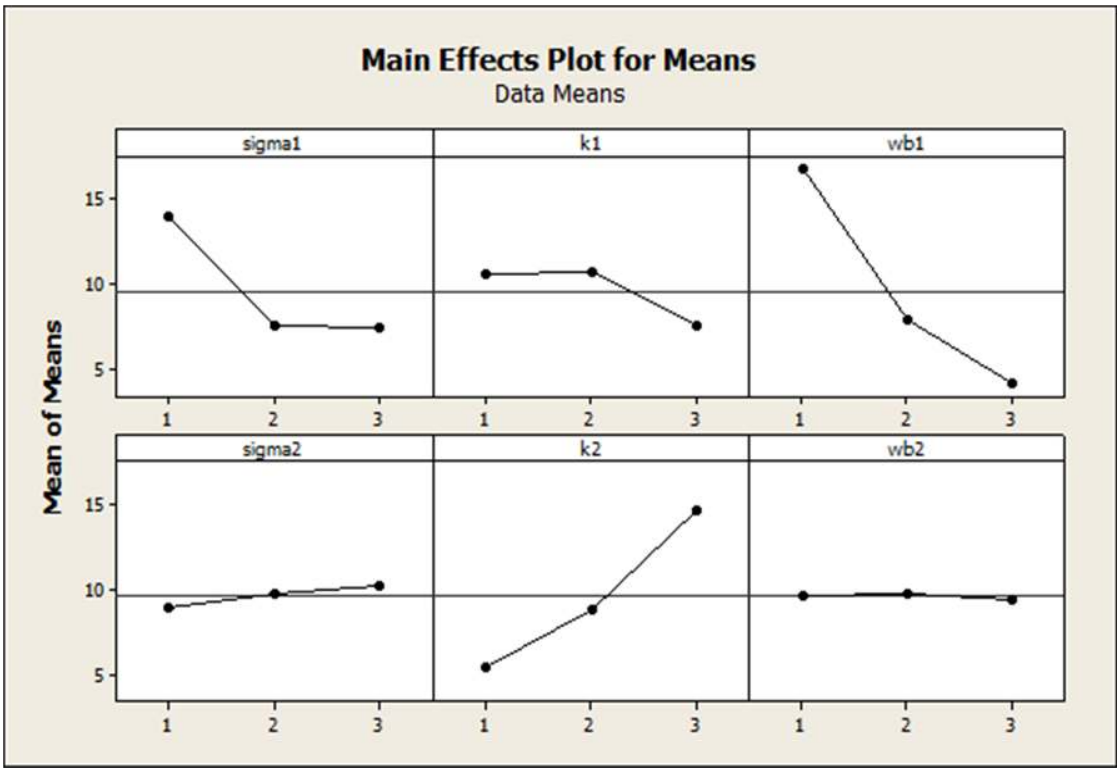

(a) 2cm tumour

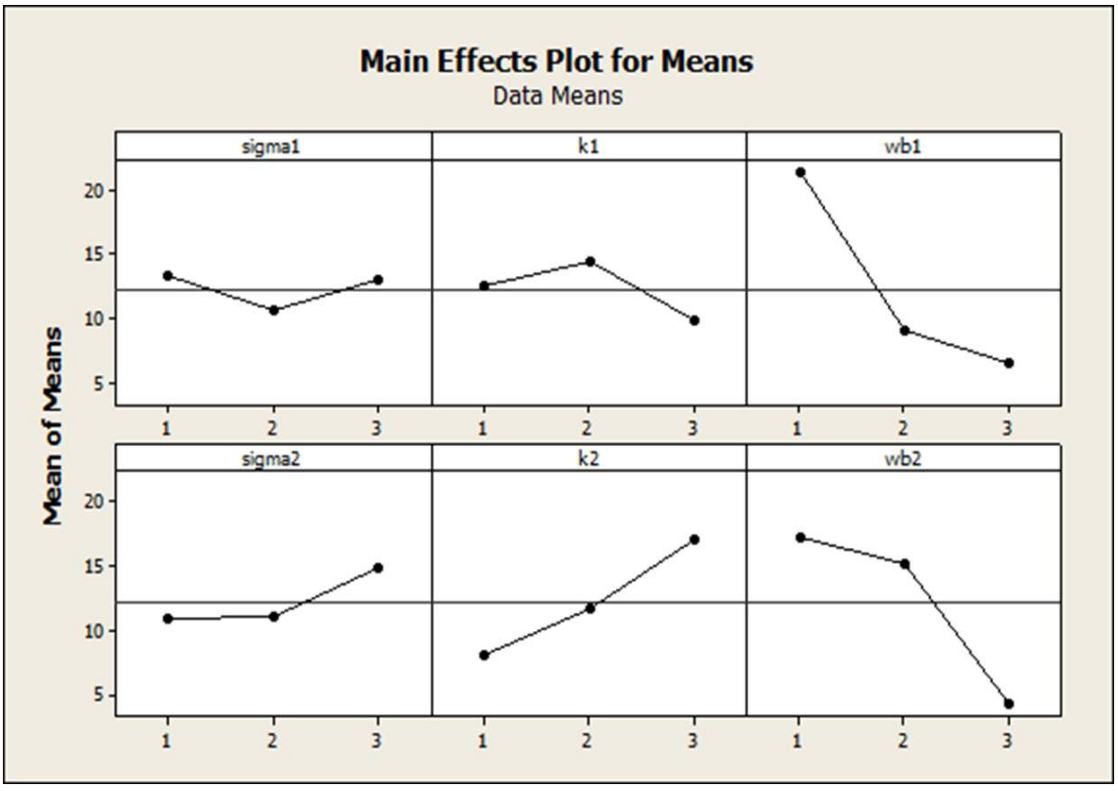

(b) 3cm tumour

Figure 6.10: Main effects plot for means for RFA with automatic temperature control for concentric tumour model with 2cm (a) and 3cm (b) tumour sizes with L=0.75*D

Another important factor to consider is the effect of tumour size. For smaller tumour (2cm) the effect of tissue electrical conductivity is more pronounced whereas for larger tumour (3cm) the ablation volume is less sensitive to the electrical conductivity.

6.3.4.2 Effect of Thermal Conductivity

From Figure 6.10 and 6.11 it can be seen that an increased thermal conductivity of the tumour results in a larger ablation volume. This effect seems to be similar for both the tumour sizes.

But as the surrounding thermal conductivity of the tissue is increased, the ablation volume decreases. The tumour in contact with the electrode gets heated directly. The energy delivered by the electrode needs to be conducted away to avoid overheating and to obtain larger ablation volume. The excess energy should preferably be localized to the tumour only. It signifies that higher thermal conductivity is beneficial for RFA and results in increased ablation volume. This is also elaborated by the higher S/N with increased thermal conductivity.

Likewise, a higher thermal conductivity of the surrounding tissue results in adverse gradient and flushes away the heat from the target zone which is undesirable. This is also verified by a decrease in S/N in response to increased thermal conductivity of peripheral tissue.

6.3.4.3 Effect of Blood Perfusion

It can be seen from Figure 6.10 and 6.11 that as the blood perfusion increases, it results in a corresponding decrease in the ablation volume. This effect is consistent for both the tissue and tumour perfusions.

Importantly, the effect of perfusion rate on the ablation volume is different for varying tumour size. For similar change in tumour blood perfusion rate, the change of ablation volume in 3 cm tumour is markedly higher compared to 2 cm tumour. This is evident from the higher gradients observed in S/N for 3 cm tumour.

It is also observed that for 2 cm tumour the ablation volume is less sensitive to the perfusion rate in tumour. This can be attributed to the fact that the negative effect of tumour perfusion for smaller tumour is to some extent overcome by the energy delivered by power delivery system. This phenomenon is also in accordance with the results reported elsewhere [152]. Furthermore, for a smaller 2 cm tumour, the change in S/N is more for surrounding tissue perfusion than the tumour perfusion. This implies that ablation volume is more sensitive to surrounding tissue perfusion rate.

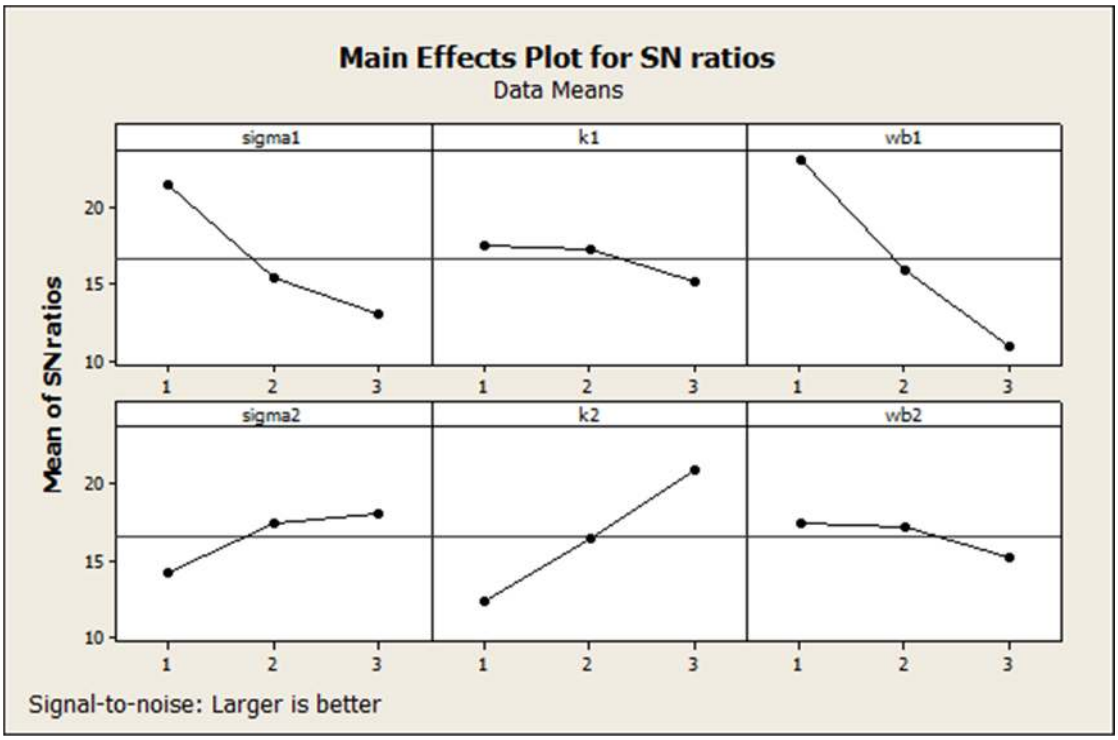

(a) 2cm tumour

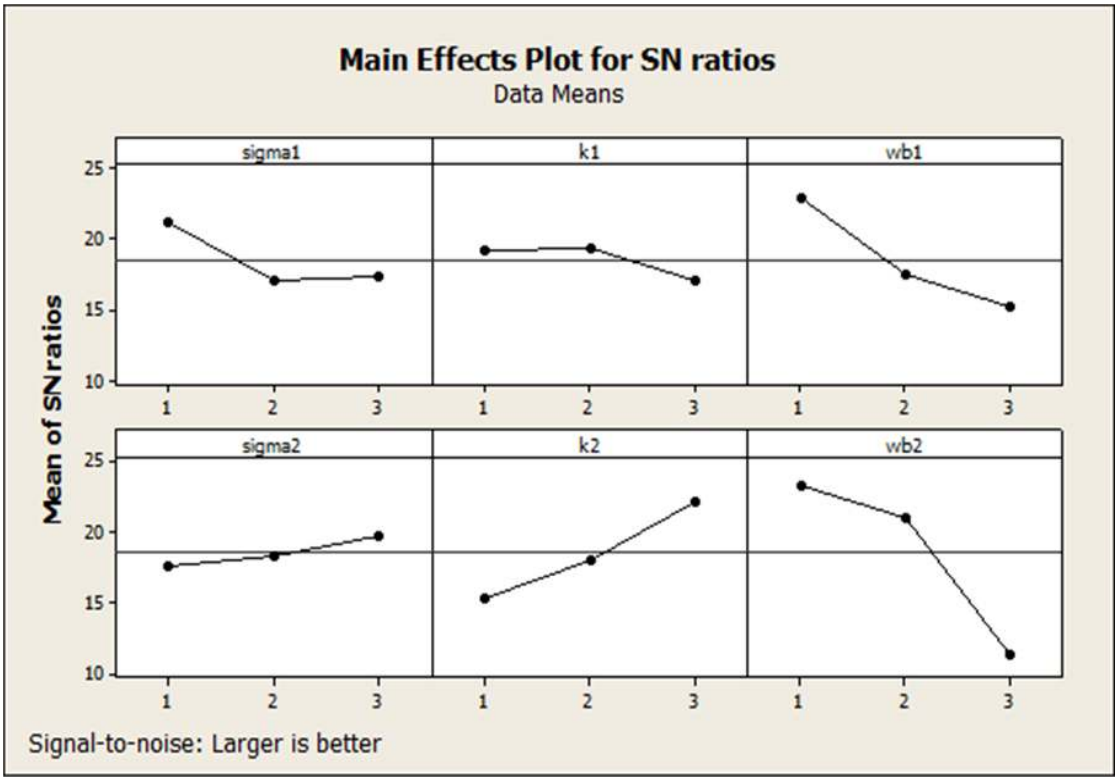

(b) 3cm tumour

Figure 6.11: Main effects plot for S/N ratio for RFA with automatic temperature control for concentric tumour model with 2cm (a) and 3cm (b) tumour sizes with L = 0.75*D

6.3.4.4 Evolution Dynamics of Ablation Volume

Figure 6.12 shows the evolution of ablation volume for the numerical experiments performed. Curves numbered from 1 to 27 represent the experiment number. It can be seen that the ablation volume increases at a different rate. This can be attributed to different tumour and surrounding tissue electrical and thermal properties. Initially, the ablation volume develops quickly which is signified by the initial higher gradient observed in Figure 6.12. After some finite time the ablation volume curve stabilizes and becomes asymptotic. This implies that within the physical constraints, maximum size of the lesion is limited. At some point away from the electrode, the heat lost to perfusion is more than the heat conducted by the ablation setup hence ablation volume beyond that cannot be obtained.

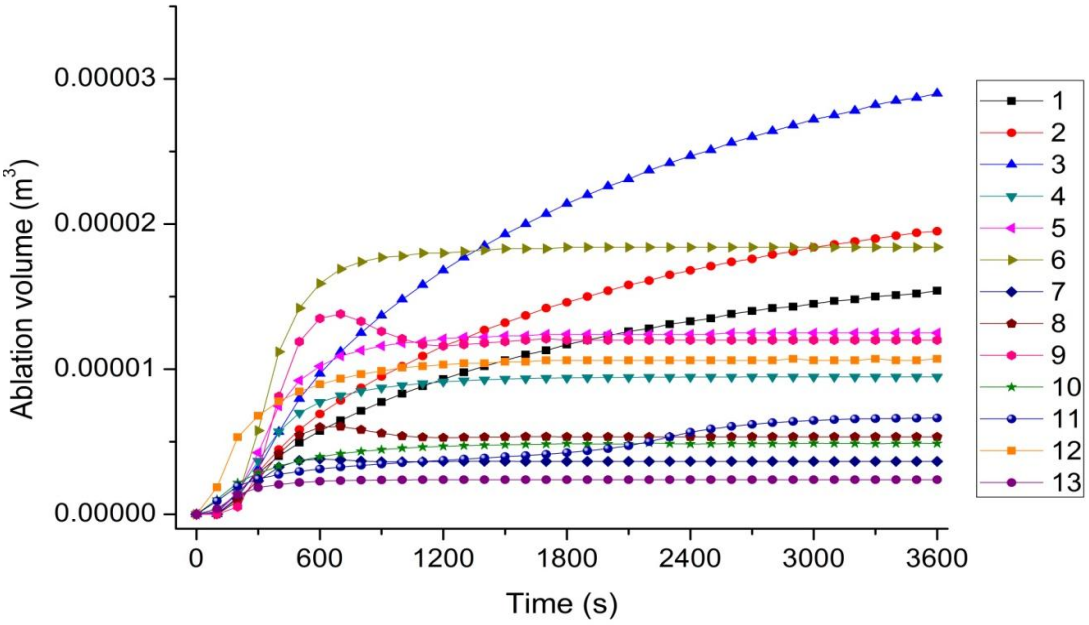

(a)

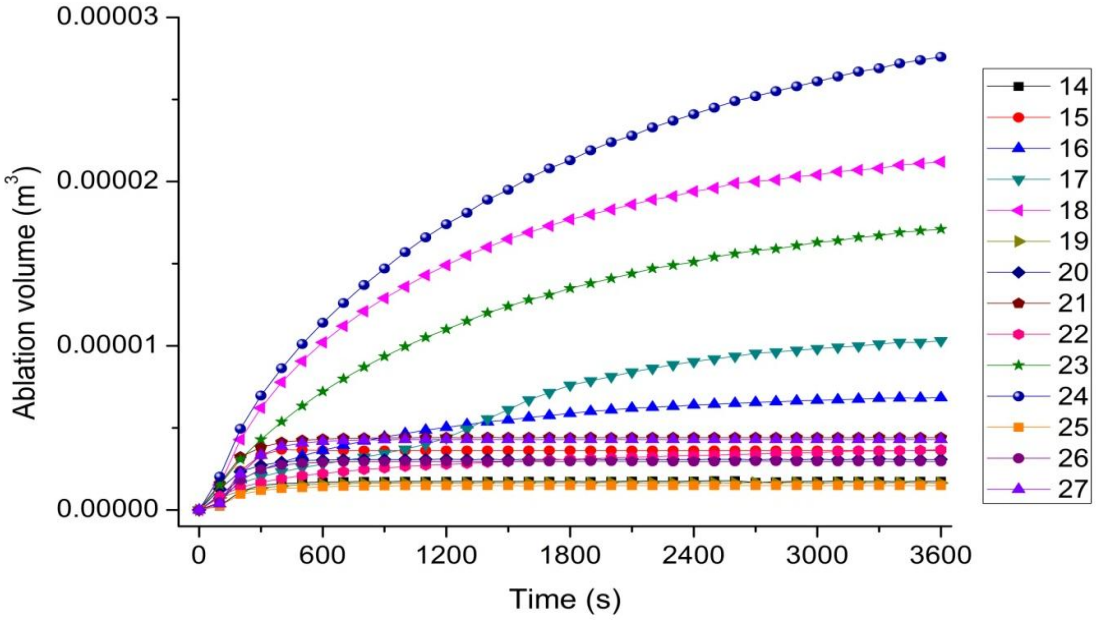

(b)

Figure 6.12: Evolution of ablation volume for RFA with automatic temperature control for concentric tumour model with 2cm tumour size with L = 0.75*D

6.3.4.5 Effect of Surrounding Tissue Properties

Figure 6.13 shows the temperature at the interface between tissue and tumour along the horizontal direction (interface with z=0 in Figure 6.5). The dashed line represents the critical or threshold temperature of 323.15 K. For experiments having temperature above the critical temperature, complete ablation has been achieved. The interface temperature for 2cm is consistently higher than 3 cm tumour. This is expected as for smaller size heat can be conducted easily away from the electrode and complete ablation is readily achieved. As can be seen from Figure 6.13, for 2cm tumour model, complete ablation is achieved in 14 out of 27 experiments. Conversely, in 3 cm tumour model complete ablation is achieved in only 6 experiments. This result underlines the inherent limitation of single electrode in achieving complete necrosis of large tumours and its inability of producing larger ablation volumes.

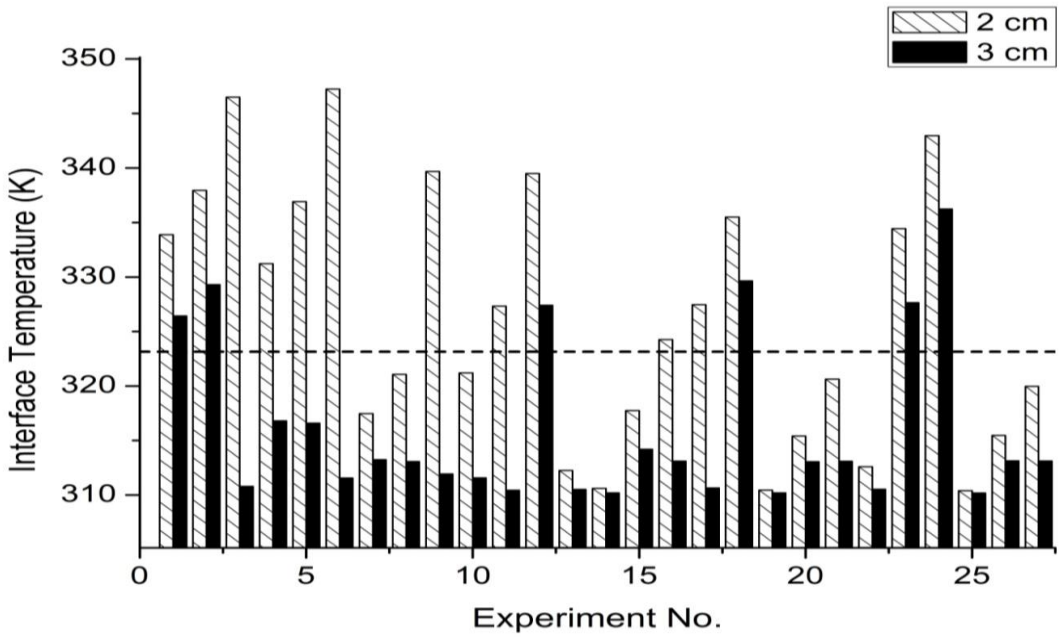

Figure 6.13: Interface Temperature along the horizontal line for RFA with automatic temperature control for concentric tumour model with 2cm and 3cm tumour with L = 0.75*D

Figure 6.14 shows the temperature at a point (r, z) = (0.01 m, 0) for tumour diameter of 2 cm and 3 cm with the same electrode length i.e. L = 0.75 * D_{2cm}. For 3 cm tumour this point lies inside the tumour domain whereas for 2 cm tumour it is situated at the interface. A meticulous observation of the graph reveals the effect of the surrounding tissue at the interface. It can be seen that the change in interface temperature of the 2 cm tumour is attributed to combined influence of surrounding tissue properties of electrical conductivity, blood perfusion rate and thermal conductivity because of the simultaneous changes in tissue properties dictated by Taguchi's orthogonal array (Table 6.4).

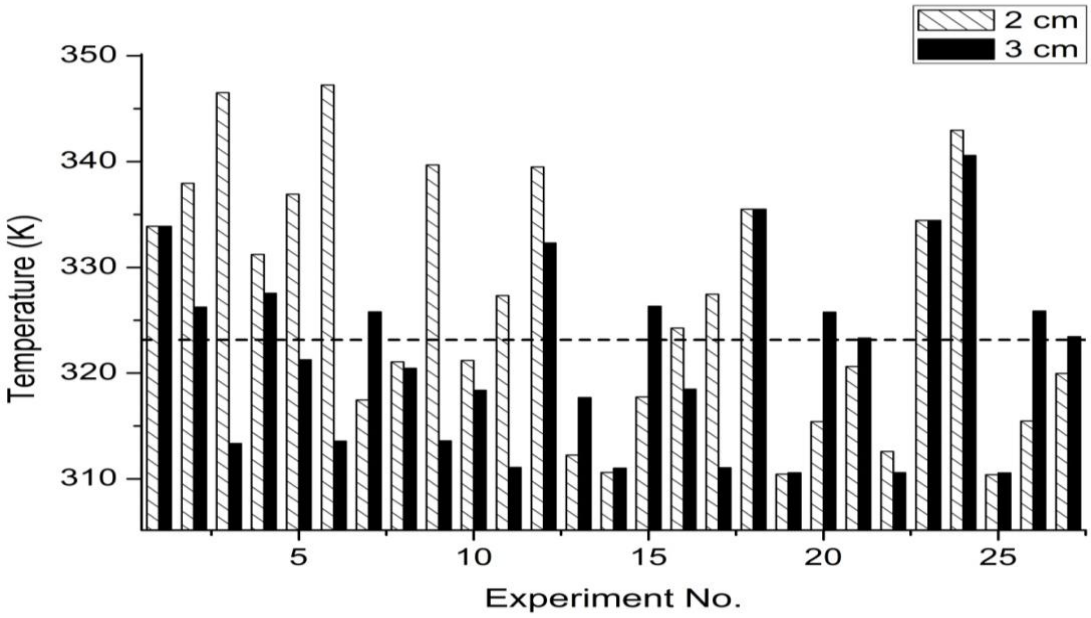

Figure 6.14: Temperature along the horizontal line at (r,z)=(0.01 m,0) for RFA with automatic temperature control for concentric tumour model with 2cm and 3cm tumour sizes with same active electrode length L = 0.75*D_{2cm}

Figure 6.15 shows the effect of surrounding tissue properties along the horizontal line at a point (r, z) = (0.01 m, 0). The surrounding tissue can cause an increase in temperature (i.e., Exp. No. 2-6, 8-12, 16, 17, 22, 24) which is most evident for Exp.

No. 3 and 6 where the temperature differential is more than 30 degrees. Similarly, the temperature can also decrease (i.e., Exp. No. 7, 13-15, 19-21, 25-27) which is most significant for Exp. No. 20 and 26 where there is temperature difference of more than 10 degrees. It is important to note that the overall change of temperature cannot be attributed to a single factor, instead it is the cumulative effect of the electrical and thermal properties of the surrounding tissue.

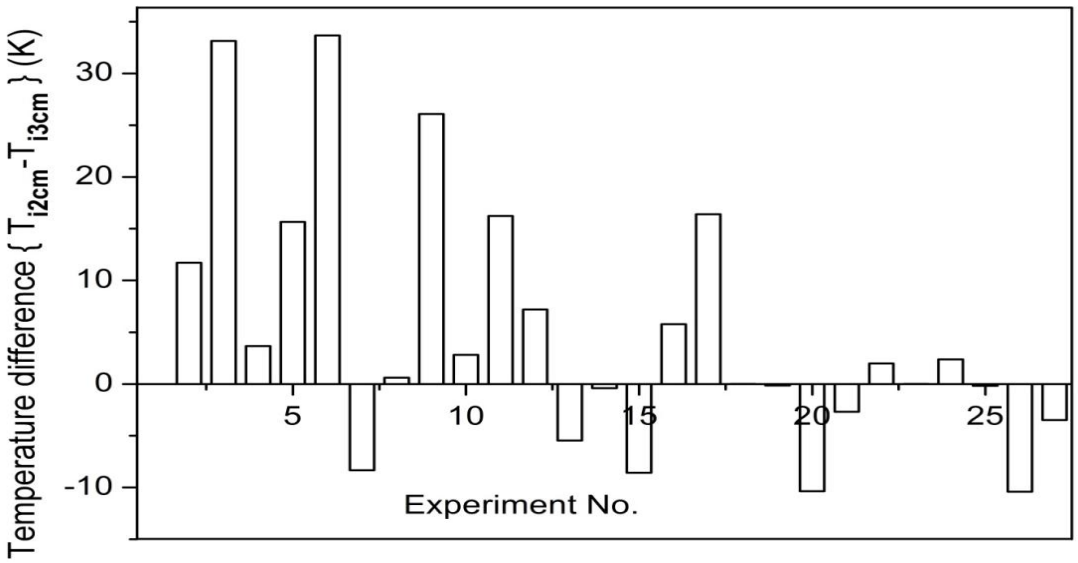

Figure 6.15: Temperature difference at along horizontal line at (r,z)=(0.01 m,0) for RFA with automatic temperature control for concentric tumour model with 2cm and 3cm tumour sizes with same active electrode length L = 0.75*D_{2cm}

6.4 Therapeutic Outcome Predictions Utilizing Simplified Models

6.4.1 Background

This study aims at developing the simplified models for the prediction of therapeutic output in radiofrequency ablation (RFA) and specifically deals with the RFA administration under automatic temperature control for needle type electrodes. The automatic temperature control is achieved by using a PID controller. These models hold promise for quick outcome prediction especially when the RFA has been applied to different tissues that include bone, kidney, liver, fat and heart tissues. The resulting outcome of the procedure is the ablation volume produced. In this research the RFA has been simulated for different tissues and simplified prediction models have been used to predict the ablation volume based on the evolving shape of the thermal lesion. The simplified models include spherical and ellipsoidal models that are characterized by 1 and 2 parameters respectively. The models are superimposed on the shape of the thermal lesion produced by the electrode in FEM COMSOL multiphysics simulation (i.e. called observed volume here forth) and their applicability was assessed by calculating the difference between the observed volume produced and the output predicted by the simplified models. In RFA the maximum temperature plays a pivotal role in delineating the efficacy of the therapy. The performance of the simplified models in response to different preset tip temperatures was also assessed.

For RFA ablation volume is the therapeutic output and for this study 50 ^{o}C isotherm contour has been used as the boundary of thermal damage. During the RFA the ablation volume slowly develops and achieves maxima after some time. Based on the

properties of the surrounding tissue, the shape of the thermal lesion varies. This research aims to predict the shape of the thermal lesion produced by using simplified models. The comparative analysis is carried out by comparing model predictions with the FEM simulation output.

6.4.1.1 Spherical Model (1 Parameter Model)

In this model, the observed RFA ablation shape is mimicked by fitting a spherical shape on it. It requires only one parameter i.e. radius of the ablation as shown in Figure 6.16. The difference between the simulated or the observed shape and the predicted shape is the error.

The centre of the sphere is at the midpoint of the active electrode length along the centreline. The volume predicted by the spherical model can be defined as:

$$V_{spherical} = \frac{4}{3}\Pi R^3 - V_e \tag{6.8}$$

where subscript e refers to electrode and V_e is the volume of part of the electrode inside the spherical shape and R is the radius of the spherical ablation shape. The percentage error between the observed volume and the volume predicted by spherical shape model is given by:

$$\text{Percentage error of prediction} = \left(\frac{V_{observed} - V_{spherical}}{V_{observed}} \right) \times 100\,\% \tag{6.9}$$

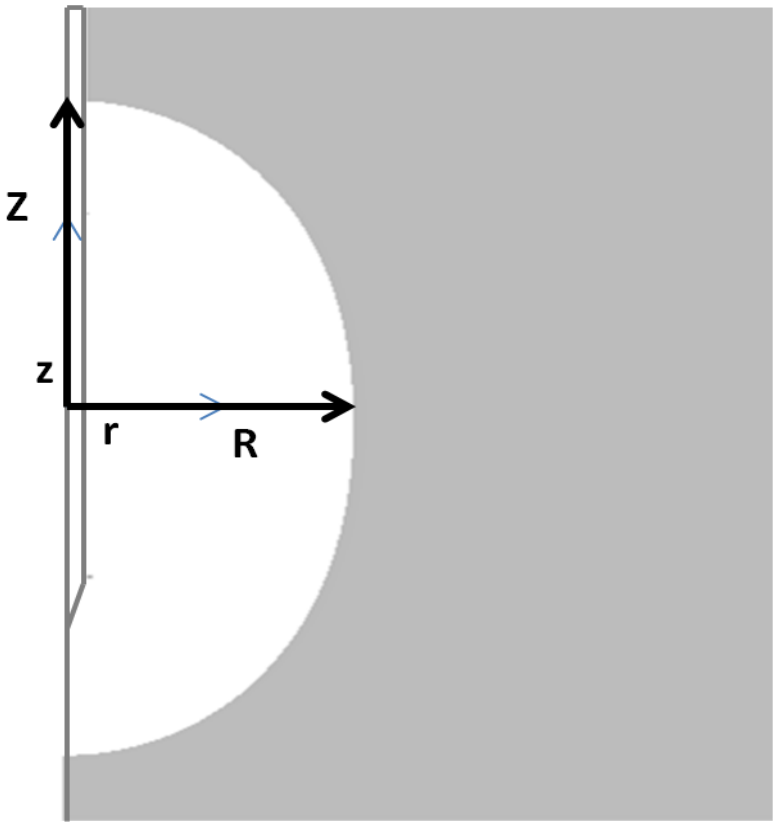

Figure 6.16: Nomenclature for simplified prediction models

6.4.1.2 Ellipsoidal Model (2 Parameters Model)

The ellipsoid model represents the shape of the model based on the ellipsoidal approximation. As shown in Figure 6.16, the ellipsoidal model can be characterized by two parameters i.e. radius of ablation R as the minor axis diameter and longitudinal distance Z as the major axis diameter i.e,

$$V_{elipsoidal} = \frac{4}{3}\Pi R^2 Z - V_e' \qquad (6.9)$$

where V_e' represents the volume of the electrode inside the ellipsoidal shape and Z represents the major axis diameter of the ellipsoid. The percentage error of prediction is defined as:

$$\text{Percentage error of prediction} = \left(\frac{V_{observed} - V_{elipsoidal}}{V_{observed}} \right) \times 100\,\% \qquad (6.10)$$

By utilizing these simplified models for the prediction of ablation shape, the ablation shape can be predicted very easily based on one or two parameters for spherical and ellipsoidal models respectively.

6.4.2 Modelling and Simulation

In this study the RFA has been applied to various tissue types that include bone, liver, lung, kidney and fat under automatic temperature control. The respective properties used are shown in Table 6.1. For mathematical modelling Equations 6.1-6.4 apply and COMSOL multiphysics was used for FEM simulation. COMSOL calculates the ablation volume (i.e. called observed volume here) by numerical integration over the domain. Automatic temperature regulation is achieved by utilizing PID controller and the simulation setup is shown in Figures 6.7-6.9. For the modelling purposes, same geometry as shown in Figures 6.5-6.6 is used with homogeneous tissue properties. Details regarding geometry and mesh have already been discussed earlier in section 6.3.2.

6.4.3 Results and Discussions

Table 6.6 shows the percentage error in prediction the ablation zone volume by utilizing spherical model. As can be seen that for bone and fat tissues, the spherical model results in least error of prediction at all setpoint temperatures. Similarly, applying spherical model for kidney resulted in highest error of prediction at all setpoint temperatures.

Table 6.6: Percentage error for spherical model for various tissues at different setpoint temperatures in ^{o}C

Setpoint temperature (^{o}C)	Bone	Liver	Lung	Kidney	Fat
60	43.10645	62.38923	52.63217	77.26958	42.39317
70	26.64134	44.89696	35.37322	62.50502	26.51985
80	19.02701	34.32643	26.0153	50.49575	19.00558
90	14.69305	27.89225	20.19239	42.30735	15.04103
100	11.92471	23.27707	16.43861	36.02215	12.47026

It can also be seen that as the setpoint temperature increases with extended heating duration, the error of prediction decreases for spherical model for all the tissues. For instance, for kidney tissue the error of prediction decreases from 77% to 36% as the setpoint temperature is increased from 60 ^{o}C to 100 ^{o}C. In short, the spherical model may be appropriate for bone, lung and fat where the location of the tumour is not critical and some error can be tolerated. But for liver and kidney the spherical model results in high errors of prediction and is not recommended that is cumulative effect of their electrothermal properties.

Table 6.7 shows the percentage error for ellipsoidal model for various tissues at different setpoint temperature. As can be observed for all the cases ellipsoidal model results in lesser error percentages as compared to spherical model. Kidney and Liver tissue result in prediction error of 22.18 % and 13.59% respectively at low setpoint temperature of 60 ^{o}C. Since these tissues have higher blood perfusion rates and at lower setpoint temperatures, the heat cannot be conducted far away from the electrode and the ablation shape resembles an ellipsoid. Similar to the case of spherical model, as the setpoint temperature is increased, the error of prediction

decreases for all the tissues. This suggests that the simplified models are better suited for predictions at higher setpoint temperatures. Since at higher temperatures the heat from the electrodes is conducted further away from the electrode and hence results in a larger ablation zone which resembles either an ellipsoid or a sphere.

Table 6.7: Percentage error for ellipsoidal model for various tissues at different setpoint temperature

Temperature (^{0}C)	Bone	Liver	Lung	Kidney	Fat
60	5.022539	13.59739	8.300829	22.18022	4.785699
70	1.665046	6.599583	3.562197	15.60979	1.783755
80	0.844741	3.472152	1.84419	9.399611	0.772086
90	0.451041	2.287943	0.99679	6.365512	0.455232
100	0.13985	1.536555	0.654729	4.283495	0.269936

The highest error for the ellipsoidal model results in kidney tissue (22.18 %) that gradually decreases (4.28 %) as the setpoint temperature is increased.

Figure 6.17 shows the variation of percentage prediction error with time for bone tissue at setpoint temperature of 100 ^{o}C. As is evident from Figure 6.17 that simplified models become more accurate as time progresses, until the prediction error settles down to a steady state error.

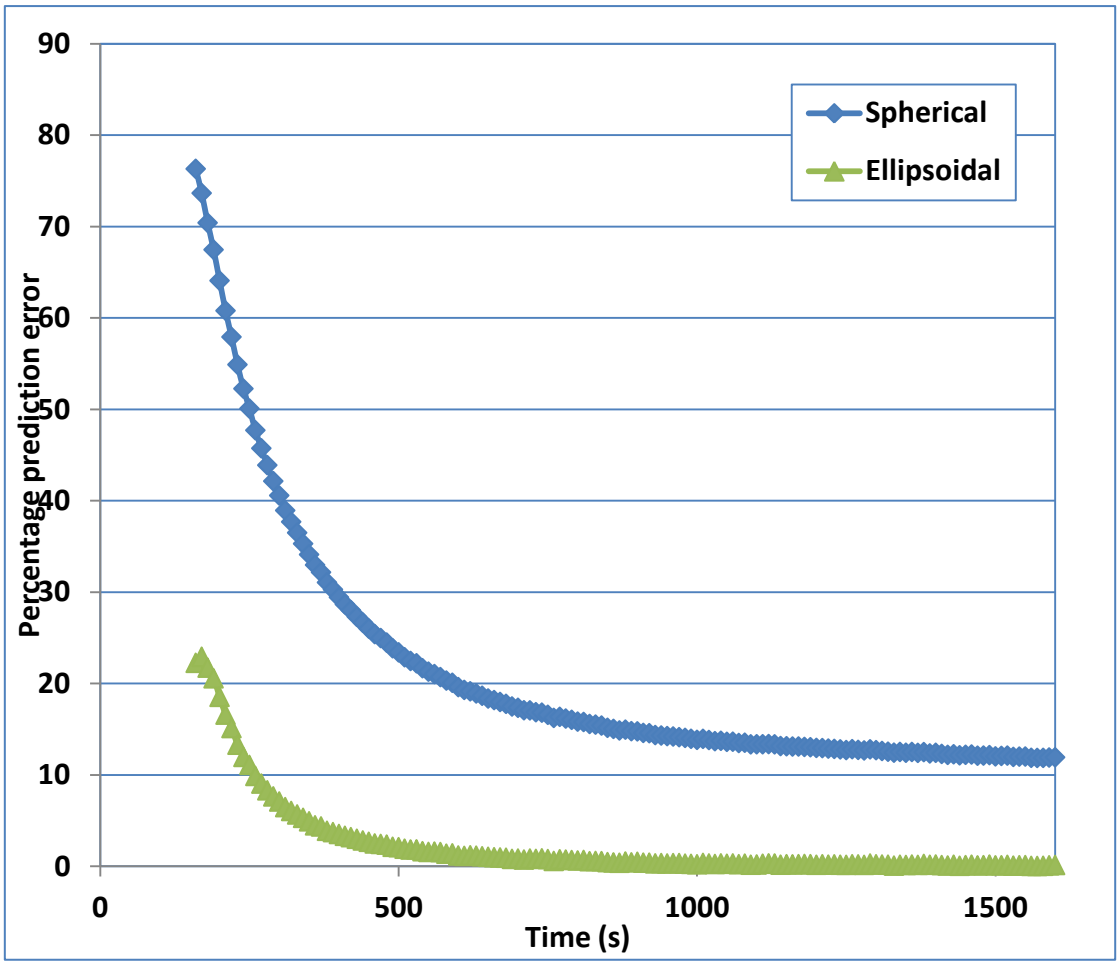

Figure 6.17: Percentage error vs. time for simplified prediction models for bone tissue at the setpoint temperature of 100 ^{o}C

Figure 6.18 presents the percentage prediction error for bone tissue with time at setpoint temperature of 60 ^{o}C. As can be seen that the percentage error decreases with time and becomes constant at longer times. A comparison of Figure 6.17 and Figure 6.18 reveals that the error reduction gradient is more for higher setpoint temperature case.

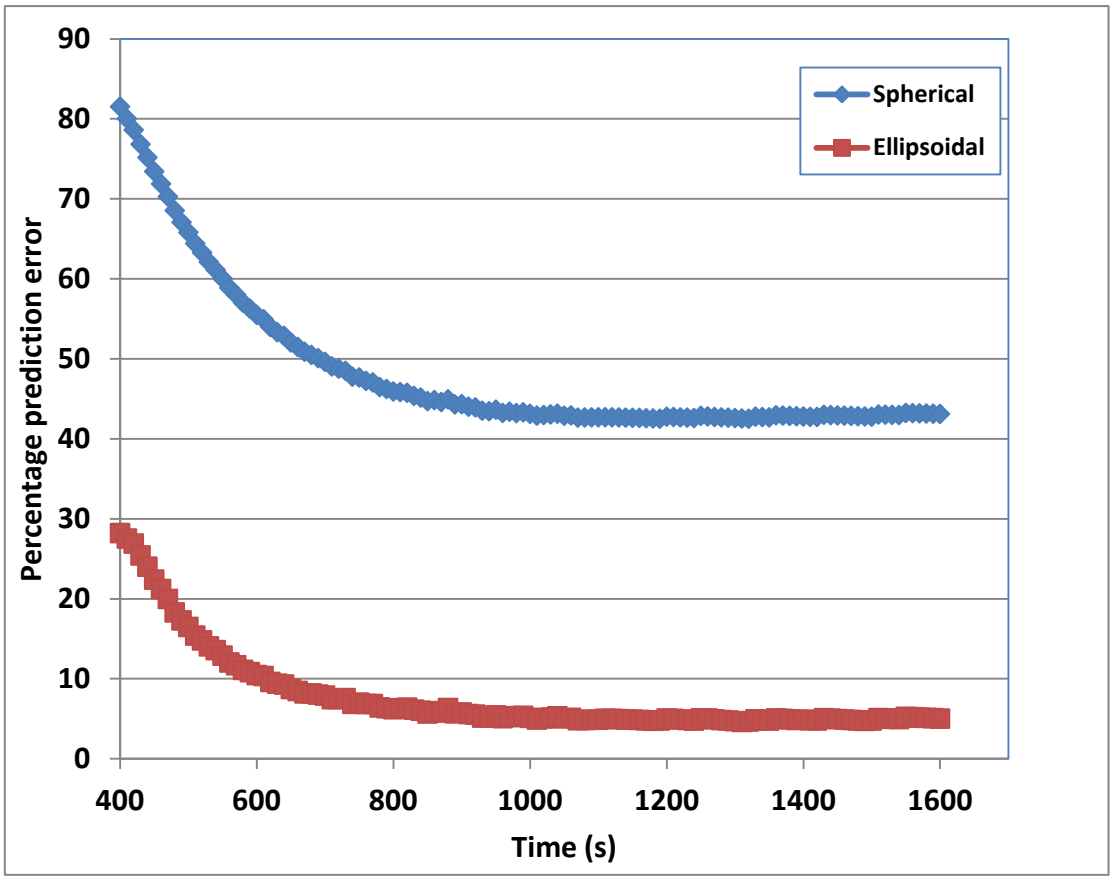

Figure 6.18: Percentage error vs. time for simplified prediction models for bone tissue at setpoint temperature of 60 ^{o}C

Chapter 7: Conclusions and Future Work

The conclusions drawn from the previous chapters can be summarized into three sections which deal with capacitive hyperthermia, meshless methods and radiofrequency ablation studies respectively.

7.1 Conclusions Related to Electromagnetic Heating in Capacitive Hyperthermia

1. Taguchi's design of experiments was used in an attempt to rank the parameters in hyperthermia therapy treatment planning which is based on Pennes bioheat equation. Six parameters namely tumour metabolic rate, tissue metabolic rate, tissue blood perfusion, tumour blood perfusion, voltage and frequency were considered and it was concluded that voltage and frequency are the most important factors to consider during the hyperthermia treatment planning. It is also important for a medical practitioner to appreciate that blood perfusion in tissue and tumour can also have significant effect on the maximum achieved temperature. As per the literature on characteristic of the tumour, in some cases tumour gets its supply of oxygen and nutrients from a single large vein. If this blood supply is reduced partially or completely by plugging the vein, it shall greatly improve the efficacy of the treatment. From medical practitioner's point of view, the information regarding the parameters involved in the therapy is of utmost importance and any irregularity, out of lack of knowledge or negligence on the part of the practitioner, could result in lethal outcome. This study concludes that applied voltage and frequency are the two most important parameters that could affect the outcome of the therapy. The

practitioner must prioritize the parameters involved and careful consideration must be made for the selection of most important parameters involved i.e. voltage and frequency.

2. In this research, the capacitive hyperthermia was analyzed from the physical perspective. Physical dimensions were treated as parameters and total of six parameters were selected including two tunable parameters namely frequency and applied voltage. Maximum achieved temperature inside the domain was treated as the relevant quality characteristic. Following a systematic analysis underlined by Taguchi's L27 orthogonal array, the effect of each selected parameter was quantified. Moreover, under the framework of capacitive hyperthermia it was concluded that for reliable treatment promising optimum results, thermal damage to the tissue as well as to the tumour needs to be taken into account. Results were analyzed from two perspectives, from treatment objective point of view and from the aspect of tumour killing efficiency. In this context two indices namely treatment index and damage index were defined which highlight the respective perspective quantitatively. It was concluded that treatment objective may be achieved but it may not represent the most efficient treatment protocol. Higher values of both, treatment and damage indices, would qualify a treatment protocol to be the optimum one.

3. The work demonstrated the use of multiple linear regression analysis for the prediction of maximum achievable temperature inside the biological tissue for electrode based thermal therapy. Electrode based thermal is a coupled electro-thermal problem. To obtain an accurate temperature field inside the biological tissue, complex bioheat and Maxwell's equations need to be solved simultaneously that

require considerable effort and resources. Multiple regression presents itself as an alternative to the rigorous numerical software. Original linear model was able to explain most of the data but modified linear model performed even better and was able to explain approximately 90 % of the variation in the response variable. It was concluded that multiple regression model can provide accurate prediction of maximum achieved temperature for current problem of electrode based thermal therapy.

7.2 Conclusions Related to Radial Basis Collocation Method

Calculation of temperature field inside the biological tissue is imperative in view of the thermal therapies whose outcome is dependent on the final achieved temperature. Numerical simulation presents itself as a cheap and inexpensive alternative to the experimental measurement which for the most cases is impractical because of the difficulties associated with the accurate measurements in vivo, high cost or the variety of problems. Moreover, special care is required to deal with the problems involving strong heterogeneity. To overcome such issues, a meshfree method known as Radial Basis Collocation Method (RBCM) was successfully applied to simulate steady state heterogeneous heat conduction and bioheat transfer. RBCM was able to provide accurate information about the temperature field for the cases of heterogeneous heat conduction and bioheat transfer. The solutions remained continuous for problems involving heterogeneous heat conduction with extreme heterogeneity and heat source. Features of RBCM such as accuracy, point based data dependency, ease of implementation together with meshless property make it an attractive alternative to the other numerical methods available.

7.3 Conclusions Related to Radiofrequency Ablation (RFA)

1. Radiofrequency ablation is increasingly being used for treatment of various tissues. Each tissue possesses its own characteristic parameter values and RFA efficacy in one particular tissue cannot be generalized to all the tissues. To tackle this variability based on tissue type, the effect of thermal conductivity, electrical conductivity and blood perfusion was firstly quantified using the efficient Taguchi's design of experiment approach. It was concluded that higher values of electrical conductivity and blood perfusion tend to decrease the final ablation volume whereas higher thermal conductivity has an additive effect for the ablation volume. RFA results were obtained for different tissue types and it was concluded that least ablation volume resulted for kidney tissue whereas highest volume was achieved for muscle tissue. The effect of individual parameters and a comparative analysis of various tissues provide an insight to application of RFA for different tissues. Furthermore, it would prove helpful in designing of optimal control system for various tissues which regulates the input parameters based on the system parameter sensitivity. It is intended that these conclusions will help the radiologist in treatment planning stage and would serve as broad guidelines for the application of RFA in varying biological environment.

2. Radiofrequency ablation as a treatment modality has been increasingly utilized for treatment of cancer especially for non resectable tumours. In order to apply RFA as an alternative treatment modality, the factors that influence the outcome of the therapy need to be dealt with perceptively.

In this study the effect of tissue as well as tumour properties on the RFA was quantitatively analyzed using the Taguchi's design of experiment technique. The temperature was controlled via PID controller and the ablation volume was considered as the response variable. The behaviour of the ablation volume is dynamic owing to the dynamic properties of the tissue and tumour. The temperature dependency of the electrothermal properties was also accommodated in the model for better correlation with the clinical environment. It was concluded that increasing the electrical and thermal conductivity of the tumour and surrounding normal tissue has an opposing effect on the achieved ablation volume. Increasing the conductivities of the tumour encourages the ablation volume whereas increase in conductivities of the surrounding tissue decreases the ablation volume. Similarly increase in blood perfusion has a homogenous effect of decreasing the ablation volume. Juxtaposedly, the effect of thermal conductivity, electrical conductivity and blood perfusion rate is not harmonious for different tumour size which is manifested by different gradient in ablation volume for same change in the parameter values. It was also observed that for small tumour the ablation volume is less affected by the tumour blood perfusion rate. These findings can be useful to further our understanding the RFA and hold promise towards achieving successful treatment objective as well as enhanced therapeutic output via improved treatment planning and strategy.

3. Radiofrequency ablation has been utilized for various tissue types. The protocols for RFA depend on the size and location tumour and electrode as well as on the type of tissue. The bottleneck in RFA administration is the limitation on the maximum temperature which should not increase above a threshold temperature.

Various numerical methods have been utilized for prediction of results in different tissue types. These methods are rigorous but require costly computational resources. To predict the accurate outcome of the therapy these methods can take longer time. To overcome this, generic simplified models that depend on geometric parameters are used which can efficiently predict outcome with minimal effort. These include spherical model and ellipsoidal model. It was concluded that for tissues like kidney, the ellipsoidal model can provide a good estimate of the ablation zone with more than 95% accuracy. Similarly for tissues like fat and bone, circular model provides more realistic prediction with an accuracy of more than 80 percent. In general, the accuracy of both these models is poor at smaller times and their prediction becomes more accurate as the ablation zone develops fully. In additional to that, the accuracy of these models increases with increase in setpoint temperature.

7.4 Contributions of the Thesis

1. With regard to capacitive hyperthermia the parameters were ranked quantitatively using Taguchi's experimental design and ANOVA. This will provide the order of preference in dealing with each parameter and would supplement and extend the radiologist's ability to treat cancer.

2. The physical dimensions like size of tumour, depth of tumour, size and position of electrodes were considered as parameters and their effect on the overall objective was quantified along with the tunable parameters.

3. The therapy was analyzed from the perspective of achievement of treatment objective and efficiency of tumour killing and subsequently two indices namely

treatment index and damage index, were defined that deal with the former and the latter perspective respectively.

4. Multiple linear regression model was formulated which presents itself as an attractive alternative to prevailing rigorous numerical models to predict the maximum achievable temperature inside the domain with physical and tunable parameters as model inputs. Inferential statistics was used to remove the inadequacies as well as to discriminate the location of maximum temperature between tissue and tumour domain.

5. A novel meshless method Radial Basis Collocation Method (RBCM) was applied to simulate the heterogeneous conduction and bioheat transfer problems which gave encouraging results even in the case of strong heterogeneities.

6. Within the purview of RFA with limitation on maximum temperature, the effect of individual factors and their combined effect for various tissues was quantified.

7. In the context of RFA with fixed temperature control, analysis was supplemented by efficient experimental design to quantify the effect of various parameters for concentric tumour model surrounded by normal tissue.

8. Predictive models requiring few geometric inputs were presented for different tissue types that can provide fast and efficient therapeutic output.

7.5 Limitations of the Present Work

1. For capacitive hyperthermia studies 2D geometry with simplified tumour shape was used but in reality the tumour shapes are complex and better perspective

can be achieved by modelling the full 3D geometry. Similarly, in RFA studies the modelled tumour shape epitomizes a simplification.

2. In these studies temperature isocontour is considered as the demarcation for thermal damage and effect of electrode is not included exclusively. Clinically more congruent results can be obtained by making use of time, temperature and tissue specific damage models i.e. Arrhenius damage model, provided that the tissue specific parameters are available.

3. For RBCM application the results presented in this thesis are based on the Inverse Multiquadratic (IMQ) RBFs and equally distributed points. For other RBFs and point distributions, the results may change.

4. The results presented are for single needle type electrode and are relevant only to system response generated by the control parameters used in this study. Moreover, the thermoregulatory response of the body owing to temperature increase is not considered in this study.

7.6 Future work

The author would like to recommend the following future directions to extend and supplement the current research work.

1. In the context of capacitive hyperthermia, the current research is based on the 2D modelling with simplified tumour shape. This can be extended to 3D modelling and complex real tumour shape tracing. The 2D results can be pitched against the 3D results obtained by utilizing the 3D geometry and accompanying incongruencies in parameter effects can be explored. This will provide a more

holistic purview of the therapeutic outcome. Moreover, the rigorousness in terms of tri-dimensional modelling and complex tumour shape, would lead to more comprehensive database which subsequently will contribute in developing more general and reliable predictive models.

2. In this research single needle type electrode is used. In future work it can be expanded to include more electrode types and sizes. By including multitude of electrode types, it can be seen whether the results presented in this research can be integrated to all types of electrodes or not.

3. Additionally, the case of multiple electrode insertions for larger tumours can be tackled. It would be insightful to observe the ablation volume sensitivity to size, arrangement and number of electrodes.

4. Pennes bioheat equation incorporates the effect of small blood vessels by an additional term containing the blood perfusion rate. Future research can be carried out to exclusively model the large blood vessels. It will be interesting to explore the effect of blood vessels and their size on the evolution of ablation volume and whether there is any change in the effect of parameters in the presence of blood vessels.

5. Future research can be directed for the application of RBCM for 3D geometries along with complex tumour shapes and the effect of different point distributions. RBCM can be applied utilizing other RBFs. It would be interesting to observe the performance of other RBFs under the framework of RBCM.

6. In this research, RBCM has been applied to heterogeneous conduction and bioheat transfer simulation by catering to only the thermal phenomenon. Further work can be carried out in extending the application of RBCM for fully coupled electrothermal problem which would provide results that are more congruent to the clinical environment.

7. In this research, the performance of simplified models was gauged for the case of single needle type electrode. Future research can be carried out to explore the performance of these models for other electrode types. It is expected that for electrodes of complicated shapes, the modified models may require more number of input parameters. Furthermore, it will be insightful how their predictive capability is affected by the presence of large blood vessels and their sensitivity to vessel size and location.

8. In this research, same control parameters were used for all types of tissues. Further research can be directed towards optimisation of control parameters for each tissue type to obtain the optimum results. Lastly, the thermoregulatory response of each tissue type can be incorporated in the modelling phase and the implications for control algorithm can be explored.

References

[1] Globocan 2008, IARC, 2010.

http://globocan.iarc.fr/factsheets/populations/factsheet.asp?uno=900 (last access: March 2013).

[2] Cancer facts and figures 2013.

www.cancer.org/acs/groups/content/.../documents/.../acspc-036845.pdf (last access: April 2013).

[3] Ministry of Health. Principal Causes of Death. Health Facts Singapore.

www.moh.gov.sg/content/moh_web/home/statistics/Health_Facts_Singapore/Principal_Causes_of_Death.html (last access:March 2013).

[4] Taguchi G. Computer based robust engineering: Essentials for DFSS. WI: ASQ Quality Press: Milwoukee, 2004.

[5] Kacker RN, Lagergren ES, Filliben JJ. Taguchi based orthogonal arrays are classical designs of experiments. Journal of Research of the National Institute of Standards and Technology. 1991; 96: 577-591.

[6] Kacker RN, Lagergren ES, Filliben JJ. Taguchi fixed-element arrays are fractional factorials. Journal of Quality Technology. 1991; 23: 107-116.

[7] Habash RWY, Bansal R, Krewski D, Alhafid HT. Thermal Therapy, Part IV: Electromagnetic and Thermal Dosimetry. 2007; 35: 123-182.

[8] Stuchly MA, Athey TW, Stuchly SS, Samaras GM, Taylor G. Dielectric properties of animal tissues in vivo at frequencies 10 MHz – 1 GHz. Bioelectromagnetics. 1981; 2: 93-103.

[9] W. Y. Habash RB, Daniel Krewski and Hafid T. Alhafid. Thermal Therapy, Part IV: Electromagnetic and Thermal Dosimetry. Critical Reviews™ in Biomedical Engineering. 2007; 35: 123-182

[10] Douglas A. Christensen CF, Carl H. Durney. Electric and Magnetic Fields. Basic Introduction to Bioelectromagnetics, Second Edition. CRC Press, 2009, p. 1-43.

[11] Khanafer K, Vafai K. Synthesis of Mathematical Models Representing Bioheat Transport. Advances in Numerical Heat Transfer, Volume 3. CRC Press, 2009, p. 1-28.

[12] Pennes HH. Analysis of tissue and arterial blood temperature in the resting human forearm. Journal of Applied Physiology. 1948; 1: 93-122.

[13] Lv YG, Deng ZS, Liu J. 3-D numerical study on the induced heating effects of embedded micro/nanoparticles on human body subject to external medical electromagnetic field. IEEE Transactions on Nanobioscience. 2005; 4: 284-294.

[14] Deng Z-S, Liu J. Theoretical Evaluation on the Thermal Effects of Extracellular Hyperthermia and Intracellular Hyperthermia. ASME Conference Proceedings. 2007; 2007: 827-828.

[15] Rosensweig RE. Heating magnetic fluid with alternating magnetic field. Journal of Magnetism and Magnetic Materials. 2002; 252: 370-374.

[16] Wulff W. The Energy Conservation Equation for Living Tissue. Biomedical Engineering, IEEE Transactions on. 1974; BME-21: 494-495.

[17] Klinger H. Heat transfer in perfused biological tissue—I: General theory. Bulletin of Mathematical Biology. 1974; 36: 403-415.

[18] Holmes MMCaKR. Microvascular Contributions in Tissue Heat Transfer. Annals NY Acad Sci. 1980; 335: 137-150.

[19] Weinbaum S, Jiji LM. A new simplified bioheat equation for the effect of blood flow on local average tissue temperature. Journal of Biomechanical Engineering-Transactions of the Asme. 1985; 107: 131-139.

[20] Xu F, Lu T. Skin Bioheat Transfer and Skin Thermal Damage. Introduction to Skin Biothermomechanics and Thermal Pain. Springer Berlin Heidelberg, 2011, p. 23-68.

[21] Tzou DY. Macro- to Microscale Heat Transfer: The Lagging Behavior. 1997.

[22] Stauffer PR. Evolving technology for thermal therapy of cancer. International Journal of Hyperthermia. 2005; 21: 731-744.

[23] Douglas A. Christensen CF, Carl H. Durney. Electromagnetics in Medicine. Basic Introduction to Bioelectromagnetics, Second Edition. CRC Press, 2009, p. 229-251.

[24] B. Zhang MM, E. Zhang, W. J. Zhang. Radiofrequency ablation technique in the treatment of liver tumours: review and future issues. Journal of Medical Engineering & Technology. 2013; 37: 150-159.

[25] Roti JLR. Cellular responses to hyperthermia (40-46 degrees C): Cell killing and molecular events. International Journal of Hyperthermia. 2008; 24: 3-15.

[26] Moritz AR. Studies of thermal injury.III. The pathology and pathogenesis of cutaneous burns - An experimental study. American Journal of Pathology. 1947; 23: 915-941.

[27] Moritz AR, Henriques FC. Studies of thermal injury .II. The relative importance of time and surface temperature in the causation of cutaneous burns. American Journal of Pathology. 1947; 23: 695-720.

[28] Henriques FC, Moritz AR. Studies of thermal injury. I.The conduction of heat to and through skin and the temperatures attained therein - A theoretical and experimental investigation. American Journal of Pathology. 1947; 23: 530-549.

[29] Zhang A, Xu LX. Numerical Bioheat Transfer in Tumor Detection and Treatment. Advances in Numerical Heat Transfer, Volume 3. CRC Press, 2009, p. 149-195.

[30] Xu YS, Qian RZ. Analysis of thermal injury process based on enzyme deactivation mechanisms. Journal of Biomechanical Engineering-Transactions of the Asme. 1995; 117: 462-465.

[31] Berjano EJ. Theoretical modeling for radiofrequency ablation: state-of-the-art and challenges for the future. Biomedical Engineering Online. 2006; 5.

[32] Montgomery DC. Introduction to statistical quality control. Canada: Wiley, 1985.

[33] Fisher RAS. Statistical methods for research workers / by R.A. Fisher. London, UK: Oliver & Boyd, 1925.

[34] Fisher RAS. The Arrangement of Field Experiments. Journal of the Ministry of Agriculture of Great Britain. 1926; 33: 503-513.

[35] Montgomery DC, Runger GC. Applied statistics and probability for engineers. New York: Wiley, 1994.

[36] Roy RK. Design of Experiments Using the Taguchi Approach: 16 Steps to Product and Process Improvement. NJ: John Wiley & Sons:Hoboken, 2001.

[37] Badkar DS, Pandey KS, Buvanashekaran G. Parameter optimization of laser transformation hardening by using Taguchi method and utility concept. International Journal of Advanced Manufacturing Technology. 2011; 52: 1067-1077.

[38] Erzurumlu T, Ozcelik B. Minimization of warpage and sink index in injection-molded thermoplastic parts using Taguchi optimization method. Materials & Design. 2006; 27: 853-861.

[39] Jones DM, Watton J, Brown KJ. Comparison of hot rolled steel mechanical property prediction models using linear multiple regression, non-linear multiple

regression and non-linear artificial neural networks. Ironmaking & Steelmaking. 2005; 32: 435-442.

[40] Oktem H, Erzurumlu T, Col M. A study of the Taguchi optimization method for surface roughness in finish milling of mold surfaces. International Journal of Advanced Manufacturing Technology. 2006; 28: 694-700.

[41] Suherman H, Sahari J, Sulung AB. Optimization mixing parameters on the electrical conductivity of polymer nanocomposites based on the Taguchi method. In: Zhou M, (ed.). Advances in Mechanical Engineering, Pts 1-3. Stafa-Zurich: Trans Tech Publications Ltd, 2011, p. 31-36.

[42] Wang SB, Pan C. Two-phase flow instability experiment in a natural circulation loop using the Taguchi method. Experimental Thermal and Fluid Science. 1998; 17: 189-201.

[43] Hsieh CT, Jang JY. Parametric study and optimization of louver finned-tube heat exchangers by Taguchi method. Applied Thermal Engineering. 2012; 42: 101-110.

[44] Chen CY, Liu KC, Chen HH, Pan LK. Optimizing the TLD-100 readout system for various radiotherapy beam doses using the Taguchi methodology. Applied Radiation and Isotopes. 2010; 68: 481-488.

[45] Lee RS, Bakthavatsalam R, Marsh CL, Kuhr CS. Ureteral complications in renal transplantation: A comparison of the Lich-Gregoir versus the Taguchi technique. Transplantation Proceedings. 2007; 39: 1461-1464.

[46] Caetano-Anolles G. DAF optimization using Taguchi methods and the effect of thermal cycling parameters on DNA amplification. Biotechniques. 1998; 25: 472-476,478-480.

[47] Goran MI. Estimating energy requirements: regression based prediction equations or multiples of resting metabolic rate. Public Health Nutrition. 2005; 8: 1184-1186.

[48] Morsi H, Yong K, Jewell A. Evaluation of the Taguchi methods for the simultaneous assessment of the effects of multiple variables in the tumour microenvironment. International Seminars in Surgical Oncology. 2004; 1: 7.

[49] Kokaly RF, Clark RN. Spectroscopic determination of leaf biochemistry using band-depth analysis of absorption features and stepwise multiple linear regression. Remote Sensing of Environment. 1999; 67: 267-287.

[50] Mac Nally R. Regression and model-building in conservation biology, biogeography and ecology: The distinction between and reconciliation of 'predictive' and 'explanatory' models. Biodiversity and Conservation. 2000; 9: 655-671.

[51] Mac Nally R. Multiple regression and inference in ecology and conservation biology: further comments on identifying important predictor variables. Biodiversity and Conservation. 2002; 11: 1397-1401.

[52] White JW, Boote KJ, Hoogenboom G, Jones PG. Regression-based evaluation of ecophysiological models. Agronomy Journal. 2007; 99: 419-427.

[53] Li WF, Miyajima C, Nishino T, Itou K, Takeda K, Itakura F. Adaptive nonlinear regression using multiple distributed microphones for in-car speech recognition. Ieice Transactions on Fundamentals of Electronics Communications and Computer Sciences. 2005; E88A: 1716-1723.

[54] Xiang S, Jin Y-X, Jiang S-X, Bi Z-y, Wang K-M. Meshless global radial point collocation method for three-dimensional partial differential equations. Engineering Analysis with Boundary Elements. 2011; 35: 289-297.

[55] Zézé DS, Potier-Ferry M, Damil N. A boundary meshless method with shape functions computed from the PDE. Engineering Analysis with Boundary Elements. 2010; 34: 747-754.

[56] Varanasi C, Murthy JY, Mathur S. A Meshless Finite Difference Method for Conjugate Heat Conduction Problems. Journal of Heat Transfer. 2010; 132: 081303-081313.

[57] Bararnia H, Jalaal M, Ghasemi E, Soleimani S, Ganji DD, Mohammadi F. Numerical simulation of joule heating phenomenon using meshless RBF-DQ method. International Journal of Thermal Sciences. 2010; 49: 2117-2127.

[58] Ahmadi I, Sheikhy N, Aghdam MM, Nourazar SS. A new local meshless method for steady-state heat conduction in heterogeneous materials. Engineering Analysis with Boundary Elements. 2010; 34: 1105-1112.

[59] Fries TP, Belytschko T. The intrinsic XFEM: a method for arbitrary discontinuities without additional unknowns. International Journal for Numerical Methods in Engineering. 2006; 68: 1358-1385.

[60] Sadat H, Dubus N, Gbahoue L, Sophy T. On the solution of heterogeneous heat conduction problems by a diffuse approximation meshless method. Numerical Heat Transfer Part B-Fundamentals. 2006; 50: 491-498.

[61] Cao L, Qin Q-H, Zhao N. An RBF-MFS model for analysing thermal behaviour of skin tissues. International Journal of Heat and Mass Transfer. 2010; 53: 1298-1307.

[62] Yao G, Tsai CH, Chen W. The comparison of three meshless methods using radial basis functions for solving fourth-order partial differential equations. Engineering Analysis with Boundary Elements. 2010; 34: 625-631.

[63] Wang L, Chen J-S, Hu H-Y. Subdomain radial basis collocation method for fracture mechanics. International Journal for Numerical Methods in Engineering. 2010; 83: 851-876.

[64] Li Z, Mao X-Z. Global space–time multiquadric method for inverse heat conduction problem. International Journal for Numerical Methods in Engineering. 2011; 85: 355-379.

[65] Kansa EJ. Multiquadrics--A scattered data approximation scheme with applications to computational fluid-dynamics--II solutions to parabolic, hyperbolic and elliptic partial differential equations. Computers & Mathematics with Applications. 1990; 19: 147-161.

[66] Wong ASM, Hon YC, Li TS, Chung SL, Kansa EJ. Multizone decomposition for simulation of time-dependent problems using the multiquadric scheme. Computers & Mathematics with Applications. 1999; 37: 23-43.

[67] Wertz J, Kansa EJ, Ling L. The role of the multiquadric shape parameters in solving elliptic partial differential equations. Computers & Mathematics with Applications. 2006; 51: 1335-1348.

[68] Chen W, Ye L, Sun H. Fractional diffusion equations by the Kansa method. Computers & Mathematics with Applications. 2010; 59: 1614-1620.

[69] Tsai CH, Kolibal J, Li M. The golden section search algorithm for finding a good shape parameter for meshless collocation methods. Engineering Analysis with Boundary Elements. 2010; 34: 738-746.

[70] Stevens D, Power H. A scalable and implicit meshless RBF method for the 3D unsteady nonlinear Richards equation with single and multi-zone domains. International Journal for Numerical Methods in Engineering. 2011; 85: 135-163.

[71] Hu HY, Chen JS, Hu W. Weighted radial basis collocation method for boundary value problems. International Journal for Numerical Methods in Engineering. 2007; 69: 2736-2757.

[72] Chen J-S, Wang L, Hu H-Y, Chi S-W. Subdomain radial basis collocation method for heterogeneous media. International Journal for Numerical Methods in Engineering. 2009; 80: 163-190.

[73] Majchrzak E, Dziatkiewicz G, Paruch M. The modelling of heating a tissue subjected to external electromagnetic field. Acta of Bioengineering and Biomechanics. 2008; 10: 29-37.

[74] Waterman FM, Tupchong L, Nerlinger RE, Matthews J. Blood flow in human tumors during local hyperthermia. International journal of radiation oncology, biology, physics. 1991; 20: 1255-1262.

[75] Ng EYK, Tan HM, Ooi EH. Boundary element method with bioheat equation for skin burn injury. Burns. 2009; 35: 987-997.

[76] Field SB, Morris CC. The relationship between heating time and temperature: its relevance to clinical hyperthermia. Radiotherapy and Oncology. 1983; 1: 179-186.

[77] Rabin Y. Is intracellular hyperthermia superior to extracellular hyperthermia in the thermal sense? International Journal of Hyperthermia. 2002; 18: 194-202.

[78] Shih TC, Yuan P, Lin WL, Kou HS. Analytical analysis of the Pennes bioheat transfer equation with sinusoidal heat flux condition on skin surface. Medical Engineering & Physics. 2007; 29: 946-953.

[79] Curley SA. Radiofrequency Ablation of Malignant Liver Tumors. Oncologist. 2001; 6: 14-23.

[80] Eggeman AS, Majetich SA, Farrell D, Pankhurst QA. Size and concentration effects on high frequency hysteresis of iron oxide nanoparticles. IEEE Transactions on Magnetics. 2007; 43: 2451-2453.

[81] Barnes FS, Hu CLJ. Model for some nonthermal effects of radio and microwave fields on biological membranes. Ieee Transactions on Microwave Theory and Techniques. 1977; 25: 742-746.

[82] Osman MM, Afify EM. Thermal Modeling of the Malignant Woman's Breast. Journal of Biomechanical Engineering. 1986; 110: 269-276.

[83] Werner J, Buse M. Temperature Profiles with Respect to Inhomogeneity and Geometry of the Human Body. Journal of Applied Physiology. 1988; 65: 1110-1118.

[84] Deng ZS, Liu J. Monte Carlo method to solve multidimensional bioheat transfer problem. Numerical Heat Transfer Part B-Fundamentals. 2002; 42: 543-567.

[85] Jacobsen S, Stauffer PR. Multifrequency radiometric determination of temperature profiles in a lossy homogeneous phantom using a dual-mode antenna with integral water bolus. Ieee Transactions on Microwave Theory and Techniques. 2002; 50: 1737-1746.

[86] Thiebaut C, Lemonnier D. Three-dimensional modelling and optimisation of thermal fields induced in a human body during hyperthermia. International Journal of Thermal Sciences. 2002; 41: 500-508.

[87] Barauskas R, Gulbinas A, Vanagas T, Barauskas G. Finite element modeling of cooled-tip probe radiofrequency ablation processes in liver tissue. Computers in Biology and Medicine. 2008; 38: 694-708.

[88] Minitab 15 http://www.minitab.com (last access: Sept. 2012)

[89] Jamil M, Ng EYK. Ranking of parameters in bioheat transfer using Taguchi analysis. International Journal of Thermal Sciences. 2013; 63: 15-21.

[90] Antony J. Design of experiments for engineers and scientists. Butterworth-Heinemann, 2003.

[91] Ng EYK, Ng WK, Huang J, Tan YK. The engineering analysis of bioheat equation and penile hemodynamic relationships in the diagnosis of erectile dysfunction: part II - model optimization using the ANOVA and Taguchi method. International Journal of Impotence Research. 2008; 20: 285-294.

[92] Sudharsan NM, Ng EYK. Parametric optimization for tumour identification bioheat equation using ANOVA and the Taguchi method. Proceedings of the Institution of Mechanical Engineers Part H-Journal of Engineering in Medicine. 2000; 214: 505-512.

[93] Dewey WC, Hopwood LE, Sapareto SA, Gerweck LE. Cellular Responses to Combinations of Hyperthermia and Radiation. Radiology. 1977; 123: 463-474.

[94] Gomonov SV, Efanov VM. Theoretical Model of Irreversible Intracellular Electroporation (Supra-Electroporation) in a Single Cell. IEEE International Power Modulators and High Voltage Conference, Proceedings of the 2008. 2008, p. 330-333.

[95] Saniei N. Hyperthermia and Cancer Treatment. Heat Transfer Engineering. 2009; 30: 915-917.

[96] Lanzafame RJ. Applications of Laser Technology in Breast Cancer Therapy. Seminars in Surgical Oncology. 1995; 11: 328-332.

[97] Rebillard X, Davin JL, Soulie M, Ccafu. Treatment by HIFU of prostate cancer : survey of literature and treatment indications. Progres En Urologie. 2003; 13: 1428-1456.

[98] Neukam FW, Stelzle F. Laser Tumor Treatment in Oral and Maxillofacial Surgery. In: Schmidt M, Vollertsen F and Geiger M, (eds.). Laser Assisted Net Shape Engineering 6, Proceedings of the Lane 2010, Part 1. Amsterdam: Elsevier Science Bv, 2010, p. 91-100.

[99] Jamil M, Ng EYK. Ranking of parameters in bioheat transfer using Taguchi analysis. International Journal of Thermal Sciences.

[100] Agah R, Pearce JA, Welch AJ, Motamedi M. Rate process model for arterial tissue thermal damage implications on vessel photocoagulation. Lasers in Surgery and Medicine. 1994; 15: 176-184.

[101] Beckham JT, Wilmink GJ, Opalenik SR, Mackanos MA, Abraham AA, Takahashi K et al. Microarray Analysis of Cellular Thermotolerance. Lasers in Surgery and Medicine. 2010; 42: 752-765.

[102] Beckham JT, Wilmink GJ, Mackanos MA, Takahashi K, Contag CH, Takahashi T et al. Role of HSP70 in Cellular Thermotolerance. Lasers in Surgery and Medicine. 2008; 40: 704-715.

[103] Habash RWY, Bansal R, Krewski D, Alhafid HT. Thermal Therapy, Part 2: Hyperthermia Techniques. 2006; 34: 491-542.

[104] Grossman YL, Ustin SL, Jacquemoud S, Sanderson EW, Schmuck G, Verdebout J. Critique of stepwise multiple linear regression for the extraction of leaf biochemistry information from leaf reflectance data. Remote Sensing of Environment. 1996; 56: 182-193.

[105] Jensen AL. Comparison of theoretical derivations, simple linear regressions, multiple linear regression and principal components for analysis of fish mortality, growth and environmental temperature data. Environmetrics. 2001; 12: 591-598.

[106] Simon H, Bhave PV, Swall JL, Frank NH, Malm WC. Determining the spatial and seasonal variability in OM/OC ratios across the US using multiple regression. Atmospheric Chemistry and Physics. 2011; 11: 2933-2949.

[107] O'Neil AJ, Jee RD, Moffat AC. The application of multiple linear regression to the measurement of the median particle size of drugs and pharmaceutical excipients by near-infrared spectroscopy. Analyst. 1998; 123: 2297-2302.

[108] Seresht RJ, Jahanshahi M, Toubi F. Applying the Multiple Linear Regressions and Taguchi Design Method for Controlled Fabrication of Carbon Nanotubes in Solution. Fullerenes Nanotubes and Carbon Nanostructures. 2010; 18: 148-159.

[109] Chatterjee S, Hadi AS. Multiple Linear Regression. Regression Analysis by Example. John Wiley & Sons, Inc., 2006, p. 53-84.

[110] Chatterjee S, Hadi AS. Regression Diagnostics: Detection of Model Violations. Regression Analysis by Example. John Wiley & Sons, Inc., 2006, p. 85-120.

[111] Ng EYK, Ooi EH. Ocular surface temperature: A 3D FEM prediction using bioheat equation. Computers in Biology and Medicine. 2007; 37: 829-835.

[112] Ng EYK, Chua LT. Comparison of one- and two-dimensional programmes for predicting the state of skin burns. Burns. 2002; 28: 27-34.

[113] Fang J, Zhao G-F, Zhao J, Parriaux A. On the Truly Meshless Solution of Heat Conduction Problems in Heterogeneous Media. Numerical Heat Transfer, Part B: Fundamentals. 2008; 55: 1-13.

[114] Hu H-Y, Li Z-C. Combinations of collocation and finite-element methods for Poisson's equation. Computers & Mathematics with Applications. 2006; 51: 1831-1853.

[115] Hu H-Y, Li Z-C. Collocation methods for Poisson's equation. Computer Methods in Applied Mechanics and Engineering. 2006; 195: 4139-4160.

[116] Comsol Multiphysics. 3.5a Ed.

http://www.math.nju.edu.cn/help/mathhpc/doc/comsol/modeling.pdf (last access: Sept. 2012).

[117] Divo E, Kassab AJ. A meshless method for conjugate heat transfer problems. Engineering Analysis with Boundary Elements. 2005; 29: 136-149.

[118] Yao GM, Siraj ul I, Sarler B. Assessment of global and local meshless methods based on collocation with radial basis functions for parabolic partial differential equations in three dimensions. Engineering Analysis with Boundary Elements. 2012; 36: 1640-1648.

[119] Kameda K, Kondo T, Tanabe K, Zhao QL, Seto H. The role of intracellular Ca2+ in apoptosis induced by hyperthermia and its enhancement by verapamil in U937 cells. International Journal of Radiation Oncology Biology Physics. 2001; 49: 1369-1379.

[120] Kapp DS, Cox RS, Fessenden P, Meyer JL, Prionas SD, Lee ER et al. Parameters predictive for complications of treatment with combined hyperthermia and radiation therapy. International Journal of Radiation Oncology Biology Physics. 1992; 22: 999-1008.

[121] Bornstein BA, Zouranjian PS, Hansen JL, Fraser SM, Gelwan LA, Teicher BA et al. Local hyperthermia, radiation therapy and chemotherapy in patients with local regional recurrent of breast carcinoma. International Journal of Radiation Oncology Biology Physics. 1993; 25: 79-85.

[122] Gasselhuber A, Dreher MR, Negussie A, Wood BJ, Rattay F, Haemmerich D. Mathematical spatio-temporal model of drug delivery from low temperature

sensitive liposomes during radiofrequency tumour ablation. International Journal of Hyperthermia. 2010; 26: 499-513.

[123] Anai H, Uchida BT, Pavcnik D, Seong CK, Baker P, Correa LO et al. Effects of blood flow and/or ventilation restriction on radiofrequency coagulation size in the lung: An experimental study in swine. Cardiovascular and Interventional Radiology. 2006; 29: 838-845.

[124] Athanassiou E, Sioutopoulou D, Vamvakopoulos N, Karasavvidou F, Tzovaras G, Tziastoudi E et al. The fat content of small primary breast cancer interferes with radiofrequency-induced thermal ablation. European Surgical Research. 2009; 42: 54-58.

[125] Berjano EJ, Hornero F. Thermal-electrical modeling for epicardial atrial radiofrequency ablation. IEEE Transactions on Biomedical Engineering. 2004; 51: 1348-1357.

[126] Gervais DA, Arellano RS, Mueller PR. Percutaneous radiofrequency ablation of renal cell carcinoma. European Radiology. 2005; 15: 960-967.

[127] Brace CL. Radiofrequency and microwave ablation of the liver, lung, kidney, and bone: What are the differences? Current Problems in Diagnostic Radiology. 2009; 38: 135-143.

[128] Shibata T, Maetani Y, Isoda H, Hiraoka M. Radiofrequency ablation for small hepatocellular carcinoma: Prospective comparison of internally cooled electrode and expandable electrode. Radiology. 2006; 238: 346-353.

[129] Ng KK, Poon RT. Radiofrequency ablation for malignant liver tumor. Surgical Oncology. 2005; 14: 41-52.

[130] Goetz MP, Callstrom MR, Charboneau JW, Farrell MA, Maus TP, Welch TJ et al. Percutaneous image-guided radiofrequency ablation of painful metastases involving bone: A multicenter study. Journal of Clinical Oncology. 2004; 22: 300-306.

[131] Bitsch RG, Dux M, Helmberger T, Lubienski A. Effects of vascular perfusion on coagulation size in radiofrequency ablation of ex vivo perfused bovine livers. Investigative Radiology. 2006; 41: 422-427.

[132] Yoon SK, Choi JC, Cho JH, Oh JY, Nam KJ, Il Jung S et al. Radiofrequency Ablation of Renal VX2 Tumors With and Without Renal Artery Occlusion in a Rabbit Model: Feasibility, Therapeutic Efficacy, and Safety. Cardiovascular and Interventional Radiology. 2009; 32: 1241-1246.

[133] Steinke K, Glenn D, King J, Morris DL. Percutaneous pulmonary radiofrequency ablation: difficulty achieving complete ablations in big lung lesions. British Journal of Radiology. 2003; 76: 742-745.

[134] Esra N, Maarten MP, Gerard CvR, Niels K. Numerical modeling for simulation and treatment planning of thermal therapy. Physics of Thermal Therapy. Taylor & Francis, 2012, p. 119-136.

[135] Llovet JM, Vilana R, Bru C, Bianchi L, Salmeron JM, Boix L et al. Increased risk of tumor seeding after percutaneous radiofrequency ablation for single hepatocellular carcinoma. Hepatology. 2001; 33: 1124-1129.

[136] Kuvshinoff BW, Ota DM. Radiofrequency ablation of liver tumors: Influence of technique and tumor size. Surgery. 2002; 132: 605-611.

[137] Livraghi T, Solbiati L, Meloni MF, Gazelle GS, Halpern EF, Goldberg SN et al. Treatment of focal liver tumors with percutaneous radiofrequency ablation: Complications encountered in a multicenter study. Radiology. 2003; 226: 441-451.

[138] Cuschieri A, Bracken J, Boni L. Initial experience with laparoscopic ultrasound-guided radiofrequency thermal ablation of hepatic tumours. Endoscopy. 1999; 31: 318-321.

[139] Ishikawa T, Kohno T, Shibayama T, Fukushima Y, Obi S, Teratani T et al. Thoracoscopic thermal ablation therapy for hepatocellular carcinoma located beneath the diaphragm. Endoscopy. 2001; 33: 697-702.

[140] Dieter H, Chris B. Interstitial electromagnetic devices for thermal ablation. Physics of Thermal Therapy. Taylor & Francis, 2012, p. 159-176.

[141] Diederich CJ. Thermal ablation and high-temperature thermal therapy: Overview of technology and clinical implementation. International Journal of Hyperthermia. 2005; 21: 745-753.

[142] Song CW, Park HJ, Lee CK, Griffin R. Implications of increased tumor blood flow and oxygenation caused by mild temperature hyperthermia in tumor treatment. International Journal of Hyperthermia. 2005; 21: 761-767.

[143] Andreuccetti D, Zoppetti N. Quasi-static electromagnetic dosimetry: From basic principles to examples of applications. International Journal of Occupational Safety and Ergonomics. 2006; 12: 201-215.

[144] Mulier S, Ni Y, Miao Y, Rosiere A, Khoury A, Marchal G et al. Size and geometry of hepatic radiofrequency lesions. European Journal of Surgical Oncology. 2003; 29: 867-878.

[145] Jamil M, Ng EYK. Evaluation of meshless radial basis collocation method (RBCM) for heterogeneous conduction and simulation of temperature inside the biological tissues. International Journal of Thermal Sciences. 2013; 68: 42-52.

[146] Yi M, Podhajsky RJ, Mahajan RL. Investigation of temperature elevation and saline miection induced electrical conductivity change of hepatic tissue by using micro probe - art. no. 64400N. In: Ryan TP, (ed.). Thermal Treatment of Tissue: Energy Delivery and Assessment IV. Bellingham: SPIE-Int Soc Optical Engineering, 2007, p. N4400.

[147] Bhattacharya A, Mahajan RL. Temperature dependence of thermal conductivity of biological tissues. Physiological Measurement. 2003; 24: 769-783.

[148] Dewhirst M, Gross JF, Sim D, Arnold P, Boyer D. The effect of rate of heating or cooling prior to heating on tumor and normal tissue microcirculatory blood flow. Biorheology. 1984; 21: 539-558.

[149] Pop M, Molckovsky A, Chin L, Kolios MC, Jewett MAS, Sherar M. Changes in dielectric properties at 460 kHz of kidney and fat during heating: importance for radio-frequency thermal therapy. Physics in Medicine and Biology. 2003; 48: 2509-2525.

[150] Pop M, Davidson SRH, Gertner M, Jewett MAS, Sherar MD, Kolios MC. A Theoretical Model for RF Ablation of Kidney Tissue and Its Experimental Validation. In: Bello F and Cotin S, (eds.). Biomedical Simulation, Proceedings. Berlin: Springer-Verlag Berlin, 2010, p. 119-129.

[151] Schutt D, Berjano EJ, Haemmerich D. Effect of electrode thermal conductivity in cardiac radiofrequency catheter ablation: A computational modeling study. International Journal of Hyperthermia. 2009; 25: 99-107.

[152] Haines DE, Watson DD. Tissue heating during radiofrequency catheter ablation - A thermodynamic model and observations in isolated perfused and superfused

canine right ventricular free wall. Pace-Pacing and Clinical Electrophysiology. 1989; 12: 962-976.

[153] Jamil M, Ng EYK. To optimize the efficacy of bioheat transfer in capacitive hyperthermia: A physical perspective. Journal of Thermal Biology. 2013; 38: 272-279.

[154] Ng EYK, Ng WK. Parametric study of the biopotential equation for breast tumour identification using ANOVA and Taguchi method. Medical and Biological Engineering and Computing. 2006; 44: 131-139.

[155] Jamil M, Ng EYK. Statistical modeling of electrode based thermal therapy with Taguchi based multiple regression. International Journal of Thermal Sciences. 2013; 71: 283-291.

[156] Weng WC, Yang F, Elsherbeni AZ. Linear antenna array synthesis using Taguchi's method: A novel optimization technique in electromagnetics. IEEE Transactions on Antennas and Propagation. 2007; 55: 723-730.

[157] Roache PJ. Perspective - A method for uniform reporting of grid refinement studies. Journal of Fluids Engineering - Transactions of the ASME. 1994; 116: 405-413.

[158] Schwer LE. Is your mesh refined enough? Estimating discretization error using GCI. 7th LS-DYNA Anwenderforum I-I-45-54, . Bamberg2008.

[159] Seiler J, Roberts-Thomson KC, Raymond JM, Vest J, Delacretaz E, Stevenson WG. Steam pops during irrigated radiofrequency ablation: Feasibility of impedance monitoring for prevention. Heart Rhythm. 2008; 5: 1411-1416.

[160] Topp SA, McClurken M, Lipson D, Upadhya GA, Ritter JH, Linehan D et al. Saline-linked surface radio-frequency ablation - Factors affecting steam popping and depth of injury in the pig liver. Annals of Surgery. 2004; 239: 518-527.

List of Publications

Journal Publications

[1] M. Jamil, E.Y.K. Ng, Ranking of parameters in bioheat transfer using Taguchi analysis, International Journal of Thermal Sciences 63 (2013) 15-21.

[2] M. Jamil, E.Y.K. Ng, Evaluation of meshless radial basis collocation method (RBCM) for heterogeneous conduction and simulation of temperature inside the biological tissues, International Journal of Thermal Sciences 68 (2013) 42-52.

[3] M. Jamil, E.Y.K. Ng, Statistical modelling of electrode based thermal therapy with Taguchi based multiple regression, International Journal of Thermal Sciences 71 (2013) 283-291.

[4] M. Jamil, E.Y.K. Ng, To optimize the efficacy of bioheat transfer in capacitive hyperthermia: A physical perspective, Journal of Thermal Biology 38 (2013) 272-279.

[5] M. Jamil, E.Y.K. Ng, Parametric sensitivity analysis of radiofrequency ablation with efficient experimental design **(Accepted: In press)**

[6] M. Jamil, E.Y.K. Ng, Quantification of the effect of electrical and thermal parameters on radiofrequency ablation for concentric tumour model of different sizes **(Submitted to International Journal of Thermal Sciences)**

[7] M. Jamil, E.Y.K. Ng, Temperature control finite element simulation of radiofrequency ablation for various tissue types: Outcome prediction by using simplified models. **(To be submitted in Physics in Medicine and Biology)**

Conference Publications

[1] M. Jamil, E.Y.K. Ng, Simulation of heterogeneous conduction and bioheat transfer utilizing subdomain radial basis collocation method, Proceedings of the 23rd International symposium on transport phenomena, 19-23 November 2012, Auckland, New Zealand.